# BOND OF LAP SPLICED BARS IN SELF-COMPACTING CONCRETE

A THESIS SUBMITTED TO
THE GRADUATE SCHOOL OF NATURAL AND APPLIED SCIENCE
OF
MIDDLE EAST TECHNICAL UNIVERSITY

BY

MEHRAN GHASABEH

IN PARTIAL FULLFILMENT OF THE REQUIREMENTS
FOR
THE DEGREE OF MASTER OF SCIENCE
IN
CIVIL ENGINEERING

JANUARY 2013

Approval of the thesis:

Submitted by **MEHRAN GHASABEH** in partial fulfillment of the requirements for the degree of **Master of Science in Civil Engineering Department**, **Middle East Technical University**, by,

Prof. Dr. Canan Özgen _____
Dean, Graduate School of **Natural and Applied Sciences**

Prof. Dr.Ahmet Cevdet Yalçıner _____
Head of Department, **Civil Engineering**

Assoc. Prof. Dr. Erdem Canbay _____
Supervisor,**Civil Engineering Department, METU**

**Examining Committee Members**

Prof. Dr. Güney Özcebe _____
Civil Engineering Department, METU

Assoc. Prof. Dr. Erdem Canbay _____
Civil Engineering Department, METU

Prof. Dr. Barış Binici _____
Civil Engineering Department, METU

Assoc. Prof. Dr. Özgür Anıl _____
Civil Engineering Department, Gazi University

Asst. Prof. Dr. Burcu Burak _____
Civil Engineering Department, METU

**Date: 01.02.2013**

**I hereby declare that all information in this document has been obtained and presented in accordance with academic rules and ethical conduct. I also declare that, as required by these rules and conduct, I have fully cited and referenced all material and results that are not original to this work.**

Name, Last Name: Mehran Ghasabeh

Signature :

## ABSTRACT

BOND OF LAP-SPLICED BARS
IN SELF-COMPACTING CONCRETE

GHASABEH, Mehran
M.S., Department of Civil Engineering
Supervisor: Assoc. Prof. Dr. Erdem CANBAY

January 2013, 82 Pages

Self-compacting concrete is an innovative construction material; its priority to normal vibrated concrete is that there is not any vibration requirement. Bond strength of reinforcement is one of the key factors that ensures the usefulness of any reinforced concrete structure. In this study, 6 full-scale concrete beams spliced at the mid-span were tested under two-point symmetrical loading. Test variables were bottom cover, side cover, free spacing between longitudinal reinforcement, lap-splice length and presence of transverse reinforcements within the lap-splice region.

Specimen SC_22_44_88_800 had cover dimensions close to the code limits and had $36d_b$ lap splice length. This specimen showed flexural failure. Specimen SC_44_44_44_710 had $32d_b$ lap splice and cover dimensions greater than code minimums. This specimen showed yielding primarily. With the increasing loading, however, bond failure occurred with side splitting.

ACI 408 descriptive equation for normal vibrated concrete predicted bar stresses of the unconfined specimens produced with self-compacting concrete acceptably well. The predicted values were lower than the measured values to be on the safe side. The error varied between 3.4% and 6.5%.

All predictions of the ACI408 descriptive equation was higher than the measured bar stresses of the confined specimens produced with SCC. All the calculated values were unsafe. The error varied between 10.6% and 34.5%.

Specimen SC_44_22_22_530_T4 with $24d_b$ lap splice length had side cover and spacing between bars 63.3% and 56.7% less than the ACI 318 limits. The calculated bar stress was 21.6% higher than the measured value. The main reason of the deviation was inadequate cover dimensions.

In specimen SC_44_22_22_530_T6, number transverse reinforcement was increased to 6 stirrups to overcome the small cover and spacing problem. However, increased number of stirrups inside a small side and face cover caused weak plane and measured bar stress decreased.



Keywords: Self-Compacting Concrete, Full-scale beam test, Bond, Lap Splice, Transverse Reinforcement.

# ÖZ

KENDİNDEN YERLEŞEN BETONDA
BİNDİRMELİ EKLERİN ADERANSI

GHASABEH, Mehran
Yüksek Lisans, İnşaat Mühendisliği Bölümü
Danışman: Doç. Dr. Erdem CANBAY

Ocak 2013, 82 Sayfa

Kendinden yerleşen beton yenilikçi bir inşaat malzemesidir; normal betona göre üstünlüğü vibrasyon ihtiyacı göstermemesidir. Donatının aderansı betonarme yapıların kullanılabilirliğin anahtar etmenlerindendir. Bu çalışmada 6 tam ölçekli orta açıklığında bindirmeli ek yapılmış kiriş simetrik iki nokta altında test edilmiştir. Deney değişkenleri alt beton pas payı, yan beton pas payı, boyuna donatı arasındaki serbest açıklık, bindirmeli eklerin uzunluğu ve bindirmeli ek boyunca yatay donatının bulunup bulunmamasıdır.

SC_22_44_88_800 deney elemanının şartname limitlerine yakın pas payı vardır ve $36d_b$ bindirme boyu vardır. Bu elemanda eğilme kırılması olmuştur. SC_44_44_44_710 deney elemanının $32d_b$ bindirme boyu ve şartname minimumlarından daha büyük pas payı vardır. Bu elemanda ilk önce akma gerçekleşmiştir. Ancak artan yüklemeyle yan yüz aderans kırılması gerçekleşmiştir.

ACI 408 normal vibrasyonlu beton için olan denklemi, sargılanmamış kendinden yerleşen beton ile imal edilmiş deney elemanlarının donatı gerilmelerini kabul edilir sınırlarda tahmin etmiştir. Hesaplanan değerler ölçülen değerlerin altında güvenli taraftadır. Hesap hatası %3,4 ile %6,5 arasındadır.

ACI 408 denkleminin kendinden yerleşen betonla üretilmiş sargılı elemanlarla ilgili tüm tahminleri ölçülen değerlerin üstündedir. Tüm hesaplanan değerler güvensiz yöndedir. Hata %10,6 ile %34,5 arasında değişmektedir.

$24d_b$ bindirme boyu olan deney elemanı SC_44_22_22_530_T4 yan pas payı ile donatı arası mesafeleri ACI 318 limitlerine göre %63,3% ve %56,7 azdır. Hesaplanan donatı gerilmesi ölçülen değere göre %21.6 fazladır. Bu sapmanın ana sebebi yetersiz pas payıdır.

SC_44_22_22_530_T6 deney elemanında enine donatı sayısı 6'ya çıkarılarak yetersiz pas payı problem aşılmaya çalışılmıştır. Ancak, yetersiz beton pas payı içinde artırılan yatay donatı zayıf bir yüzey oluşturmuştur ve ölçülen gerilme değerleri daha da düşmüştür.

Anahtar Kelimeler: Kendinden Yerleşen Beton, Tam Boyutlu Kiriş Deneyi, Aderans, Bindirmeli Ek, Enine Donatı.

**DEDICATED TO MY DEAR PARENTS**
**Rahim Ghasabeh and Noras Eskandari**

**ACKNOWNLEDGMENT**

"**Learning never exhausts the mind."**
— Leonardo da Vinci

Foremost, I wish to express my sincere thanks and appreciation to my master thesis supervisor, Assoc. Prof. Dr. Erdem Canbay for his continuous support, patience and motivation in all the time of research and writing this thesis.

I would like to thank the examining committee members, Prof. Dr. Güney Özcebe, Prof. Dr. Barış Binici, Asst. Prof. Dr. Burcu Burak, Dr. Özgür Anıl and other faculty members with whom I have taken courses, in particular, Prof. Dr. Tanvir Wasti for his motivated suggestions.

I would like to thank the staff of the structural mechanics laboratory who were helped and supported me throughout my experimental study.

I would like to thank all my friends both in Iran and Turkey, particularly Aynaz Lotfata.

Moreover, I would like to give my especially deepest gratitude to my dear patents, during these two and half years, I have lived away from them. I am deeply indebted to them for their supports in my whole life.

**TABLE OF CONTENTS**

## LIST OF TABLES

**TABLES**

## LIST OF FIGURES

**FIGURES**

## LIST OF SYMBOLS

| | |
|---|---|
| $a$ | Distance of the point load to the support |
| $A_b$ | area of bar being developed or spliced |
| $A_{tr}$ | Total cross-sectional area of all transverse reinforcement which is within the spacing s and which crosses the potential plane of splitting through the reinforcement being developed. |
| $b_w$ | Width of specimen |
| $c_b$ | bottom concrete cover for reinforcing bar being developed or spliced |
| $c_{max}$ | maximum ($c_b$, $c_s$) |
| $c_{min}$ | maximum ($c_b$, $c_{si}$) |
| $c_s$ | minimum [$cso$ , $csi$ + 6.4 mm] |
| $c_{si}$ | ½ of the bar clear spacing |
| $c_s$ | side cover |
| $d_b$ | Diameter of reinforcing bars |
| $f'_c$ | 28 days cylinder compressive strength of concrete |
| $f_c$ | Cylinder compressive strength of concrete |
| $f_{cts}$ | Split tensile strength of concrete |
| $f_s$ | stress in reinforcing bars |
| $f_y$ | Longitudinal reinforcement yield strength |
| $K_{tr}$ | transverse reinforcement index |
| $l_s$ | Development or splice length |
| $n$ | Number of bars or wires being spliced or developed along the plane of splitting |
| $N$ | the number of transverse stirrups, or ties, within the development or splice length |
| $t_{A/C}$ | Tangential deviations between points A and C |
| $t_{B/C}$ | Tangential deviations between points B and C |
| $t_d$ | The bar diameter factor |
| $t_r$ | The relative rib area factor |
| $\Delta_A$ | Deflection at point A |
| $\Delta_B$ | Deflection at point B |
| $\Phi$ | Reinforcement bar diameter |

# CHAPTER 1

# INTRODUCTION

## 1.1. General

Concrete, along with steel, is one of the most popular construction materials of the last century. Since fresh mix of concrete is flowable, concrete can be molded into any shape as long as the formwork can be built for the desired shape. Concrete mix is very important because of the target strength and workability. To increase the strength of concrete, water/cement ratio should be decreased which arises workability problems. To avoid honeycombing in concrete, it should be properly compacted by means of vibrators when it is placed into the forms. However, compaction is carried out by unskilled workers on site and it is very tiring and demanding work. Therefore, a substantial proportion of concrete is not adequately compacted in reality. High water content can increase the level of workability whereas it causes segregation and decrease the target strength of concrete.

After the Second World War in Japan, the rapid reconstruction projects concealed the construction quality. Those structures deteriorated very rapidly in one or two decades which initiated investigation of the unsatisfactory performance of concrete. Many researches aimed improvement in the durability of concrete. The cause of deterioration of concrete was found to be mainly insufficient compaction of concrete and the solution was proposed as increasing the workability of the fresh mix so much that compaction was no longer necessary (De Schutter, Bartos, Domone, & Gibbs, 2008), (Ozawa, et al. 1989), (Tanaka, Sato, et al., 1993), (Miura, Takeda, Chikamatsu, & and Sogo, 1993), (Hayakawa, Matsouka and Shindoh 1993).

Self-compacting concrete (SCC) can be defined as specially produced concrete that flows under its own weight, fills the required space or formwork completely and produces a dense and adequately homogenous material without the need for compaction. SCC resists segregation and maintains its stable composition during transportation and placing (De Schutter, Bartos, Domone, & Gibbs, 2008). Today, SCC has been used widely all around the world. In general, SCC is produced with conventional concrete materials and viscosity-modifying admixture (VMA) (ACI 237R-07, 2007). SCC is also named as self-consolidating concrete, self-leveling concrete, and self-placing concrete in the literature.

SCC has many advantages such as reducing the labor and equipment for vibration to get appropriate compaction/consolidation, and for screeding operations to get flat surfaces. Mechanical properties of SCC are always very high. SCC also accelerates construction time. For complex formworks, it ensures high construction quality. Even at congested reinforcement, SCC places perfectly into the formwork.

## 1.2. Fresh and hardened properties of self-compacting concrete

Although SSC and traditionally vibrated concrete have similar hardened properties such as strength and elastic modulus, there are unavoidable differences in practical mix design (Domone, 2007), (De Schutter, Bartos, Domone, & Gibbs, 2008). Materials that constitute self-compacting concrete are the same as used for normal concrete. The most usual distinction lies in higher powder content and a low water/powder ratio in self-compacting concrete than normal concrete. The compressive strength increment of SCC depends on portion of additions. Limestone powder is an ordinary addition that contributes considerably to the rate of gain of strength. In addition, usage of viscosity modifying admixtures upgrades the stability of SCC. The types of superplasticiser define the effectualness of a viscosity material admixture. There are three key properties of fresh SCC, namely:

- Filling ability
- Passing ability
- Segregation resistance

Filling ability is the ability of the fresh mix to flow under its own weight and perfectly fill all the spaces in the formwork. Passing ability is the ability which demonstrates how well the fresh mix flow through constrained formwork. Segregation resistance, which is determined by the plastic viscosity and density of the cement paste, is the ability of fresh mix to keep its basic apportionment of constituent materials during transport, placing and compaction.

Some tests, which are different than normal vibrated concrete, are performed to explore the key properties of fresh SCC. These tests are Slump-flow test, $T_{500}$ time, V-funnel and L-Box.

The Slump-flow test and $T_{500}$ time is a test to evaluate flowability and the flow rate of self-compacting concrete in the absence of restrictions. Unlike the normal vibrated concrete, an unconfined horizontal spread of the sample is measured as the slump-flow. $T_{500}$ time is a time measured when horizontal spread of the sample reaches a circle of 500 mm diameter.

The V-funnel test is used to evaluate the viscosity and filling ability of self-compacting concrete. The V-funnel flow time is the period a defined volume of SCC needs to pass a narrow opening. The time measured as test result is fundamentally depends on plastic viscosity provided that blocking and/or segregation do not take place.

The L-Box test is used to evaluate the passing ability of self-compacting concrete to flow through tight openings including spaces between reinforcing bars and other obstructions without segregation or blocking.

## 1.3. Bond Behavior

In reinforced concrete construction, bond between concrete and steel is one of the essential factor affecting the member behavior. The resistance of plain concrete against tension is lower in comparison with its compressive strength; due to this fact concrete has been classified as brittle material. The role of steel bars in concrete member is to enhance the tensile strength of concrete. For this reason, perfect bond between steel bars and concrete is necessary. The features of bond depend mainly on:

- Adhesion between steel and concrete
- Friction between steel and concrete
- Bearing of the deformation on the steel surface against surrounding concrete

For deformed bars, bearing of the deformation on the steel surface against surrounding concrete has consequential role in force transfer between steel bars and concrete. Adhesion and friction have little contribution for deformed bars. For this reason, the use of plain bars is prohibited in structural members.

As it is shown in Figure 1.1, due to existence of ribs and lugs along deformed bar, a great majority of forces are transferred by bearing and friction forces act on it. The force transfer by adhesion and friction along the surface of the bar is lost after initial slip.

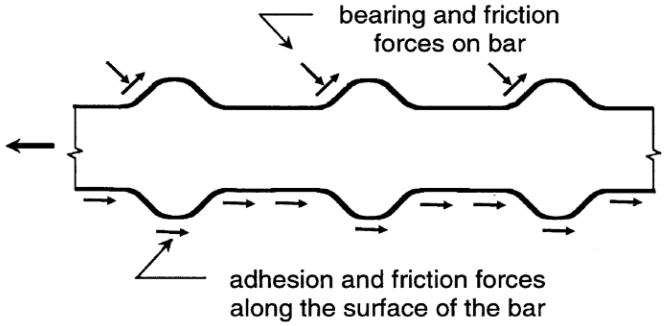


**Figure 1.1** Bond force transfer mechanism (ACI 408R-03, 2003)

Bond behavior mainly depends on the variables listed below:

- The mechanical properties of the concrete (associated with tensile and bearing strength);
- The volume of the concrete around the bars (related to concrete cover and bar spacing parameters);
- The presence of confinement in the form of transverse reinforcement which can delay and control crack propagation;
- The surface condition of the bar;
- The geometry of the bar (deformation height, spacing, width, and face angle).

According to the ACI report "Bond and Development of Straight Reinforcing Bars in Tension" (ACI 408R-03), factors affecting bond behavior are classified in three categories as structural characteristics, bar properties and concrete properties.

Two types of splitting failure can occur due to insufficient bond characteristics. Side splitting occurs if total face cover is larger than sum of side cover and bar clear spacing, Figure 1.2. If the concrete face cover is smaller than half of the free spacing between the bars, the splitting crack occurs through the cover to the free surface known as face splitting.

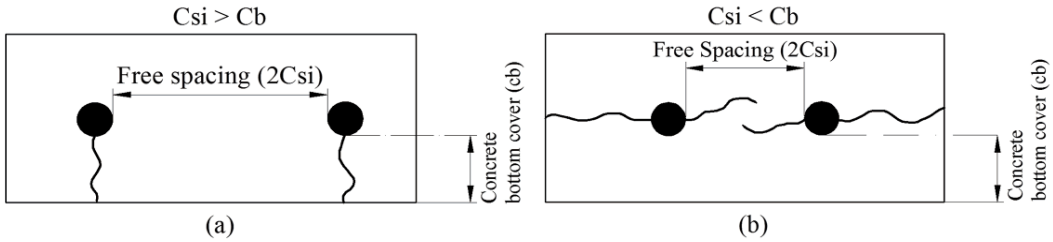


**Figure 1.2** Bond crack

## 1.4. Research Needs

Bond strength of the steel reinforcing bars has been studied by many researchers for more than 100 years. Thaddeus Hyatt (1877) is one of the first investigators, made tests to determine the bond between concrete and iron bars. In the following years, Duff A. Abrams (1913) started a project took about three years for bond between steel bars of any kind (plain and deformed) and concrete. During these years significant modifications have been done by code provisions. There are extensive numbers of researches on bond in the literature. Even, researches on bond behavior of SCC are outrageous. However, studies on bond behavior of SCC are limited with small cubical or cylindrical specimens and with pull-out tests (Canbay, 2009). In order to observe better the top-bar effect of SCC, pull-out tests were also performed on some wall or column members (Yin-Wen, et al., 2003), (Valcuende, et al., 2009). A study on small beam-end specimens was also conducted for SCC (de Almeida Filho, et al., 2008), (Desnerk, et al., 2010). There are limited studies on the literature carried out on full-scale beams with lap splices for SCC (Türk, et al., 2008), (de Almeida Filho, et al., 2008), (Pandurangan, et al., 2010). It can be concluded that there is a need for bond tests on SCC with full-scale beams to justify conclusions deduced from limited tests.

## 1.5. Objective and Scope

The objective of this study is to investigate the bond behavior between steel reinforcing bars and self-compacting concrete, and evaluate the effect of different parameters affecting the bond characteristics in SCC. In this study, three reports are followed; namely, ACI 408R-03 Bond and Development of Straight Reinforcing Bars in Tension, ACI R237-07 Self-Consolidating Concrete, and The European Guidelines for Self-Compacting Concrete. Totally six full-scale bottom cast beam specimens were prepared. The parameters affecting bond behavior and considered in this study were number of transverse reinforcing bars along lap-splice region, lap splice length of longitudinal reinforcing bars, cover dimensions, and free spacing between longitudinal bars. All specimens were simply supported beams and loaded symmetrically under two points along the length of the beams. All the longitudinal reinforcement spliced at the mid-span where the shear force is zero and moment is constant. Tip and mid deflections along with strains on longitudinal and transverse reinforcement were acquired during the tests.

In this scope, previous publications and researches were reviewed to comprehend the bond behavior for SCC. Six full scale beam specimens were designed based on ACI 408R-03 descriptive equation for lap splice length. A suitable test setup was prepared and all specimens were tested in the laboratory. All the necessary data was gathered with a data acquisition system during testing. Test results were evaluated analytically to verify the validity of the design equations.

# CHAPTER 2

## LITERATURE REVIEW

The researches and studies associated with bond behavior of reinforced normal-vibrated concrete members started by Abrams (1913). Based on comprehensive literature survey, significant observations and conclusions of the previous researches and publications are summarized below. The survey is presented in chronological order to keep the historical prospective.

*Sonebi and Bartos (1999)* operated experimental investigation to study the properties of hardened SCC and the bond with reinforcing bars. According to the RILEM test specification, bond strength was ascertained for reinforcing bars with two types of diameter embedded in concrete. The obtained results for SCC were compared with those of a vibrated concrete as reference mix. They concluded briefly that:

- Self-compacting concrete had sufficient flowablity and excellent deformability without blockage.
- The compressive strength of SCC is less dependent on curing condition than that of reference mix.
- The SCC showed greater stability than that of the reference mix.
- The drying shrinkage of SCC was lower than that of reference mix.
- In comparison with the reference mix, the bond stress of SCC was obtained higher.

*Yien-Wen Chan, Yu-Sheng Chen, and Yi-Shi Liu (2003)* performed direct pullout tests on reinforcing bar embedded in self-compacting concrete members. Full-scale reinforced concrete walls were used with a depth of 1200 mm as the pullout specimens. The reinforcing bars were set up horizontally inside the test specimens at different elevations. Comparison of the test results between the specimens both with self-compacting concrete (SCC) and ordinary Portland concrete (OPC) was done by considering the affecting factors such as development of bond strength with age, influence of compressive strength, top bar effect and effect of high-range water-reducing admixture at early age. It was concluded that the variation in bond strength at different elevations in SCC is less significant than that of OPC which is related to the more consistent nature of SCC and the non-consolidating concreting process. SCC exhibited consequentially higher bond strength and less significant top-bar effect. Because of the possible retarding effect, more attention required to be paid to the development in compressive strength and bond strength of SCC.

*Daoud and Lorrian (2003)* carried out the pull-out test to investigate the impact of reinforcing bar positions on bond strength of SCC. Five different positions of reinforcement were considered: horizontal (superior, inferior and median), and vertical (loaded in casting or against casting direction). The results expressed that when the bars cast in vertical position and loaded against the casting direction, the highest bond strength was obtained. For bars cast horizontally, by increasing the depth of concrete underneath the steel bar, the bond strength decreased. The ration between the bond strength of bars cast in vertical and horizontal position was nearly 1.5. By using image analysis, a satisfying correlation was found between the bond strength and the difference between the percentage of coarse aggregate above and below the steel bar for different positions.

*Zhu, Sonebi and Bartos (2004)* fulfilled pullout test to estimate the sequel of applying SCC on bond and interfacial properties around steel reinforcement in practical concrete element. In this study, for the elastic modulus and micro-strength of the interfacial transition zone (ITZ) around steel reinforcement determination, the depth-sensing nano-indentation technique was used. The conclusions stated that the actual bond strength of SCC mixes for the same bar diameter was higher than that of reference mix. Owing to the lower water content and specifically the higher powder volume in SCC mixes, which resulted in reducing the accumulation of bleed water under horizontally embedded reinforcing bars, the normalized bond strength was nearly 10-40% higher than that of reference mix. The elastic modulus and micro-strength of the ITZ around steel reinforcement in practical concrete were successfully studied by the depth-sensing nano/micro-indentation technique. For the vibrated, reference concrete, the elastic modulus and the micro-strength of the ITZ were greater on the top side of horizontal steel reinforcement than on the bottom side. In SCC mixes, diversity of ITZ properties between top and bottom side were less distinct. By increasing bond strength of reinforcement in the mixes, the improved micro-mechanical properties of the ITZ and their uniformity for SCC mixes were unchanging.

*Esfahani, Kianoush and Lachemi (2005)* conducted an experimental study on bond strength of reinforcing bars made of glass fiber reinforced polymers (GPRP) embedded in normal and self-compacting concrete. Pullout tests were done on 36 GFRP reinforcing bars installed inside concrete specimens. In this study, different parameters such as type of concrete, bar location, and cover thickness were encompassed. It was concluded that:

- The bond strength of bottom GFRP reinforcing bars was nearly the same for the specimens made of normal and self-compacting concrete. For the top bars, the bond strength of normal concrete was greater than that of self-compacting concrete.
- The ratio of bottom bar bond strength to top bar bond strength for GFRP embedded in self-compacting concrete was obtained greater than that embedded in normal concrete.
- The V-notch failure is common in slab. Due to occurrence of this type of failure in the middle bars, the bond strength is larger than that for other locations. Hence, the bond strength of bars in slabs should be greater than that in beams.

*Ana Lúcia H. de C. El Debs e Fernando M. de Almeida Filho (2007)* conducted the numerical approach applying Finite Element Method to assess the bond stress using beam models based in Rilem's recommendation. The result obtained for ordinary concrete and self-compacting with the same compressive strength were compared with each other, and additionally with numerical results. The results obtained for beam model with SCC and ordinary concrete are almost identical, with a small advantage for ordinary concrete. Although the slip could not be well represented, the numerical models exhibited good approach with the test results, especially for the failure load and for the displacements values. The theoretical predictions were more conservative than the test results. Finally, it could be said that good approaches for the beam tests were obtained by utilization of the numerical modes using both ordinary concrete and self-compacting concrete. Those values could be extended to models with different compressive strength and bar diameter.

*de Almeida, F.M.A., El Debs , M.K., and El Debs, A.L.H.C. (2007)* performed pull-out and beam tests according to RILEM procedures on the test specimen made of SCC with varying compressive strength, steel bar diameter and test methods to estimate the bond behavior. The following conclusions can be inferred:

- The bond behavior described by pull-out and beam tests using SCC and normal vibrated concrete are almost identical almost to each other. However, in some cases for SCC it was better than vibrated concrete.
- By comparing the Code provisions and equations reasoned out that adoption of the same procedures for vibrated concrete could be applied for SCC, which denoting that bond behavior of SCC are similar of vibrated concrete.

*Hossain and Lachemi (2008)* implemented especially developed pullout test on 72 specimens to determine the bond resistance and properties between deformed steel bar and supplementary cementing materials (SCM) (such as fly ash and slag) and viscosity modifying admixtures (VMA) based SCC as well as normal concrete (NC). Furthermore, top-bar effect on the bond behavior was examined. By comparing the bond characteristics of deformed reinforcing bars embedded in conventionally vibrated normal concrete and SCC, the following conclusions were interpreted:

- Due to the more consistent nature of SCC and the nonconsolidated concreting process, variation in bond strengths at different elevations yielded less significant effect than in NC.
- For all SCC specimens except those cast in horizontal condition, the normalized bond strength were higher than those specimens made of NC. The top-bar effect in SCC was less significant than that in NC.
- The bond measurement results as a quantitative estimation indicated that for a reinforced concrete, using SCC, would be more reliable than those using NC. Bleeding and the inhomogeneous nature of normal concrete can be minimized by using SCC.

*Valcunde and Parra (2008)* conducted experimental work studying the bond strength between reinforcing steel bars and concrete and the top-bar effect on self-compacting concrete. The pullout tests were conducted on eight different concrete, four self-compacting concrete (SCC) and four normally-vibrated concrete (NVC). The results indicated that the quality of concrete, the compressive strength and the tensile strength had extensive influence on the bond strength. By comparing the results acquired for both SCC and normal vibrated concrete (NVC), it was concluded that the SCC exhibited higher bond strength than NVC. By reason of greater fill capacity and less bleeding of SCC, for moderated load levels, SCC demonstrated a stiffer behavior than NVC. The ultimate bond strength in SCC was obtained greater than that in NVC.

*Türk, Benli and Calayır (2009)* examined experimentally the effect of self-compacting concrete and the reinforcement diameter on the bond-slip properties of tension lap-splices. Twelve full-scale beam specimens (2000×300×200 mm) were tested in positive bending. Based on the results, the conclusions were obtained and listed below:

- In spite of the concrete type, by increasing the diameter of the reinforcing bar, the maximum load increased and the deflection recorded at the center of the beam decreased, additionally the specimens with the higher reinforcing bars presented higher stiffness.

- For the embedded tension lap-spliced bars in SCC, load transfer was better than that of those embedded in normal concrete. Besides, in the beams made of SCC failure developed evenly and was particularly ductile, in comparison with the specimens made of normal concrete and with no stirrups.
- In spite of the reinforcing bar diameter, longer cracks were observed in specimens made of SCC than those of normal concrete.
- The normalized bond strengths of the SCC mixes were nearly 4% higher than those of the NC mixes.

*Canbay, E. (2009)* followed up experimental study by conducting in total six full-scale tests to evaluate the influence of main variables such as spacing between reinforcing bars, splice length, and cover dimensions on the bond of lap-spliced bars in SCC. Increasing the splice length can change the type of failure from bond to flexure. However, for specimens with large splice length with small cover dimensions, flexural failure was followed by bond failure. By carrying out the analytical study and using the equation in ACI 408-R03 for determination of reinforcement stress and comparing them with the experimentally calculated stress, it was concluded that the ACI 408 descriptive equation for normal concrete estimated tests results exceptionally good.

*Pandurangan, Kothandaraman, Sreedaran (2010)* carried out full-scale experimental investigation using pullout test to determine the effect of SCC on bond characteristics and mode of bond splitting of tension lap splices anchored in normal strength concrete (NSC). It was concluded that at low passive confinement by transverse reinforcement, the bond strength between the SCC and normal vibrated concrete were almost identical. Furthermore, at well confinement, bond strength in SCC is higher than normal vibrated concrete. For the beam specimens with confinement index lower than or equal to 2.0, lower ductility was attained and subjected to wide crack width. Specimens with ductility index higher than 3.0 demonstrated ductile performance and subjected to large number of smaller cracks. Spacing of transverse reinforcements did not have any influence on the load at first flexural crack.

*Türk, Karataş and Ulucan (2010)* carried out experimental study on a total of 27 full-scale beam specimens. All specimens were tested in positive bending under the four point loading arrangement used during the load controlled experiments to evaluate the effect of fly ash (FA) and silica fume (SF) on the bond-slip properties of tension lap-spliced bars. Following results were obtained by analyzing the results of this study:

- The experimental ultimate moment is lower than the analytical one. This designated that all specimens failed by splitting of concrete at the end of the overlapping splice. A sudden increase of the splitting cracks width occurred at the ultimate moment over the whole splice.
- All beam specimens with both NC and SCC had the same splice embedment length (300 mm), but the experimental and theoretical ultimate moment generally were close to each other.
- It was observed that, due to the hydration and pozzolanic reactions as well as the filer effects of high fineness, silica fume cause the improvement of concrete pore structures and increased the strength of concrete. The beam specimens of SCC with SF had the greatest stiffness compared to other all beam specimens.

- The bond strength of the beam specimens produced from SCC was generally higher than that of beam specimens made of NC. This was due to high volume fin grains content comparison with NC covered more effectively the reinforcements. By increasing volume fraction of fine materials the accumulation of bleed water under horizontally embedded bars reduced.

*Castel, Vidal and François (2010)* preformed four different mechanical tests such as splitting test, direct axial tension test, tension member test, and beam test in flexure to examine the possible diversities between bond and cracking properties of SCC, and vibrated concrete (VC). The conclusions are listed below:

- In terms of transfer length, there was no significant difference observed in the bond properties of both types of concrete by conducting tension member test.
- In terms of cracking, the tensile strength measured for both types of concrete was obtained almost identical by performing beam test.
- By using the splitting test, the direct axial tension test and the beam test, there was no significant difference emerged in both SCC and VC tensile strength.
- In terms of effect of the concrete skin on cracking, the comparison between the specimens mad of both SCC and VC concrete when either the concrete skin was removed or not, indicated that there was no diversity observed in the cracking load of SCC and VC specimen when the concrete cover was cast off. Therefore it was concluded that the quality of SCC skin influenced the cracking loads. SCC requires greater attention on curing condition at early age than VC in order to maintain identical cracking properties.

*Desnerk, De Schutter, Taerwe (2010)* conducted pullout tests to examine the bond strength of reinforcing bars exposed to bending. According to RILEM recommendations RC6, a total of 36 specimens were cast using 3 different concrete types including conventional vibrated concrete (CVC) and SCC. In this study, effect of bond length, concrete type and bars size on the bond behavior were investigated. The following conclusions were attained based on the results:

- For SCC specimens with the bond length of 10 times the bar diameter failed by yielding or rupture of the reinforcing bars prior to bond splitting for the concrete compressive strengths studied here (60 MPa and higher). Therefore, according to the test results, the bond length was restricted to 5 times of the bar diameter.
- When larger bar diameters were embedded in the tested specimens, the bond strengths of both SCC and CVC reached high values. But for smaller reinforcing bars, the bond strength of SCC was somewhat higher.
- Existence of the limestone filler content in SCC mixes caused higher compressive strength resulted to the greater bond strength of SCC than that of CVC; though, both concrete mixes had equal water to cement ration.
- By increasing bar diameters, the slip related to the maximum bond strength increased.

*Mazaheripour, Baros, Sena-Cruz, Pepe and Martinelli (2013)* performed experimental study to investigate the effect of bar diameter, surface configuration, thickness of concrete cover and bar embedment length on the bond behavior of Glass-Fiber Reinforced Polymers (GFRPs) in self-compacting steel fiber reinforced concrete (SFRSCC). The conclusions drawn based on experiments results indicated that unbonding was the main cause of the failure. For two types of GFRP, bond length of

more than 20 times the bar diameter led to attaining the ultimate tensile strength. Formation of single crack in the alignment of the reinforcing bars had deleterious impact on the bod characteristics of tested beams, for the specimens with 15 mm concrete cover. Since fiber reinforcement mechanism kept micro cracks away, no splitting failure took place. The bond failure generally depended on the shear resistance of GFRP surface layers. As a matter of fact, the concrete cover thickness had an important role on the bond performance of GFRP-SFRSCC, because the maximum pullout force, attained by increasing the bar diameter and the bond length, became limited by the SFRSCC splitting strength, which was in direct proportion to the concrete cover thickness. The post-peak pullout force and the average residual bond stress increased by increasing the concrete cover.

# CHAPTER 3

# EXPERIMENTAL PROGRAM

## 3.1. General

In this study, six full-scale reinforced concrete beam specimens cast with self-compacting concrete (SCC) were prepared for testing. The diameters of longitudinal and transverse steel bars were 22 mm and 8 mm, respectively. In addition, two longitudinal steel bars with 16 mm diameter were used as compression steel. All preparations including reinforcement caging, strain gauges attachment, and construction of experimental formwork were done in Structural Mechanics Laboratory; only SCC was supplied by a ready mix concrete firm.

## 3.2. Material

### *Concrete*

Self-compacting concrete was produced in the ready mix company and transferred by transmixer to the laboratory, Figure 3.2. The target strength of concrete was 50 MPa. The mix design of the SCC is given in Table 3.1. Due to improper use of viscosity modifying agent, bleeding was observed on the top about 50 mm concrete surfaces and on standard cylinder surfaces, Figure 3.1.

**Table 3.1** Concrete mix design

| **Constituent Materials** | **Weight ($kg/m^3$)** |
|---|---|
| Cement | 270 |
| Fly Ash | 180 |
| Water | 185 |
| Fine Aggregate (0-4mm) | 1114 |
| Coarse Aggregate (4-11.2 mm) | 551 |
| Super Plasticizer | 6.75 |
| Viscosity Modifying Agent | - |

**Figure 3.1** Bleeding observed during pouring of concrete

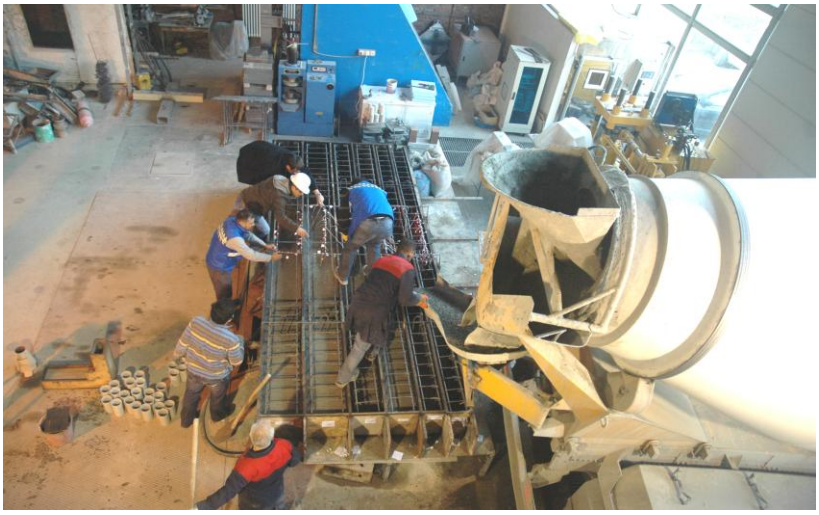

**Figure 3.2** Concrete casting

Concrete of all specimens was molded at the same time from a transmixer and test cylinders were taken arbitrarily during the placement of concrete. Concrete strength was determined by testing these standard cylinders. In this study, 35 cylinders were taken, 4 of them were standard cylinders with 150 mm in diameter and 300 mm in height and the others were standard cylinders with 100 mm in diameter and 200 mm in height.

During the experiment, the compressive and split strength of concrete was determined by testing the cylinders. Table 3.2 presented the date of cylinder tests, corresponding compressive and split strength values, and related experiments. It is not easy to produce normal strength concrete for SCC; therefore, at the beginning of the study, the target compressive strength was chosen as 50 MPa. At the end of 28 days, however, the SCC did not reach this target value. Therefore, experiments started after 141 days at an acceptable strength level.

**Table 3.2.** Concrete strength of specimens

| **Date** | **Age of Concrete (Days)** | $f_c$ **(MPa)** | $f_{ct}$ **(MPa)** | **Experiments Done** |
|---|---|---|---|---|
| 0.1.12.2011 | 4 | 19.91 | N.A. | N.A. |
| 04.12.2011 | 7 | 23.89 | N.A. | N.A. |
| 11.12.2011 | 14 | 25.78 | N.A. | N.A. |
| 18.12.2011 | 21 | 29.68 | N.A. | N.A. |
| 25.12.2011 | 28 | 35.80 | N.A. | N.A. |
| 02.01.2012 | 36 | 36.11 | N.A. | N.A. |
| 14.02.2012 | 79 | 43.88 | N.A. | N.A. |
| 22.03.2012 | 116 | 44 | 3.4 | SC_22_44_88_530<br>SC_22_44_88_800 |
| 05.04.2012 | 130 | 44.5 | 3.9 | SC_44_44_44_710<br>SC_44_44_44_530_T4 |
| 16.04.2012 | 141 | 45.6 | 3.9 | SC_44_22_22_530_T4<br>SC_44_22_22_530_T6 |

***Steel***

Six deformed steel bars were used in each beam specimen with the diameter of 22 mm as tension reinforcements and two 16 mm bars were used as compression reinforcement. All reinforcing bars were taken from the same batch. Turkish classification for bars was S420.

From each full length reinforcements, three test coupons were taken. Lengths of coupons were 600 mm, 400 mm, and 300 mm for bars with diameter of 22, 16 and 8 mm, respectively. These coupons were tested at the Material Laboratory of Civil Engineering Department. In Turkish Standards, minimum requirement of elongation is 12%. As the results showed, all bars elongations were greater than the minimum criteria. Table 3.3 and Table 3.4 show the properties of the reinforcing bars used in the specimens.

**Table 3.3** Geometrical properties of reinforcing bars

| Test Coupon | Weight (gr) | Length (cm) | Diameter (mm) | Area ($mm^2$) |
|---|---|---|---|---|
| ϕ8_1 | 131.7 | 30 | 8.41 | 55.94 |
| ϕ8_2 | 132.4 | 30 | 8.46 | 56.23 |
| ϕ8_3 | 132.0 | 30 | 8.45 | 56.06 |
| ϕ16_1 | 613.5 | 40 | 15.70 | 193.45 |
| ϕ16_2 | 614.4 | 40 | 15.79 | 195.69 |
| ϕ16_3 | 615.9 | 40 | 15.81 | 196.18 |
| ϕ22_1 | 1793.4 | 60 | 22.03 | 380.80 |
| ϕ22_2 | 1790.2 | 60 | 22.01 | 380.13 |
| ϕ22_3 | 1790.0 | 60 | 22.00 | 380.08 |

**Table 3.4** Properties of reinforcing bars

| Bar Size (mm) | Yield Strength (MPa) | Ultimate Strength (MPa) | Elongation (%) |
|---|---|---|---|
| ϕ8 | 595 | 835 | 17.5 |
| ϕ16 | 475 | 741 | 17.3 |
| ϕ22 | 459 | 721 | 17.0 |

### 3.3. Formwork

Formworks were prepared at the Structural Mechanics Laboratory. In order to construct six beams at the same time, six adjacent formworks were assembled by using steel plates and steel profiles. To get smooth surface, 5 mm thick steel plates were used as formwork. Steel plates were cut to get 4 m × 400 mm surface. The depth of the four specimens was 400 mm. For the two of the specimens, 22 mm thick wooden plates were cut and put on the bottom of the formwork to get 378 mm depth. Two steel box sections which had 20 × 20 × 2 mm dimensions and 4 m in length were welded as stiffeners on the side steel plates vertically with 250 mm spacing. Between these vertical stiffeners 430 mm diagonal cross stiffeners were also welded. Another steel plate was welded on the stiffeners and a two side smooth thick plate was produced. Figure 3.3 shows the details of the formwork.

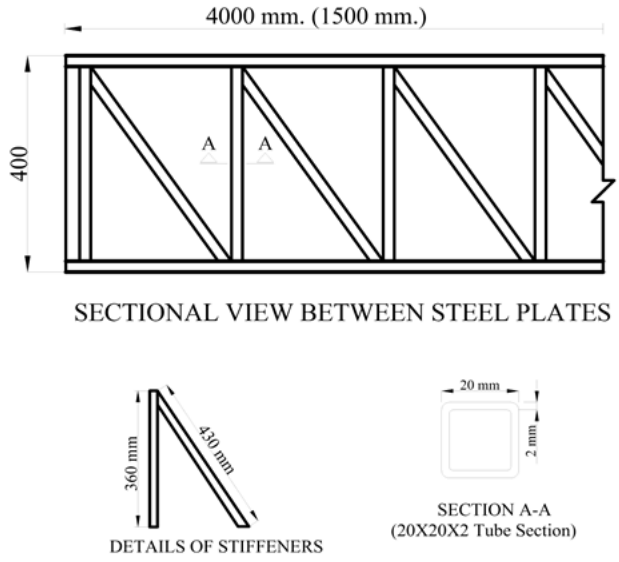


**Figure 3.3** Detail of framework

Steel plate of 1500 mm long and 30 mm thick were also set up to get a total of 5500 mm long formwork. The box steel sections provided the required stiffness to the formworks against out of plane bending.

The side parts of formwork were set on a smooth steel table according to their predefine beam widths and heights. The surface of table was also produced with 5 mm thick steel plates. The ends of formwork were closed with similar steel plates. The steel plates were precisely assembled using water level and 90° angles to form perfectly straight and orthogonal formwork. Finished view of formwork is shown in Figure 3.4. The formwork with steel caging inside is shown in Figure 3.5.

**Figure 3.4** Finished view of formwork

**Figure 3.5** Formwork with reinforcement cage

### 3.4. Test methods for SCC

During concreting, some tests were conducted on the fresh SCC to evaluate its flowability, viscosity and passing ratio. These test methods are slump flow and $T_{500}$ time, V-funnel test, and L-box test. The results of these tests are presented in Table 3.5. The principles of all these three tests are described below:

#### *Slump flow and $T_{500}$ time*

This test determines the flowability and the flow rate of self-compacting concrete in the absence of obstructions. The $T_{500}$ time is also a measure of the speed of flow and viscosity of the SCC. This test is based on the slump flow test described in EN 12350-2. The result of this test indicates the filling ability of SCC. For performing this test, the fresh concrete is poured into a cone, Figure 3.6 and Figure 3.7. When the cone is withdrawn upward, the time from beginning upward movement of the cone to when the concrete has flowed to a diameter of 500 mm is measured and defined as $T_{500}$ time, Figure 3.8. For the slump flow determination, the mean value of the measured diameters of the flow spread is used, Figure 3.9.

**Figure 3.6** Base plate with the cone

**Figure 3.7** Slump and T500 test method for fresh SCC

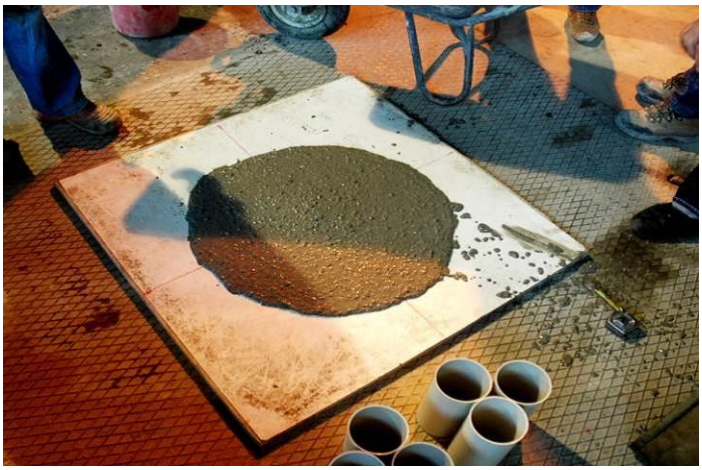

**Figure 3.8** $T_{500}$ test method

**Figure 3.9** Slump flow test method

***V-funnel test***

This test is used to determine the viscosity and filling ability of SCC. The test is carried out by filling the V shaped funnel with fresh concrete and the measured time taken for the concrete to flow out of the apparatus is recorded as the V-funnel flow time, Figure 3.10.

**Figure 3.10** V-funnel test method

***L-Box test***

The passing ability of SCC to follow through tight openings including spaces between reinforcing bars and other obstructions without segregation or blocking is evaluated by the L-Box test. The basic result of the L-Box test is the passing ability, calculated by the ratio of the height of the concrete surface remaining at the far end of the trough, after its passage through the reinforcing bars to the concrete height remaining within the vertical column of the apparatus, Figure 3.11.

**Figure 3.11** L-Box test method

Table 3.5 shows the results of the fresh SSC tests mentioned above. The mean diameter of the spread was measured as 760 mm which can be defined as a high value. Therefore, slump-flow can be classified as SF3 which indicates that this concrete can fill the form even for very congested structures or structure with very complex shapes. However, in this slump-flow class segregation resistance is more

difficult to control. The time to reach the 500 mm diameter was less than 2 seconds and therefore concrete was classified as VS1 for the $T_{500}$ test. Although, this class of concrete is capable of self-leveling and generally has the best surface finish, the probability for bleeding and segregation is very high. The flow out time in the V-Funnel test was very high (21 seconds) and classified as VF2.

**Table 3.5** Result for fresh SCC

| Test | Measurement of | Result | Class |
|---|---|---|---|
| Slump flow | Mean diameter of spread | 760 mm | SF3 |
| $T_{500}$ | Time to reach 500 mm circle | 1.5 sec. | VS1 |
| V-Funnel | Flow out time | 21.0 sec. | VF2 |
| L-Box | Concrete height at end/gate | 0.90 | PA2 |

### 3.5. Stress Calculation

For stress predictions, the steel stresses were calculated by using ACI 408 recommendation and calculated values were compared with those obtained experimentally. The theoretical steel stresses were calculated by the descriptive equations proposed by ACI Committee 408 for normal concrete. This equation is also used for the preliminary design of the specimens. The SI version of the equations is provided below for steel stress $f_s$:

$$f_s = \left[1.43\ell_s\left(c_{\min} + 0.5d_b\right) + 57.4A_b\right]\left(0.1\frac{c_{\max}}{c_{\min}} + 0.9\right)\frac{\left(f_c'\right)^{1/4}}{A_b}$$

$$+ (8.90t_r t_d\frac{NA_{tr}}{n} + 558)\frac{f_c'^{3/4}}{A_b} \quad \leq \quad f_y$$

### 3.6. Details of beam specimens

Length of all specimens was 5200 mm. The depths of the specimens were 400 mm and 378 mm. Face and side covers varied between 1 and 2 bar diameter, $d_b$. Spacing between bars changed between $2d_b$ and $4d_b$, Figure 3.12. Three different lap splice lengths were tested in the study ($24d_b$, $32d_b$, and $36d_b$). The length of the specimens was 5.2 m. The shear span, $a/d$ ratio was about 4 for all specimens. In this ratio, $a$ is the distance between the point load and support which was 1.4 m for all tests, and $d$ is the effective depth of the specimen that was 345 mm. All specimens contain three bottom-cast spliced bars. Along the shear span, 8 mm closed stirrups were used at every 150 mm in order to prevent shear failure. Three specimens contained transverse reinforcement along the splice length in order to observe the effect of confinement on bond behavior. Dimensions of beams and their shear spans $a/d$ ratios are given in Table 3.6. The details of the specimens are given through Figures 3.13 and 3.18. The width and height of the specimens were determined according to the cover dimensions and therefore these numbers are not rounded figures.

In the naming of specimens, SC_a_b_c_d type of coding was used. First two letters "SC" refers to self-compacting concrete, *a, b, c* and *d* letters stand for face cover,

side cover, net spacing between bars, and splice length respectively. Three specimens have either "T4" or "T6" at the end of designation that denotes presence of transverse reinforcement at the splice region. The number shows the quantity of transverse reinforcement. Specimen details are given in Table 3.6.

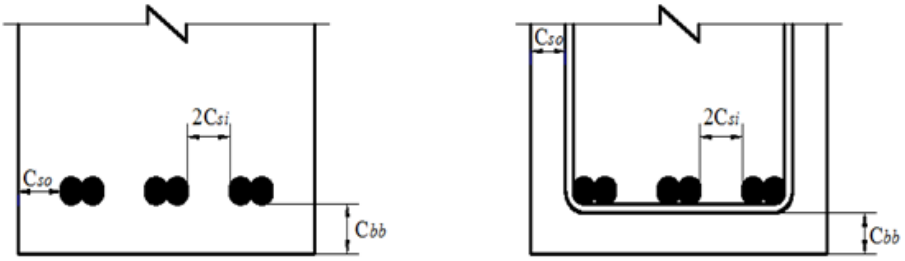


**Figure 3.12** Side cover, bottom cover and free spacing between lap spliced bars

**Table 3.6** Dimensions of Specimens

| Specimen | Dimensions (mm) ($b \times h \times l$) | Face Cover (mm) | Side Cover (mm) | Spacing Between bars (mm) | Splice Length (mm) |
|---|---|---|---|---|---|
| SC_22_44_88_530 | 396×378×5200 | 22 | 44 | 88 | $530/24d_b$ |
| SC_22_44_88_800 | 396×378×5200 | 22 | 44 | 88 | $800/36d_b$ |
| SC_44_44_44_710 | 308×400×5200 | 44 | 44 | 44 | $710/32d_b$ |
| SC_44_44_44_530_T4 | 308×400×5200 | 44 | 44 | 44 | $530/24d_b$ |
| SC_44_22_22_530_T4 | 220×400×5200 | 44 | 22 | 22 | $530/24d_b$ |
| SC_44_22_22_530_T6 | 220×400×5200 | 44 | 22 | 22 | $530/24d_b$ |

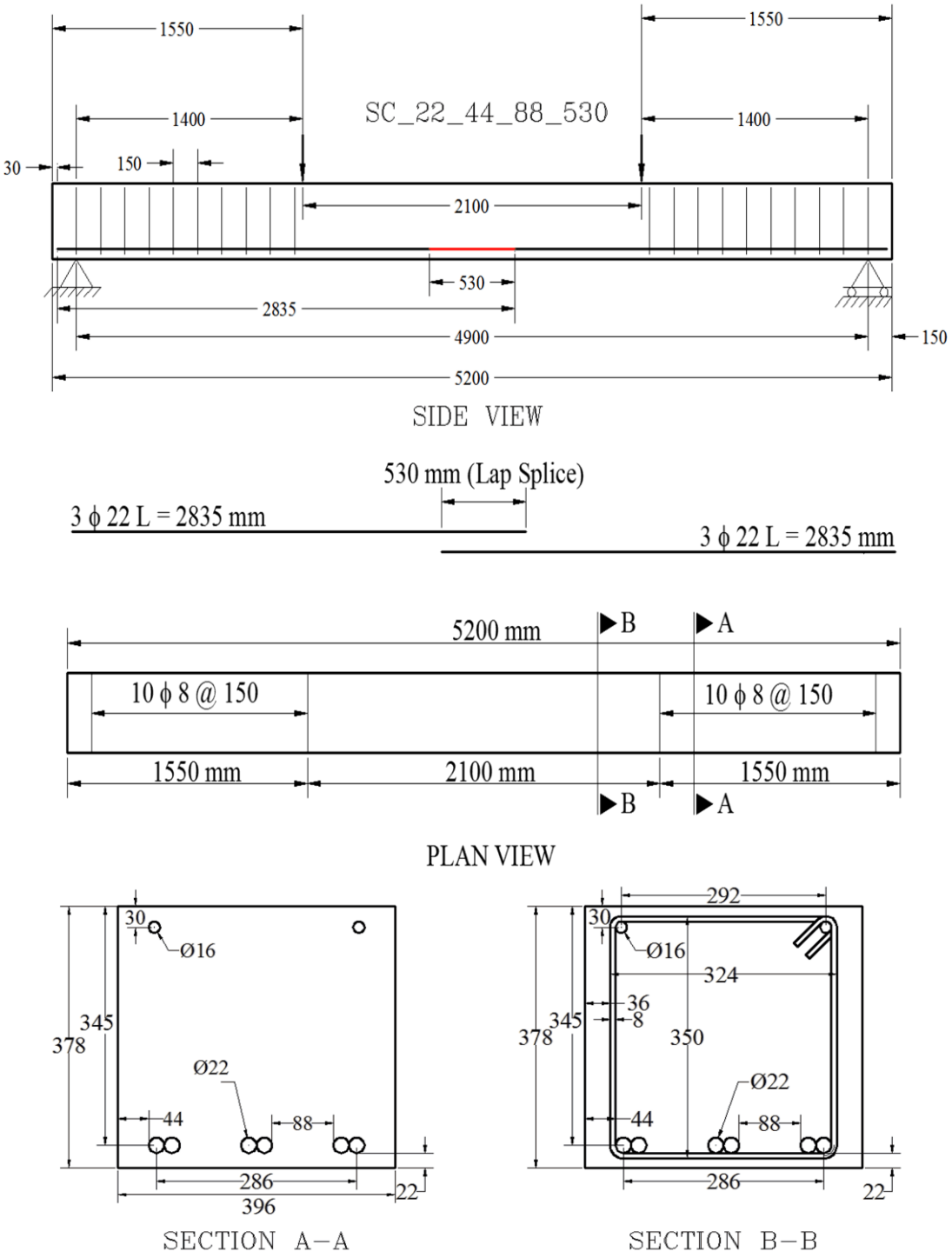


**Figure 3.13** Details of specimen SC_22_44_88_530

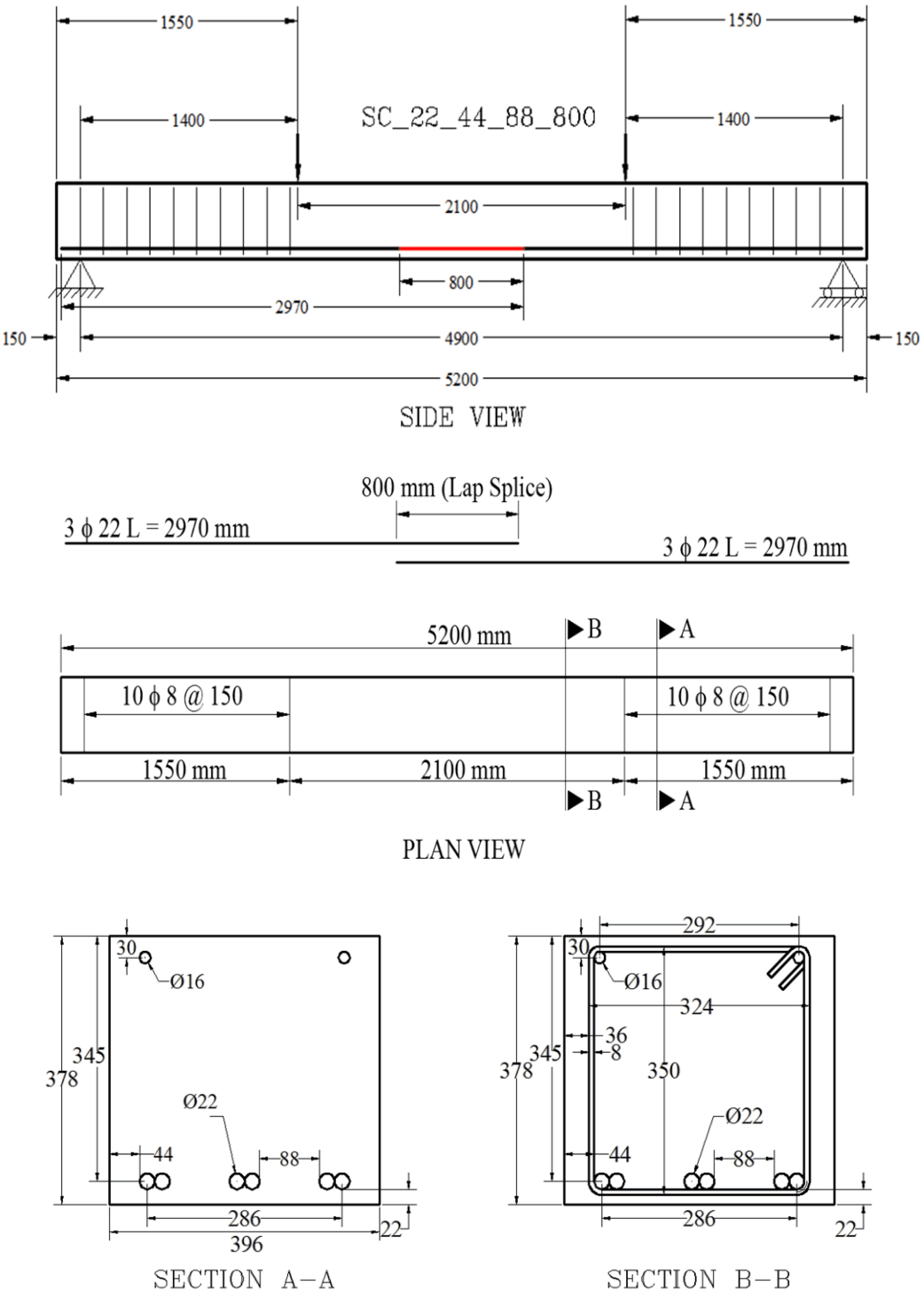


**Figure 3.14** Details of specimen SC_22_44_88_800

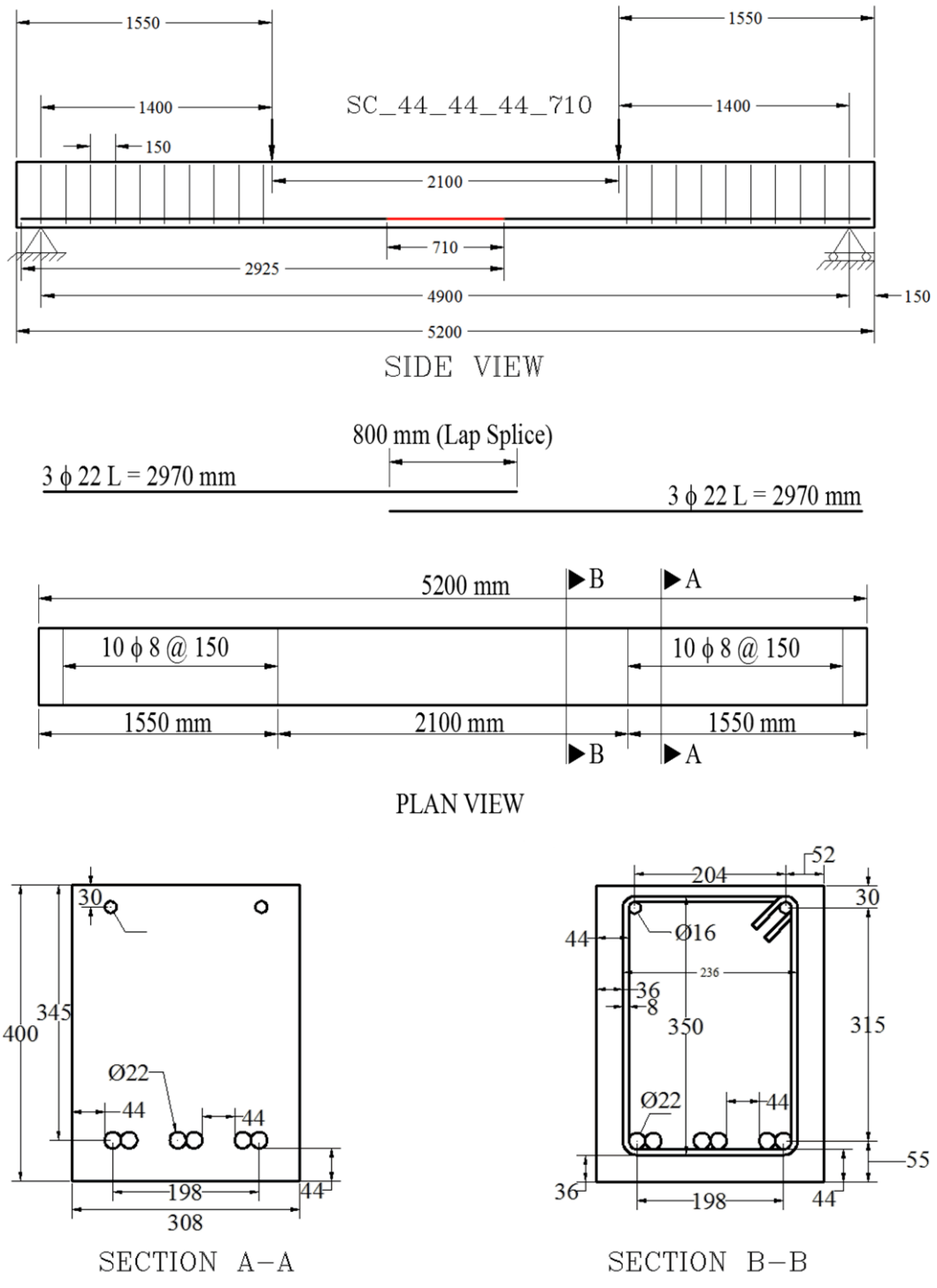


**Figure 3.15** Details of specimen SC_44_44_44_710

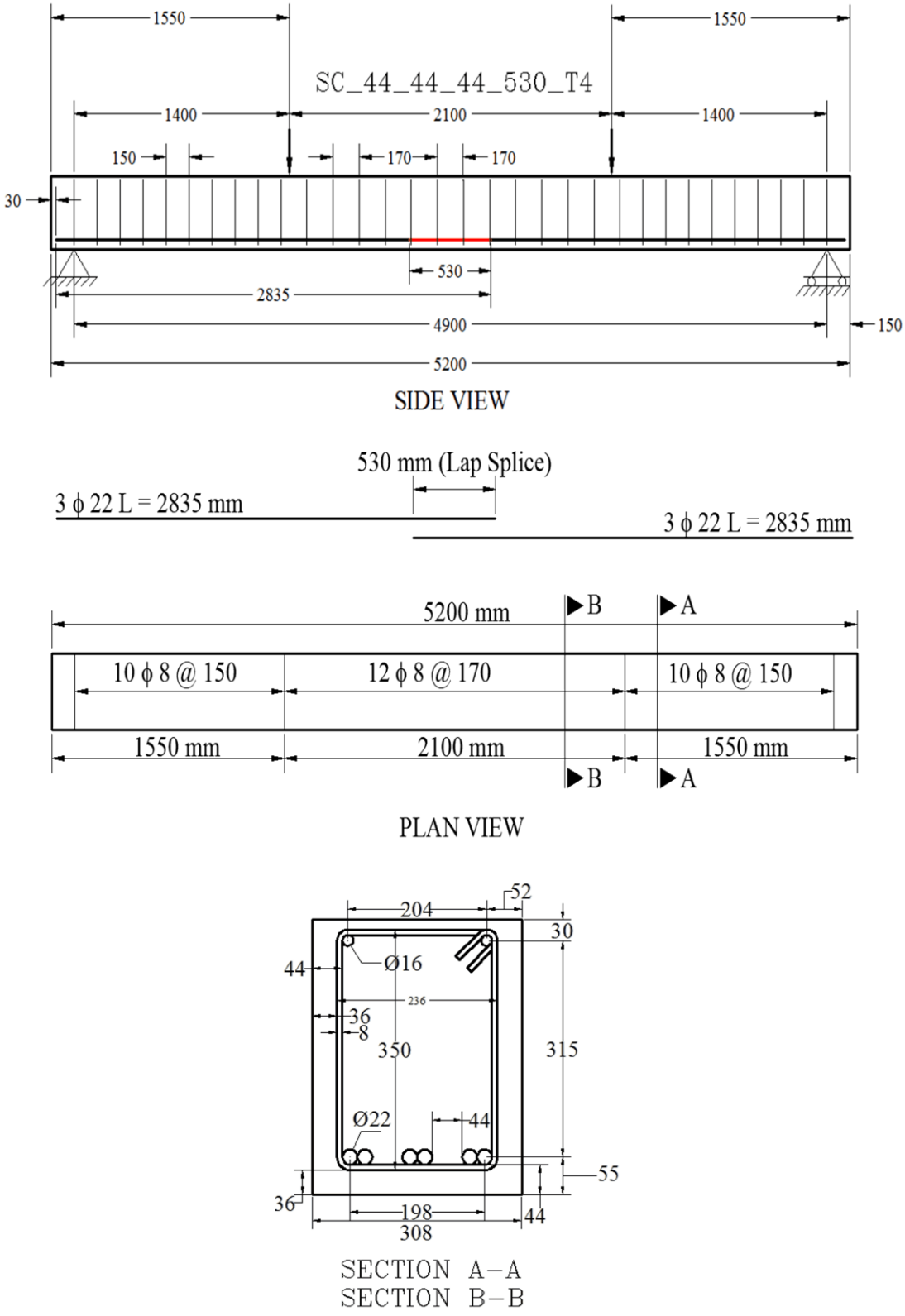


**Figure 3.16** Details of specimen SC_44_44_44_530_T4

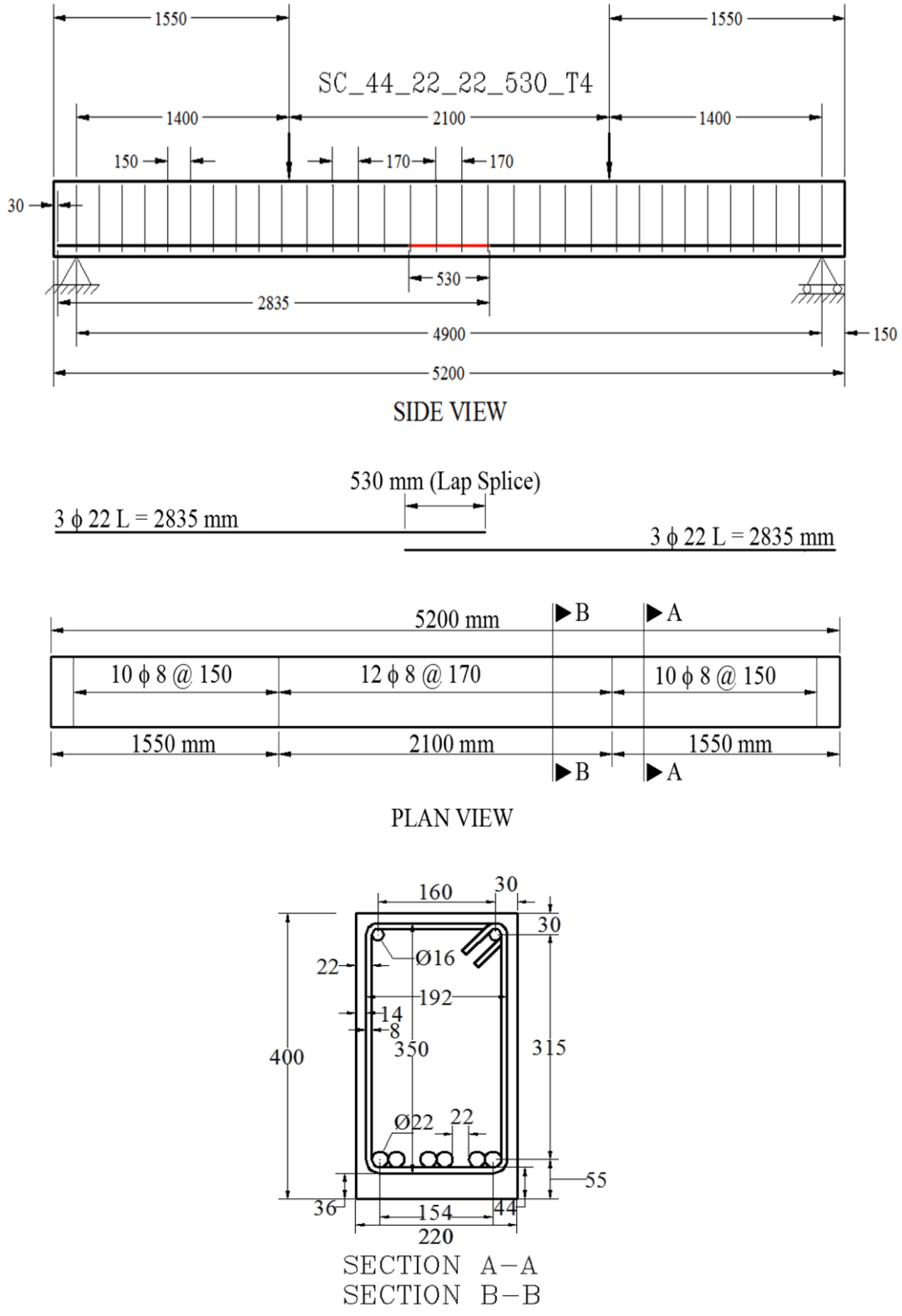


**Figure 3.17** Details of specimen SC_44_22_22_530_T4

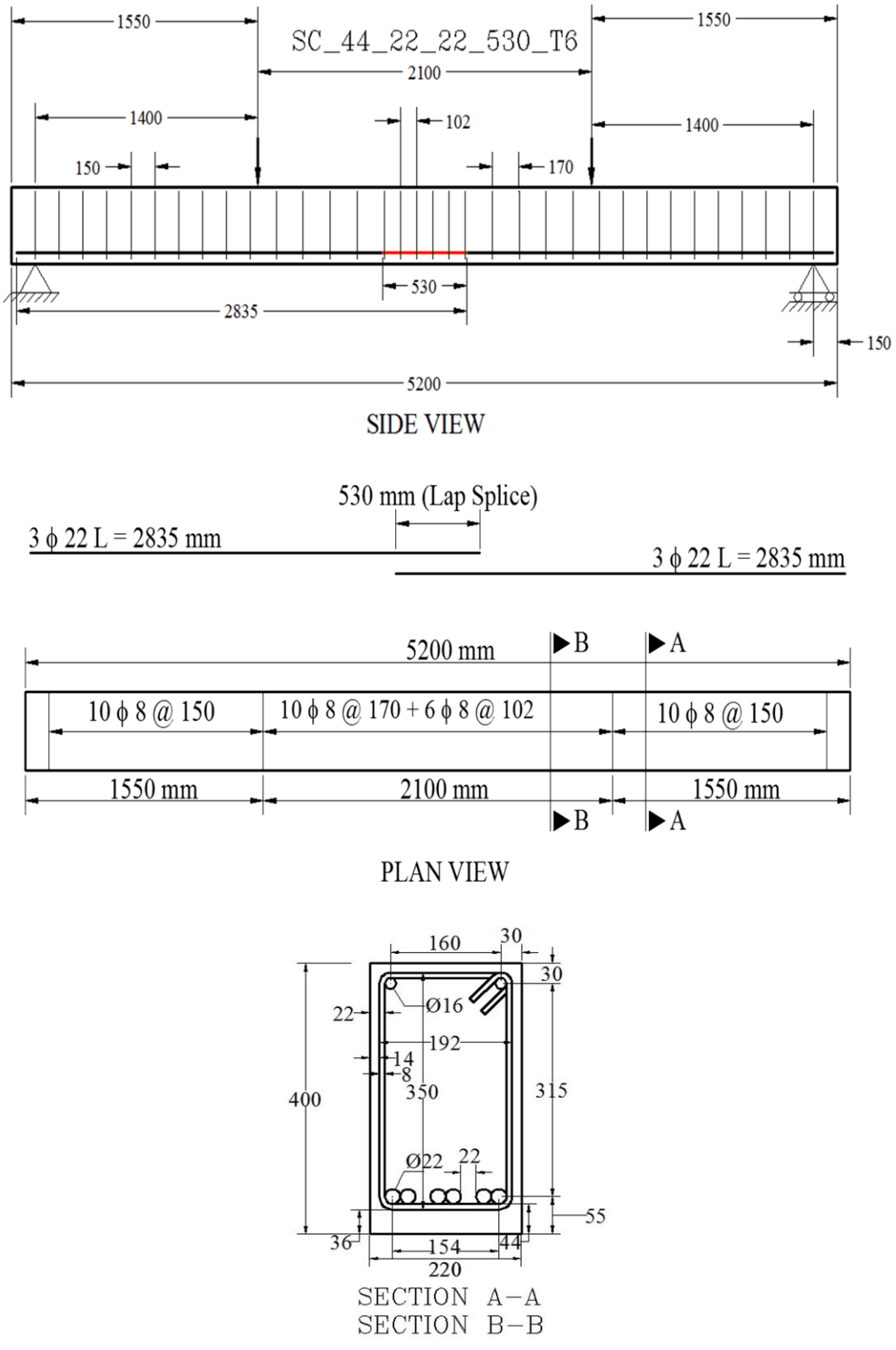


**Figure 3.18** Details of specimen SC_44_22_22_530_T6

## 3.7. Test set up and loading

Two concrete blocks were used as the abutment for the beam specimens and located inside the loading frame 1050 mm away from the midpoint, and totally for all specimens they were set 2100 mm apart from each other. These blocks were fixed on the strong floor by plaster. Specimens were put inverted on a square and on a circler steel bars to get simple and roller support action, Figure 3.19. The main reason of upside down testing of specimens was to take lap-splice region on the top and so, to better observe and mark cracks on the lap splice region.

A 20 ton-force capacity load cell was located to the bottom of the ram. A hinge at the top and a roller at the bottom were provided to the ram-load cell couple in order to ensure a rotationally free/moment free system

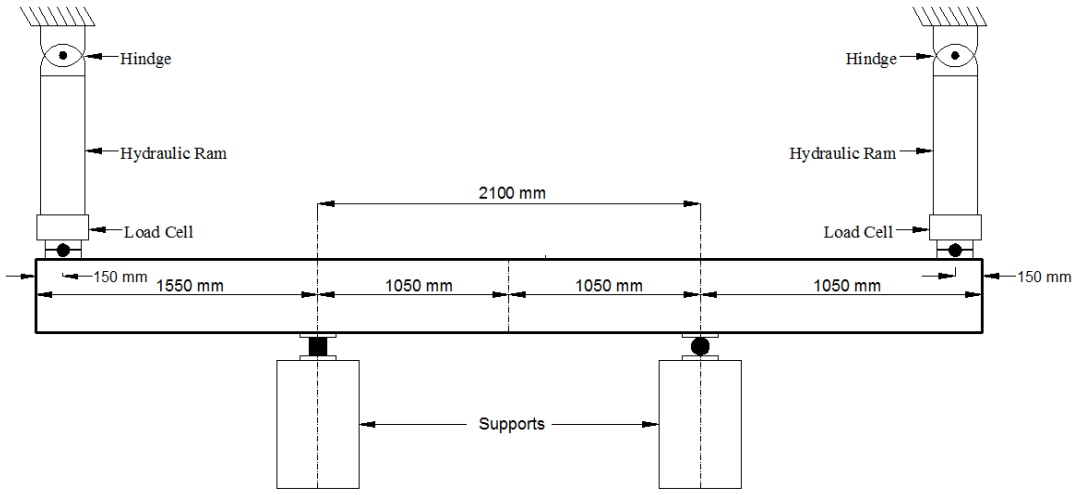


**Figure 3.19** Test set up for all beam specimens

## 3.8. Instrumentation

Displacements and deformations measurement of critical regions along the beams are necessary during the tests. Linear Variable Differential Transformers (LVDTs) and dial gages were used for displacement measurements. The strain of longitudinal and transverse reinforcements was measured using strain gages. Load cells were utilized for load measurement.

Data was recorded by a data acquisition system The data was stored as engineering units like strains, displacements and loads by means of a software. Load - displacement curve of the specimens were monitored during testing.

### *Displacement Measurement*

Vertical tip displacements were monitored at the both ends of beams, 300 mm away from the loading points. At these points two strain gage based LVDTs were located. Heavy concrete blocks with steel rods were used to fix the LVDTs to the strong floor.

The vertical mid-span deflection is one of the most important measurements of the test. Therefore, the mid-span displacement was monitored for all specimens by two LVDTs. The mean values of data collected by these two LVDTs recorded as the vertical mid-span deflection.

Support displacement was also monitored in order to examine the vertical rigid body support displacement. There was a little vertical displacement recorded at the supports, although it had to be zero. Two LDVTs were located at left and right the supports.

***Moment Curvature***

Ductility of reinforced concrete is related to the sectional property of the member. It illustrates member resistance to brittle failure when reinforce concrete member is exerted to flexural loading. Ductility is interpreted as the capability of a structural member undergoing deformation without any significant reduction in the flexural capacity of the member. Totally four LVDTs were used to collect related data to calculate displacement ductility. Displacement ductility specifically determines the type of failure. This value was obtained by dividing the ultimate mid-deflection to the corresponding yield displacement. For this purpose, on the top and bottom surfaces of the specimens two LVDTs were installed horizontally. All horizontal LVDT's were located 200 mm away from the mid-point. Therefore, curvature values are not sectional properties but average numbers over 400 mm in this study.

Locations of LVDTs are presented in Figure 3.20. As shown in the figure, totally ten LVDTs were used during the test to record tip, mid, and support displacement.

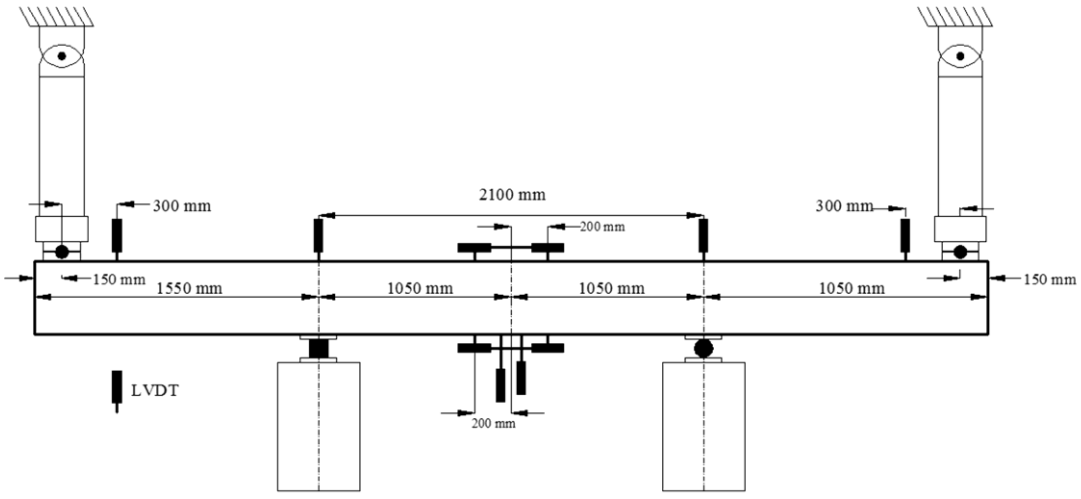


**Figure 3.20** Schematic view of instrumentation

***Load measurements***

Specimens were loaded at the ends of the specimens by means of hydraulic rams. As it was mentioned before, two concrete blocks were used as supports to create a constant moment region and all the longitudinal bars were spliced in this region. Load cells were located between the hydraulic rams and the surface of specimen. Both load cells had compressive and tensile capacity of 200 kN. Figure 3.21 shows the installed load cells:


**Figure 3.21** Load cell used in test

***Strain measurements***

Kyowa strain gauges with 120Ω resistance were used in both longitudinal and transverse bars to monitor strains. Figure 3.22 shows locations of strain gauges.

Bond stress is maximum at the continuous end of the lap splice and decreases towards the free end of the lap splice. Theoretically, it gets zero at the free end

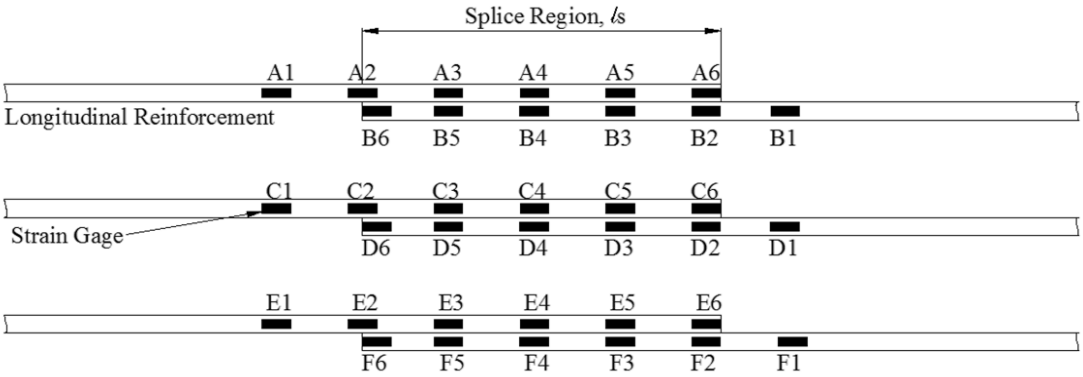


**Figure 3.22** Locations of strain gauges on the longitudinal reinforcements

For the specimens with the transverse reinforcement, totally nine strain gauges were used, and for each stirrup three strain gages were set up. Location of these gauges on the stirrups were presented in figure 3.23.

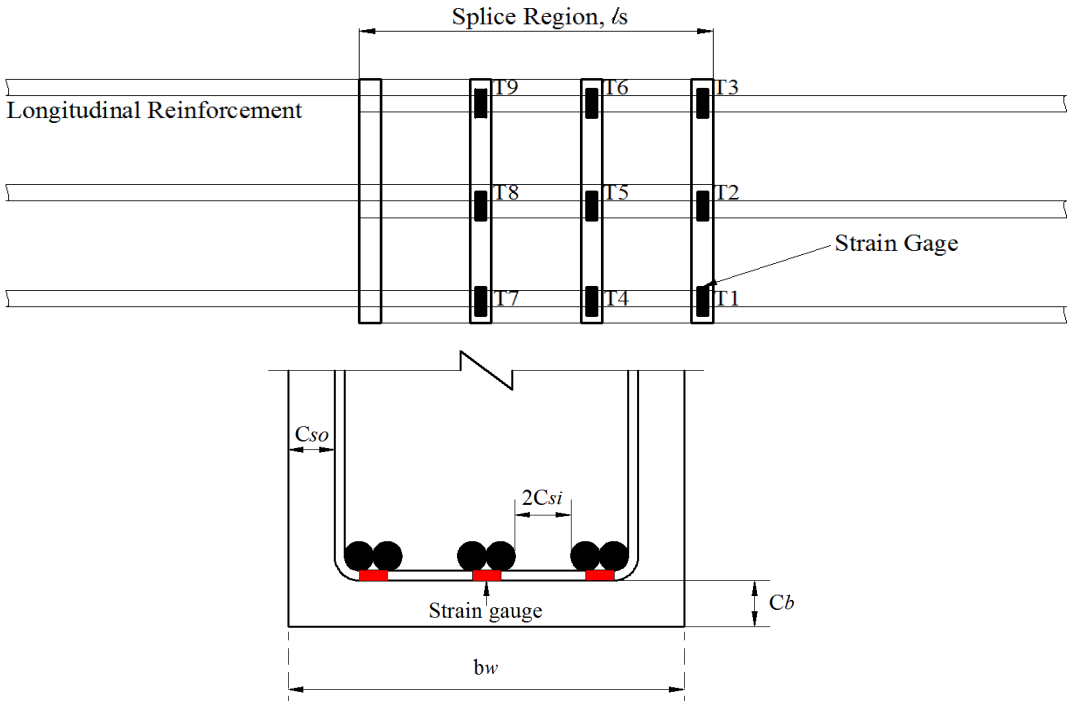


**Figure 3.23** Locations of strain gauges on the transverse reinforcements

# CHAPTER 4

# OBSERVED BEHAVIOR OF TEST SPECIMENS

## 4.1. General

In this chapter, observed behavior of the beam specimens will be presented. Using LVDTs and strain gages, displacement and strain measurements were acquired during testing. They are demonstrated in a graphical manner as Load vs. Displacement and Load vs. Strain curves.

Table 4.1 summarizes the test results. In this table, cracking load $P_{cr}$, ultimate load $P_{ult}$, and type of failure is included along with compressive $f_c$, and splitting tensile strength of concrete $f_{cts}$.

**Table 4.1** Test results

| | $f_c$ (MPa) | $f_{cts}$ (MPa) | $P_{cr}$ (kN) | $P_{ult}$ (kN) | Failure Type |
|---|---|---|---|---|---|
| SC_22_44_88_530 | 44.0 | 3.4 | 37.4 | 107.2 | Bond |
| SC_22_44_88_800 | 44.0 | 3.4 | 34.8 | 131.3 | Flexural |
| SC_44_44_44_710 | 44.5 | 3.7 | 30.8 | 125.2 | Yield+Bond |
| SC_44_44_44_530_T4 | 44.5 | 3.7 | 30.4 | 109.8 | Bond |
| SC_44_22_22_530_T4 | 45.6 | 3.9 | 21.3 | 98.3 | Bond |
| SC_44_22_22_530_T6 | 45.6 | 3.9 | 22.6 | 95.3 | Bond |

## 4.2. Information of Graphs

For all specimens, 3 types of graphs including displacement, strain measurements and moment curvatures, were drawn with respect to the acquired data during the tests. All graphs are detailed below one by one with demonstrative figures.

### 4.2.1. Deflection and Support Settlement

Displacement vs. Load figures include tip, mid-span and supports deflections. The instrumentation is illustrated in Figure 4.1.

The values of the left and right load cells are nearly close to each other as expected. The sum of these two readings is used in the load axis of all graphs.

The values of recorded data by channels No. 5 and No. 8 were presented as left and right tip deflection. The curves of the left and right tip deflections versus load were drawn separately. Mean value of the channels No. 3 and No. 4 presents middle deflection. Channels No. 6 and No. 7 were used to get the support displacement. Channels No. 9 and No. 10 on the top surface of the specimens and channels No. 11 and No. 12 on the bottom surface of the specimens were used to calculate the left and right curvatures of the specimens for the analytical part of this thesis.

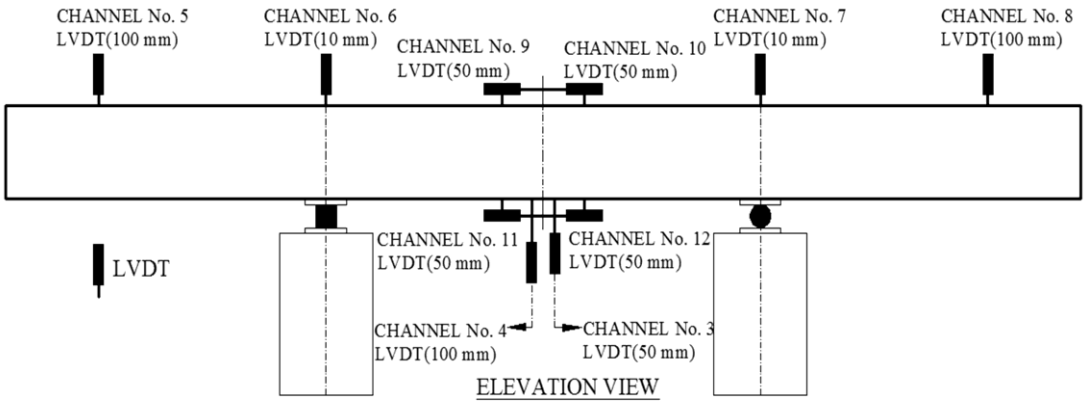


**Figure 4.1** Schematic view of measuring instruments set up

### 4.2.2. Strain Graphs

Strain graphs versus applied load for both longitudinal and transverse reinforcements were plotted for all specimens. As it is illustrated in Figure 4.2, for each longitudinal reinforcing bar there were totally six strain gauges which totally makes 36 strain gauges. Five of them were located along the splice region. These strain gauges were sorted from free end of the lap splice region. For strain gauges located at the free end of the reinforcing bars, A6, B6, C6, D6, E6, F6, the expected values of strain measurements are in vicinity of zero. The maximum values of strain are expected for the point at the continuous end of lap splices. Other strain gauges will demonstrate the strain distribution along the splice.

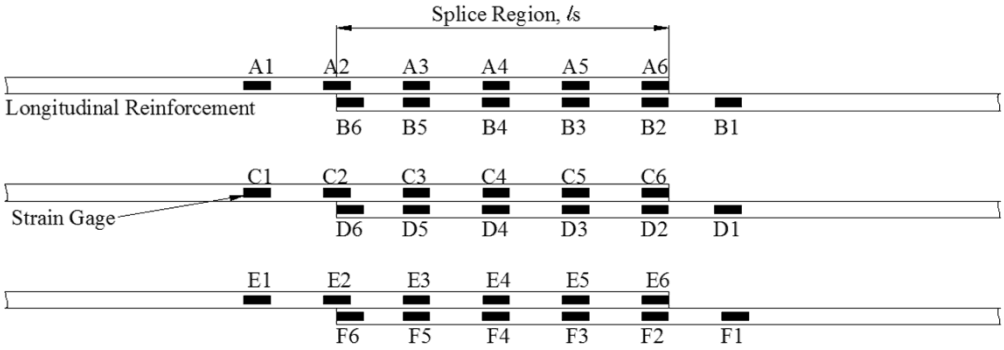


**Figure 4.2** Strain gauges instrumentation for longitudinal reinforcing bars

For three of the beam specimen, stirrups were used to investigate the effect of their presence on the bond strength and type of failure. For each specimen with the transverse reinforcement within the splice region, three stirrups were selected; namely, end, intermediate, and middle ones, and on each of them three strain gauges were attached. With this strain measurement, it is aimed to determine the effectiveness of the stirrups based on their location. For each tests with the transverse reinforcement within the splice region, the locations of the strain gages are given in Figure 4.3.

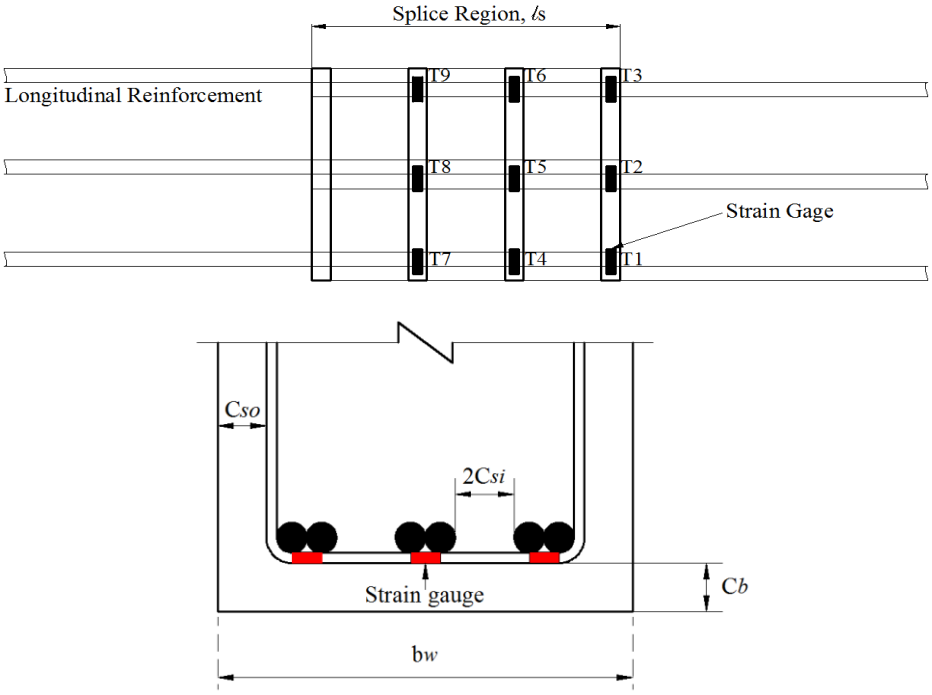


**Figure 4.3** Strain gauges instrumentation for transverse reinforcement

## 4.3. Observed Behavior of Specimens

In this section, gathered data is presented in a graphical manner as deflections, and strain gauge measurements. Also crack pattern and the observed behavior of specimens during test is discussed.

For all specimens, the load at which the first crack initiated was calculated. The first crack initiated always at the end of the lap splices. The discontinuity at the free end of lap splices resulted in cracks.

### 4.3.1. Specimen SC_22_44_88_530

Specimen SC_22_44_88_530 had only one bar diameter, $1d_b$, face cover, whereas side cover and half the spacing between bars were $2d_b$. Also, splice length ($24d_b$) was calculated as inadequate for yielding. The bar stress according to ACI 408 equation was calculated as 349 MPa. Note that, the yield strength was 459 MPa. Therefore, specimen SC_22_44_88_530 failed due to face splitting prior reaching to its flexural capacity. The calculated yield load for this was 117.9 kN. However, this specimen failed at 107.18 kN due to bond face splitting before flexural failure. Bond failure was brittle and occurred abruptly. Tip, mid deflections and support displacement of the specimen as well as strains are illustrated in Figures 4.4, 4.5, and 4.6, respectively. In this specimen, strain gauges were attached only on the mid longitudinal spliced bars. Therefore, only C and D strain gauges were presented for this specimen. Missing strain gauges mean that this data could not be gathered because of some technical difficulties.

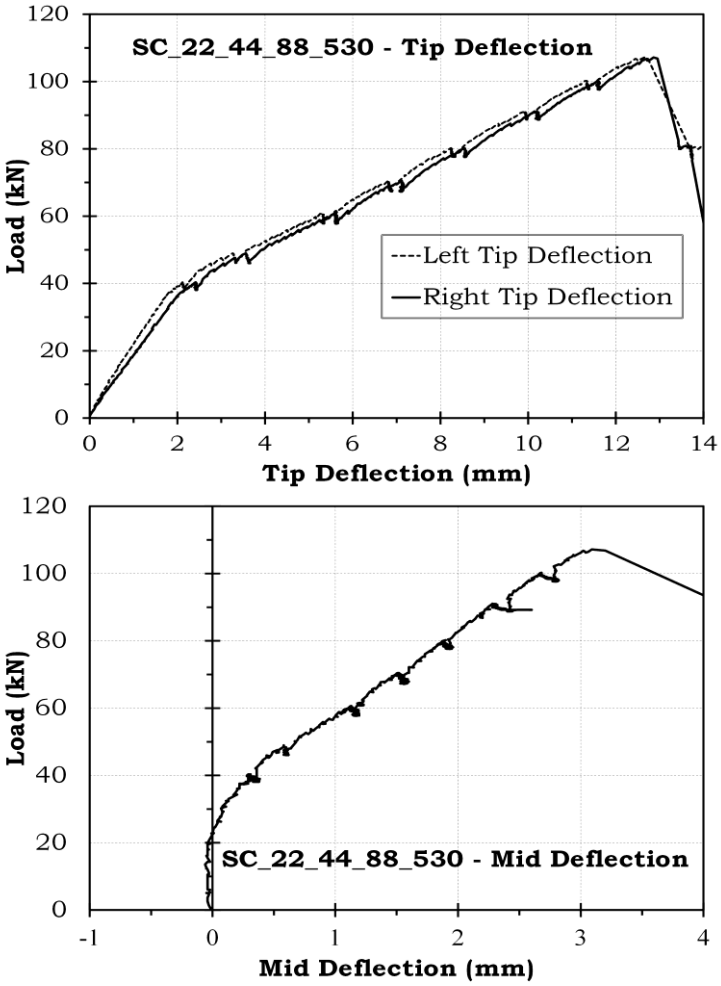


**Figure 4.4** Load versus Deflection Charts

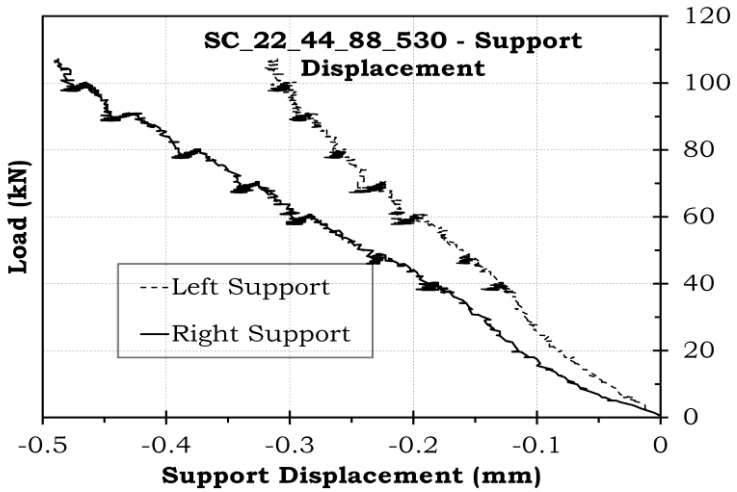


**Figure 4.5** Load versus Support Displacement

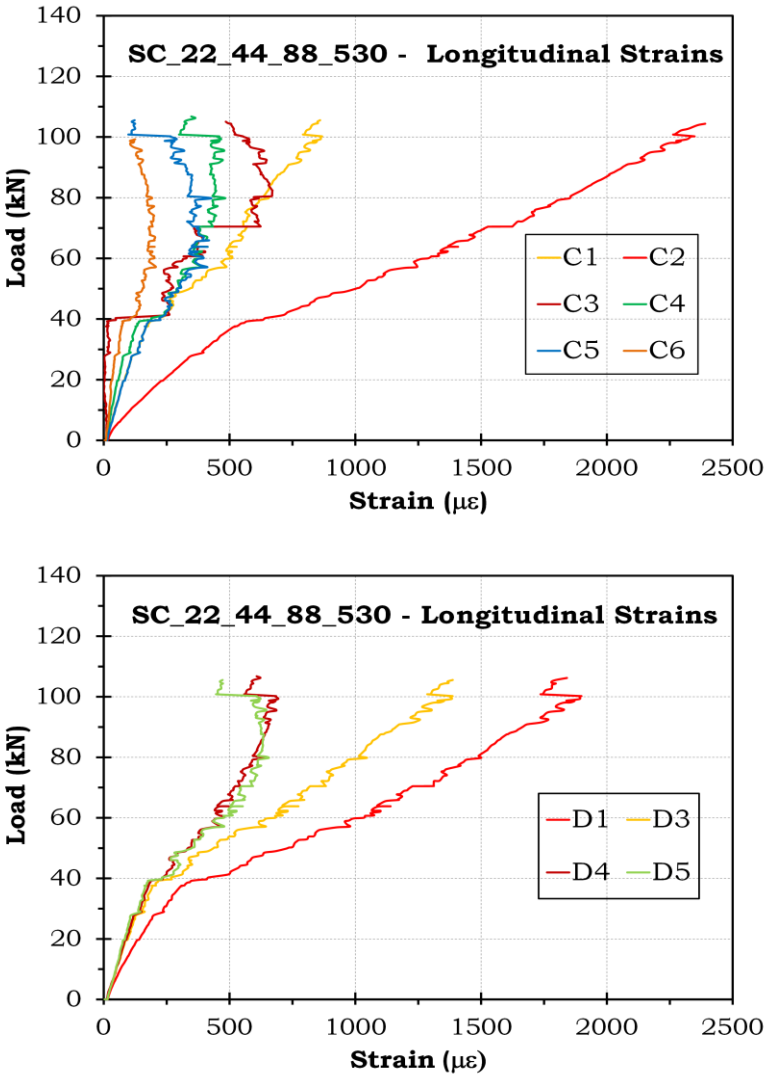


**Figure 4.6** Load versus Longitudinal Strain Charts

As can be seen from the figures, the first crack initiated at 37.4 kN. Support displacements are very low as expected. The overlap of the left and right tip deflections indicates that the load was applied symmetrically. Since the distance between the two supports is 2.1 m, the deflection in the span is low as estimated. The total deflection can be calculated by adding both the tip and mid deflections.

According to Figure 4.6, first cracking occurred in "C" strain gauges at 500 με and in the counterpart "D" strain gauges at 400 με. The average cracking strain can be taken as 400 με.

The cracks that formed at the ultimate stage on the face cover are shown in Figure 4.7. Eventually, face splitting failure was observed on the bottom cover with one distinct flexural crack.

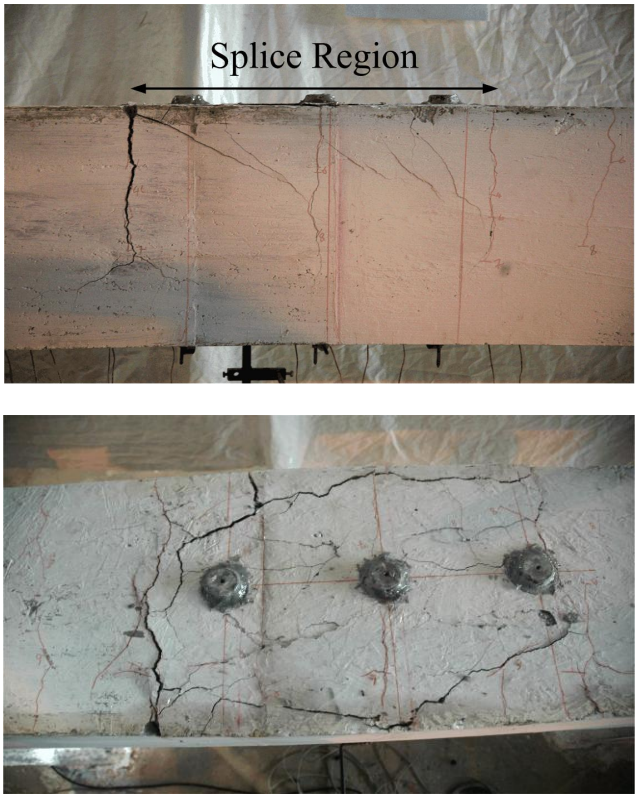


**Figure 4.7** Cracks formation on the side and bottom cover within the splice region

### 4.3.2. Specimen SC_22_44_88_800

Specimen SC_22_44_88_800 had only one bar diameter, $1d_b$, face cover whereas side cover and half the spacing between bars were $2d_b$. The bar stress for $36d_b$ splice length was calculated as 444 MPa according to ACI 408 equation which was 3% off from the yield strength of 459 MPa. Specimen SC_22_44_88_800 failed by reaching its flexural capacity. Therefore, no splitting failure was observed. The increased splice length provided the required bond stress for yielding of the bars. The first crack initiated at 34.8 kN. Specimen yielded at 112.9 kN, while some longitudinal cracks were forming and propagating on the bottom and side cover of the specimen. The theoretical yield value was calculated as 117.9 kN. The tip-, and mid deflections, support displacements and the strains are illustrated in Figures 4.8-4.10.

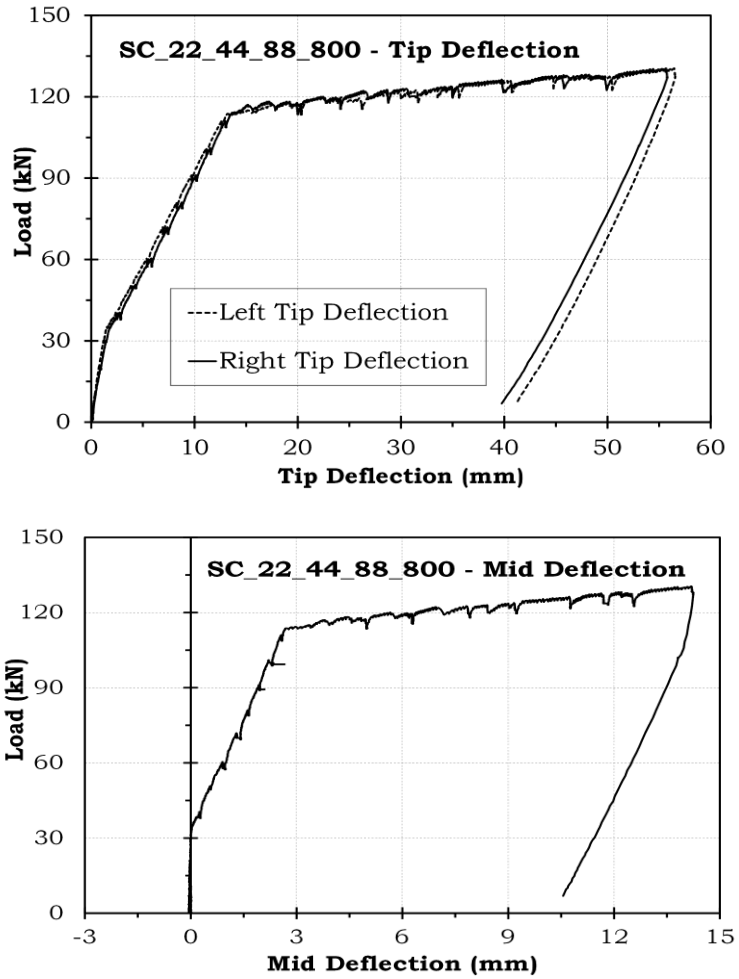


**Figure 4.8** Load versus Deflection Charts

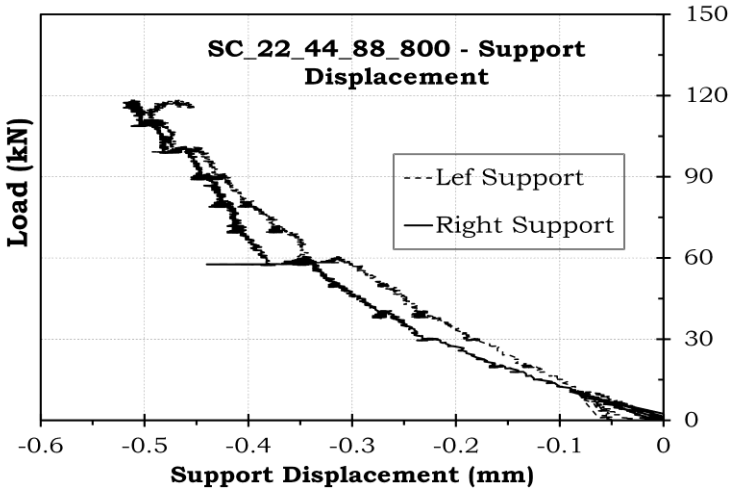


**Figure 4.9** Load versus Support Displacement

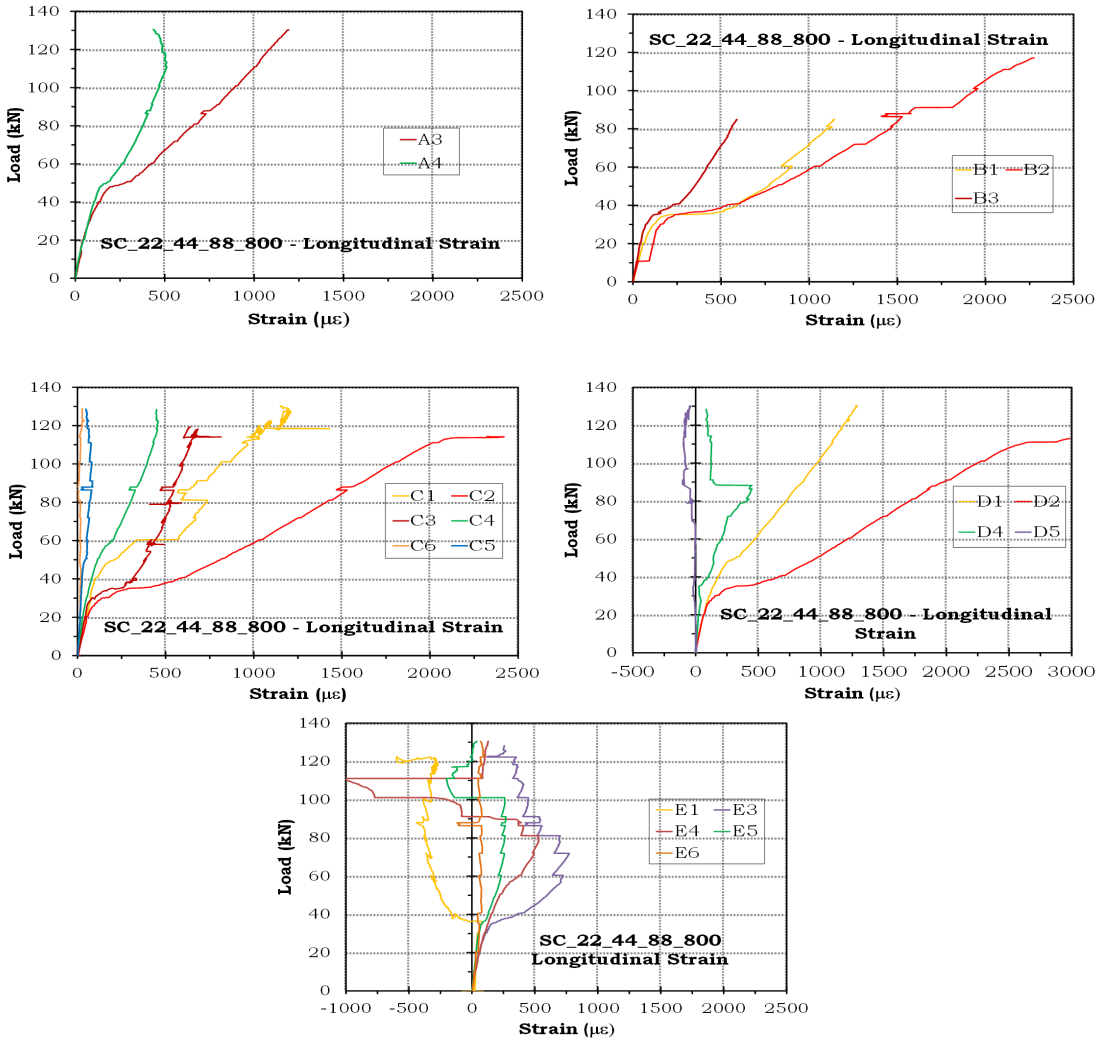


**Figure 4.10** Load versus Longitudinal Strain

Support displacements were measured very low as expected. The overlap of the left and right tip deflections indicates that the load was applied symmetrically. Since the distance between the two supports is 2.1 m, the deflection in the span was almost zero until cracking and remained low until yielding. After yielding of the longitudinal bars, deflections increased rapidly. The total deflection can be calculated by adding both the tip and mid deflections.

In Figure 4.10, longitudinal strains are linear and in the expected sequence until cracking. After cracking, strains may follow unexpected paths. The main reason of this behavior is mainly due to cracking. If a crack intersects a strain gauge, the value can deviate.

The cracks formed on the side and bottom cover of the specimen is presented in Figure 4.11. As can be seen on the figures, there was no side or bottom cover failure occurred in this specimen. All cracks were flexural cracks.

**Figure 4.11** Cracks formation on the side and bottom cover of the specimen

### 4.3.3. Specimen SC_44_44_44_710

Specimen SC_44_44_44_710 had two bar diameter, $2d_b$, face cover and side cover, whereas half the spacing between bars were $1d_b$. The total horizontal bond failure plane was less than the total vertical failure plane, and therefore, the expected failure in this specimen was side splitting. The bar stress according to ACI 408 equation for $32d_b$ splice length was calculated as 443.4 MPa. Note that, the yield strength was 459 MPa. In this specimen, the first crack initiated at 30.8 kN according to the deflection graphs. Longitudinal reinforcements yielded at about 114.9 kN based on the graph where the curve deviated sharply. After flexural yielding of the beam, however, bond failure occurred later with further loading. Theoretically, the yield load was calculated at 117.1 kN. The specimen was subjected to the bond failure and reached its maximum load capacity at 126.2 kN. The cracks formed on the side cover, and propagated on the longitudinal direction until failure. Tip-, and mid deflections, support displacement, and longitudinal strains are illustrated in Figures 4.12-4.14.

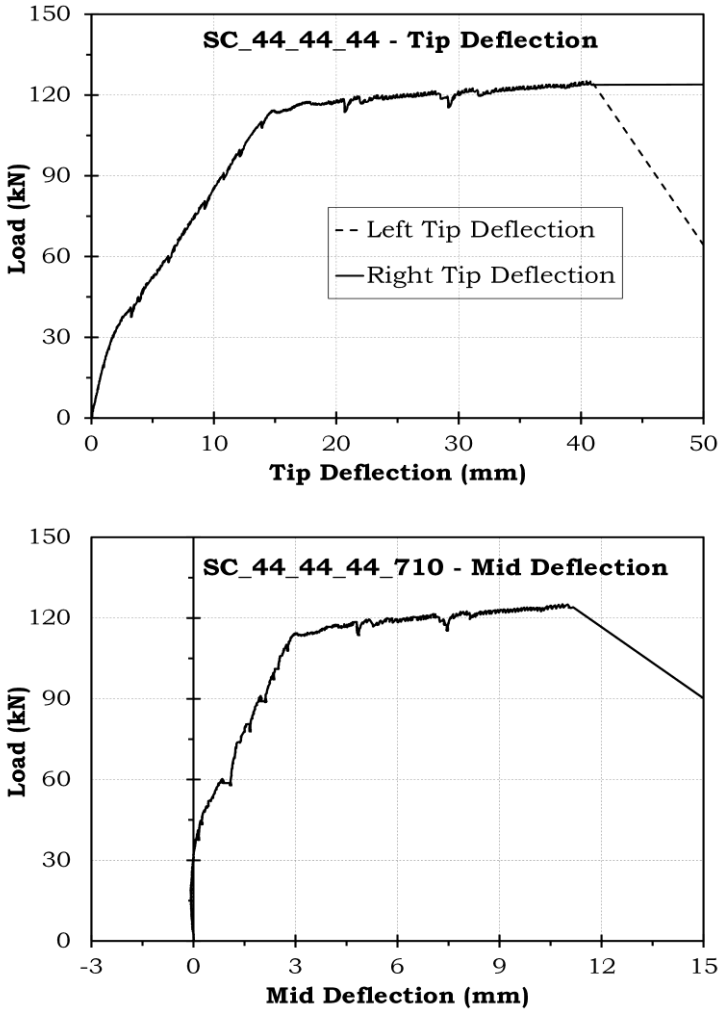


**Figure 4.12** Load versus Deflection Charts

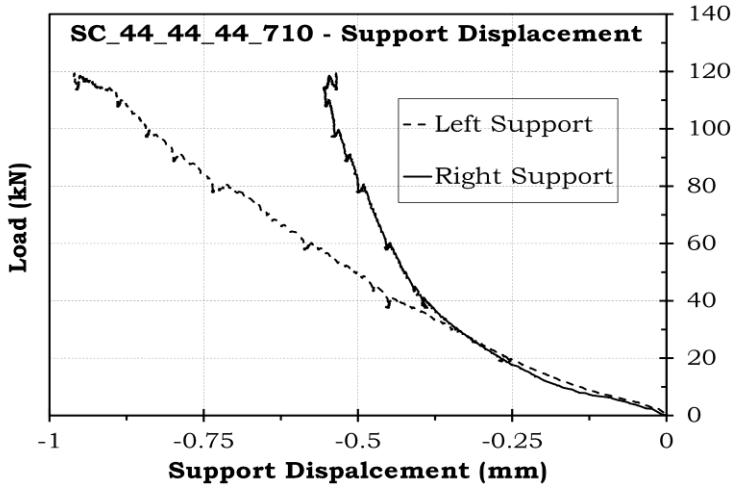


**Figure 4.13** Load versus Support Displacement

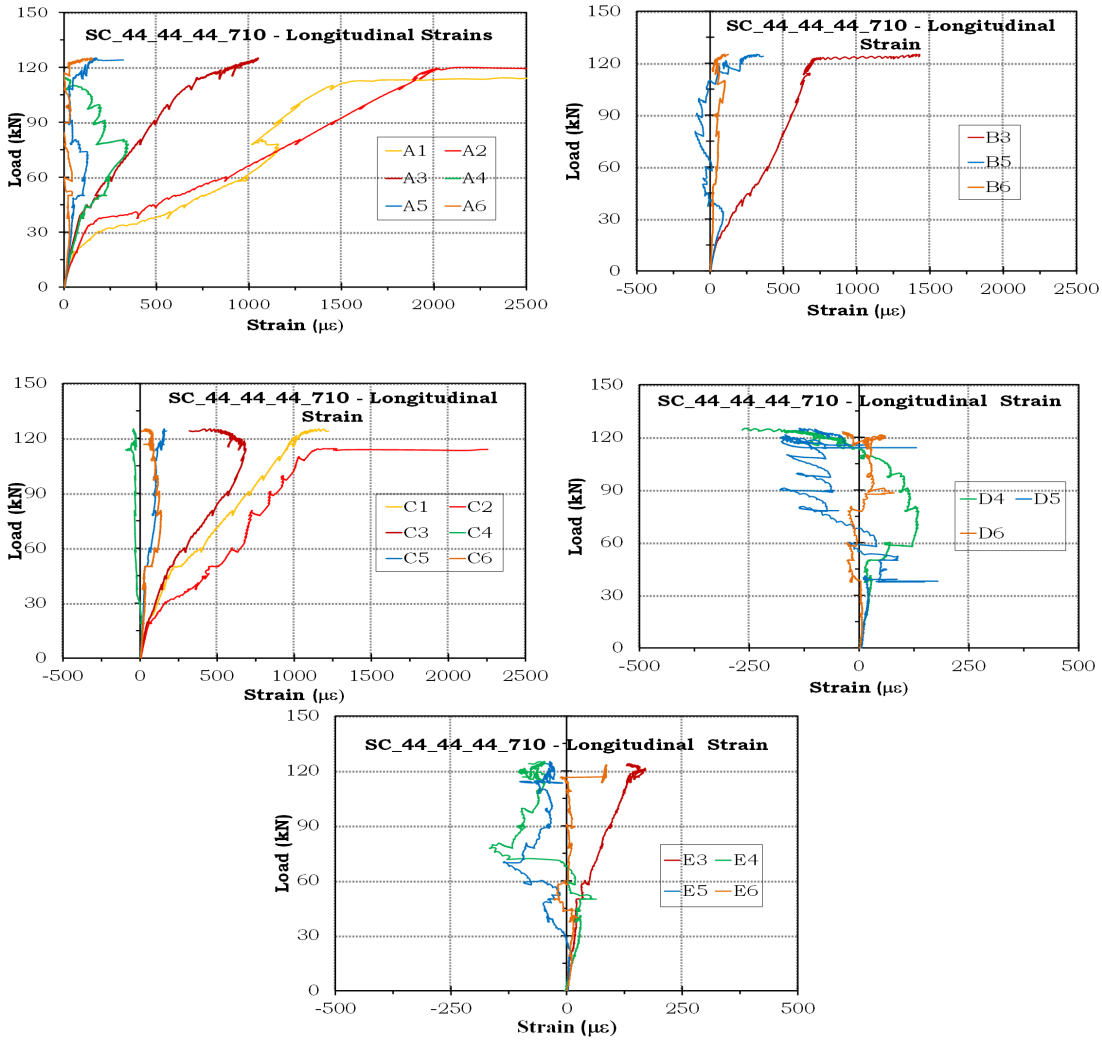


**Figure 4.14** Load versus Longitudinal Strain Charts

Support displacements were measured very low as expected. The overlap of the left and right tip deflections indicates that the load was applied symmetrically. Since the distance between the two supports is 2.1 m, the deflection in the span was almost zero until cracking and remained low until yielding. After yielding of the longitudinal bars, deflections increased rapidly. The total deflection can be calculated by adding both the tip and mid deflections.

In Figure 4.14, longitudinal strains are linear and in the expected sequence until cracking. After cracking, unpredicted strains were measured as shown in the figure. The main reason of this behavior is mainly due to cracks intersecting strain gauges.

The cracks formed on the side cover of the specimen are presented in Figure 4.15. As can be seen on the figures, side splitting occurred. Simultaneously, with the formation of side splitting cracks, two flexural cracks at the tip of laps widened excessively.

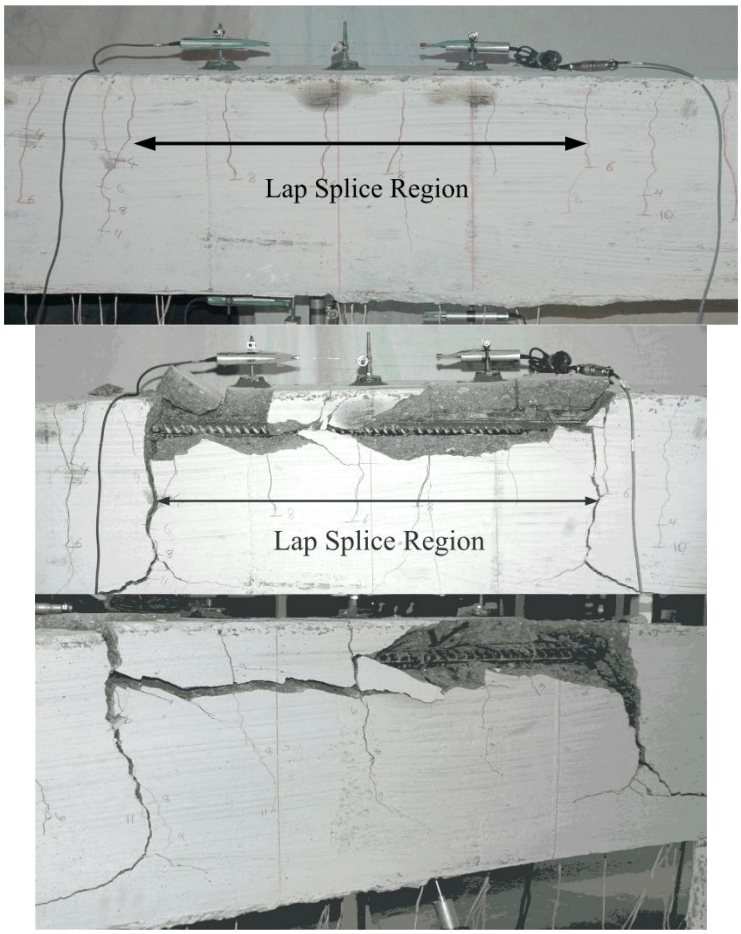


**Figure 4.15** Cracks formation and side splitting occurrence on the side cover of the specimen

### 4.3.4. Specimen SC_44_44_44_530_T4

Similar to the former specimen, specimen SC_44_44_44_530_T4 had two bar diameter, $2d_b$, face cover and side cover, whereas half the spacing between bars were $1d_b$. The total horizontal bond failure plane was less the total vertical failure plane, and therefore, the expected failure in this specimen was side splitting. In this specimen, in addition to the longitudinal reinforcements, four transverse reinforcements were used within the splice region. In order to get similar behavior to the former specimen, lap splice length was decreased to 530 mm, $24d_b$. The bar stress according to ACI 408 equation for $24d_b$ splice length was calculated as 370.6 MPa. The contribution of transverse reinforcement was calculated as 71.8 MPa. Total expected steel stress was 442.4 MPa. Note that, the yield strength was 459 MPa. In this specimen, the first crack initiated at 30.4 kN according to the deflection graphs. Prior to yielding, the beam specimen failed at 109.80 kN due to the side splitting. Failure was brittle and occurred suddenly. Tip-, and mid deflections, support displacement and longitudinal and transverse strains are illustrated in Figures 4.16-4.19.

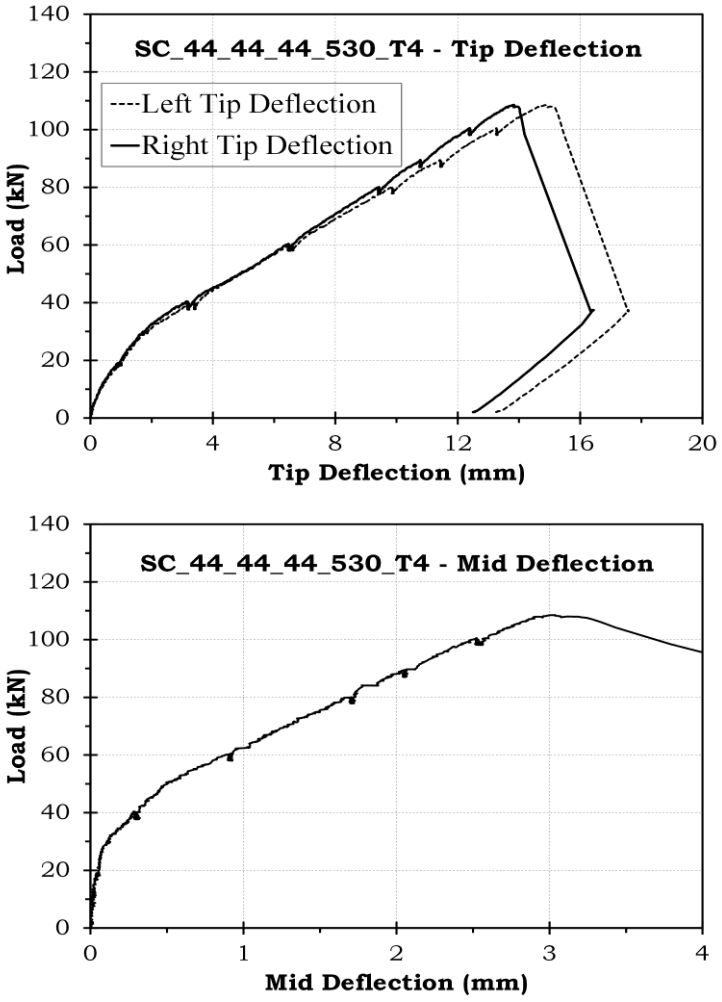


**Figure 4.16** Load versus Deflection Charts

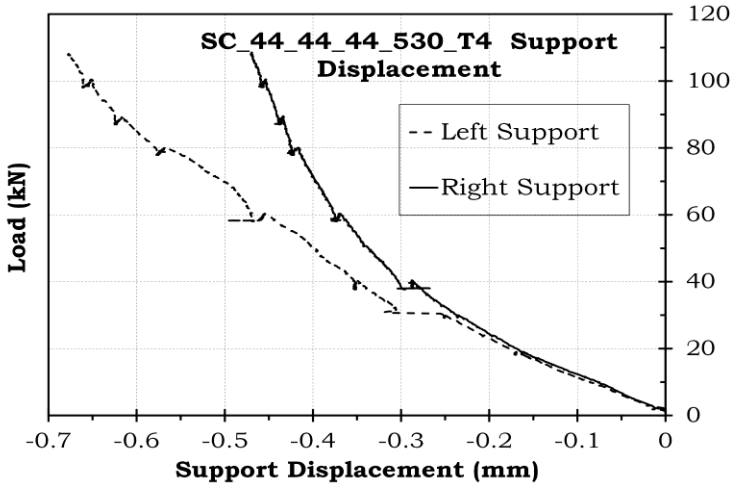


**Figure 4.17** Load versus Support Displacement

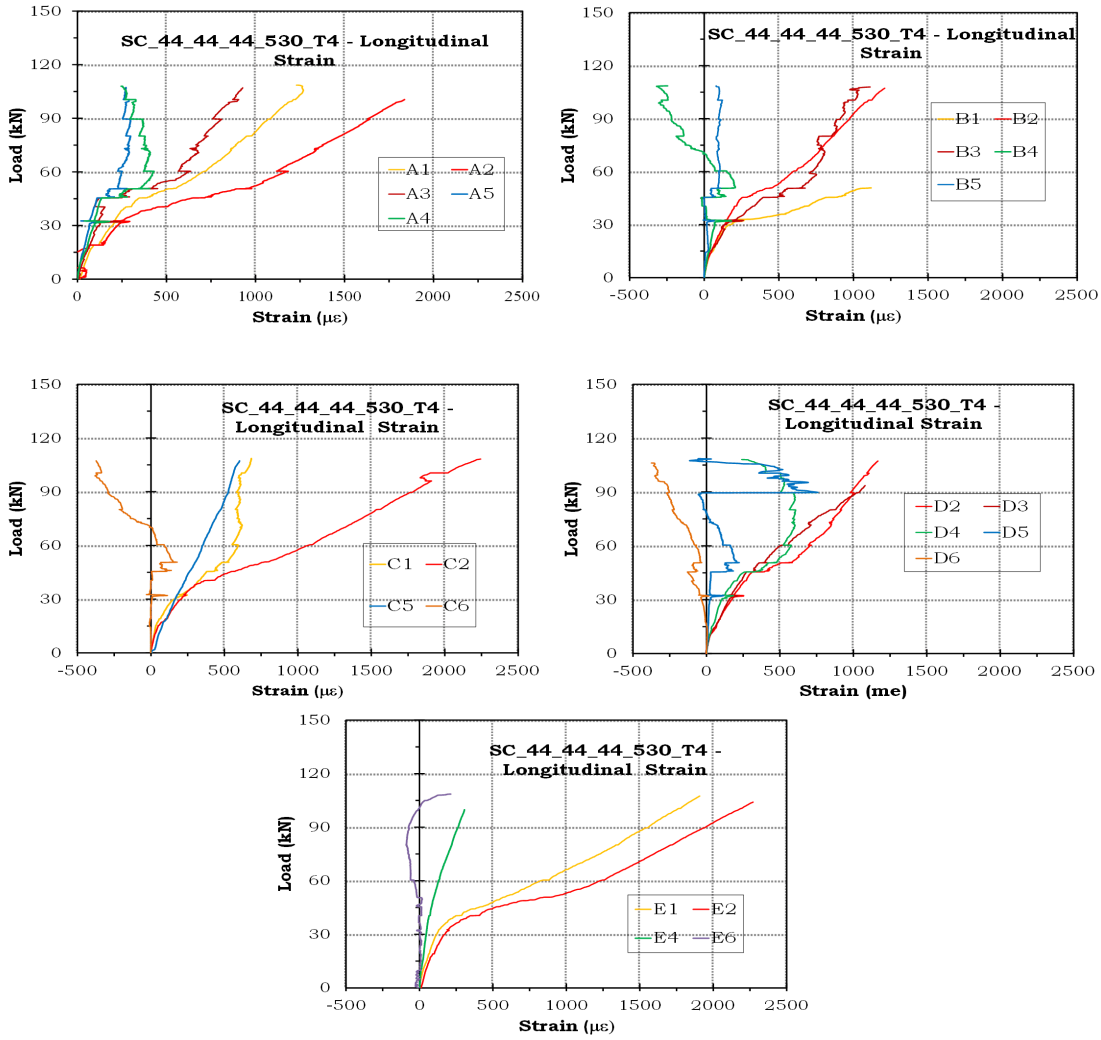


**Figure 4.18** Load versus Longitudinal Strain Charts

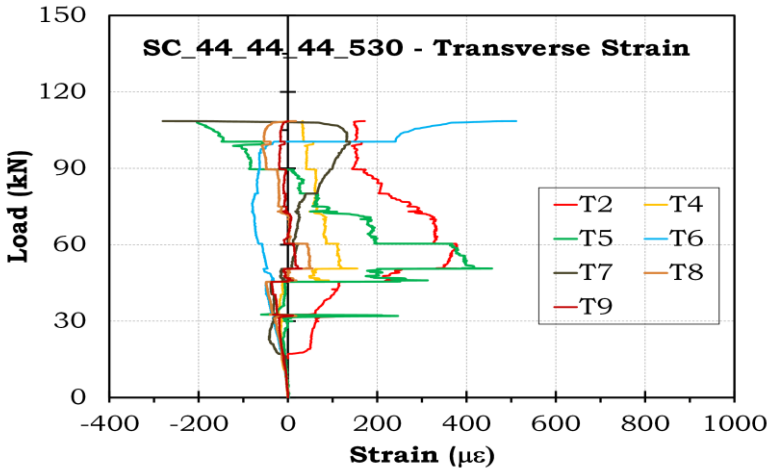


**Figure 4.19** Load versus Transverse Strain Chart

Support displacements were measured very low as expected. The overlap of the left and right tip deflections indicates that the load was applied symmetrically. The mid-deflection was much lower than the tip deflections. The total deflection can be calculated by adding both the tip and mid deflections.

Cracks initiated at approximately 250 με level. After cracking, strain distribution is not uniform along the splice length. This unpredictable inconsistency is much predominant on the transverse reinforcement as shown in Figure 4.19.

Vertical flexural cracks formed first on the bottom and side cover. Formation of the longitudinal cracks on the side cover caused side splitting failure at the ultimate stage, Figure 4.20.

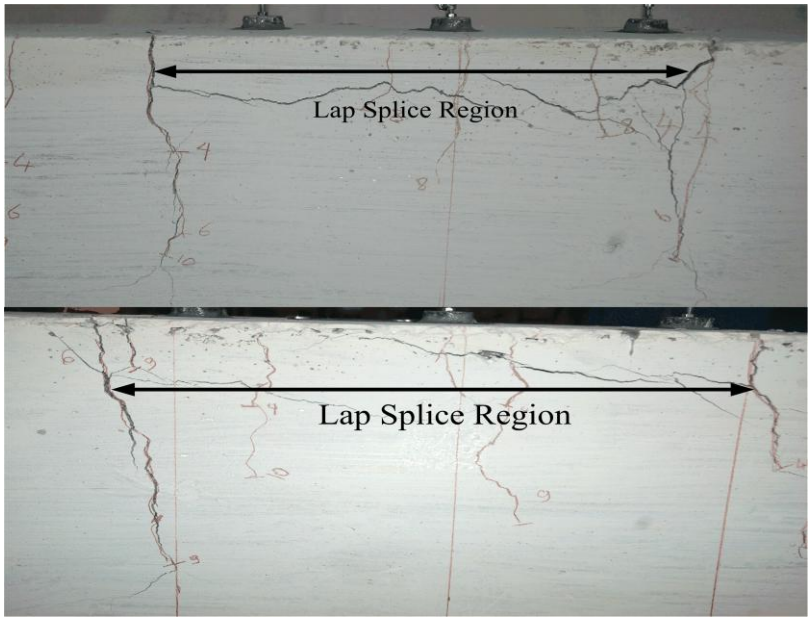


**Figure 4.20** Cracks formation and side splitting on the side cover of the specimen

### 4.3.5. Specimen SC_44_22_22_530_T4

Specimen SC_44_22_22_530_T4 had two bar diameter, $2d_b$, face cover, whereas side cover was $1d_b$, and half the spacing between bars was $½d_b$. The total horizontal bond failure plane was less the total vertical failure plane, and therefore, the expected failure in this specimen was side splitting. In this specimen, in addition to the longitudinal reinforcements, four transverse reinforcements were used within the splice region. Lap splice length was 530 mm, $24d_b$. The bar stress according to ACI 408 equation for $24d_b$ splice length was calculated as 341.7 MPa. The contribution of transverse reinforcement was calculated as 73.1 MPa. Total expected steel stress was 414.8 MPa. Note that, the yield strength was 459 MPa. In this specimen, the first crack initiated at 21.3 kN according to the deflection graphs. Prior to yielding, the beam specimen failed at 98.3 kN due to the side splitting. Failure was brittle and occurred suddenly. Tip-, and mid deflections, support displacement and longitudinal and transverse strains are illustrated in Figures 4.21-4.24.

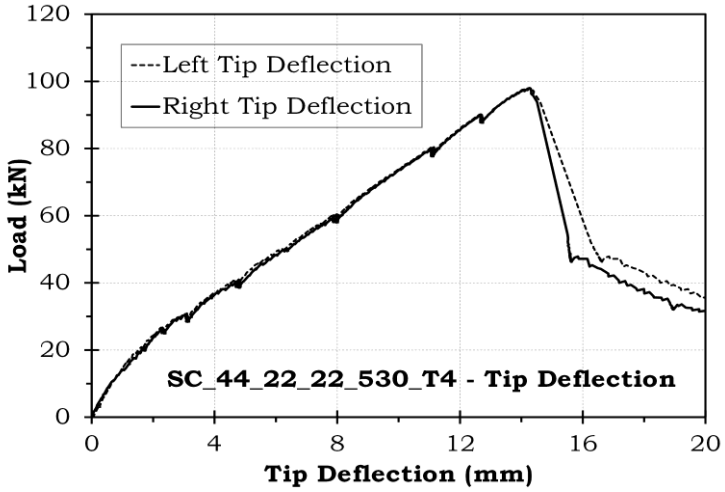


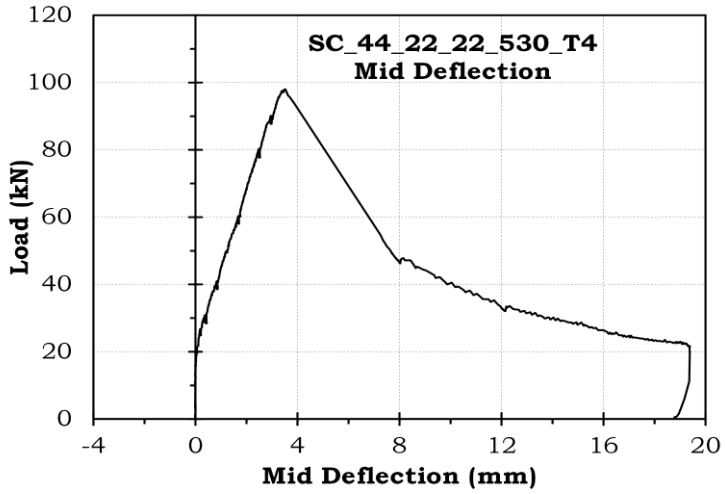


**Figure 4.21** Load versus Deflection Charts

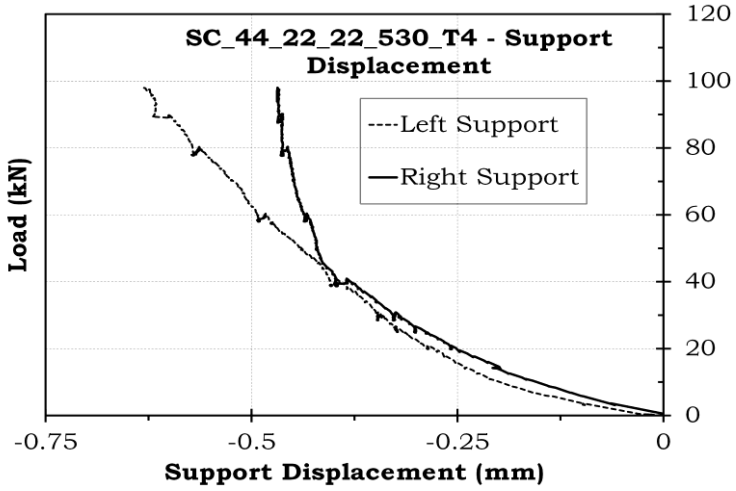


**Figure 4.22** Load versus Support Displacement

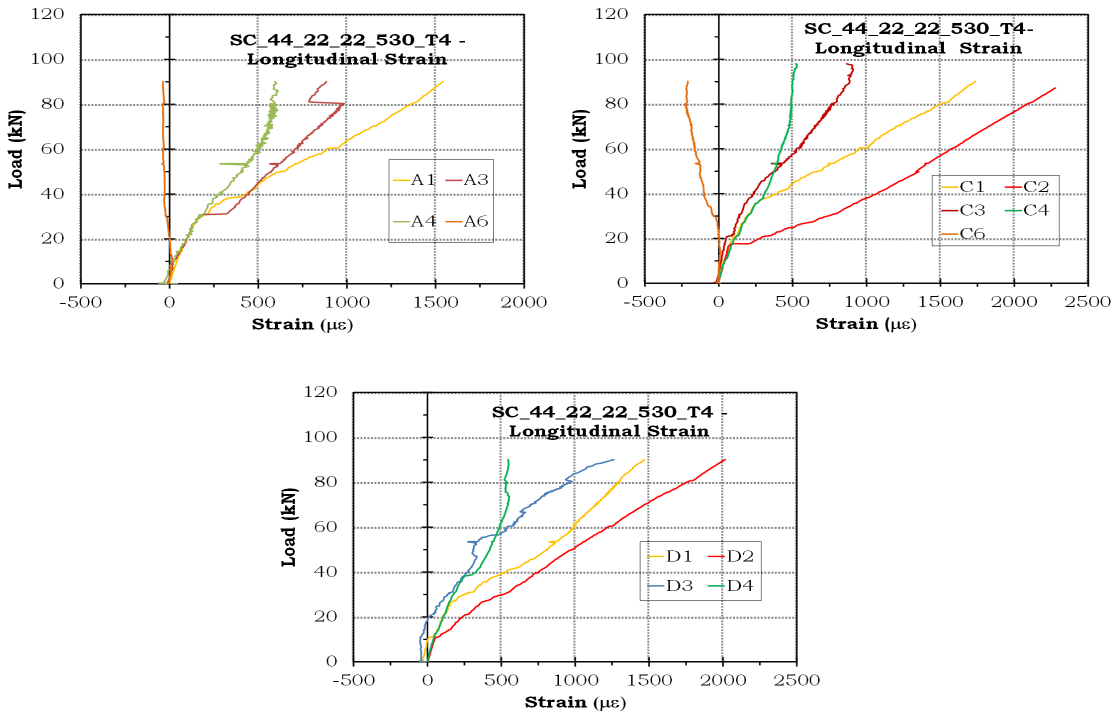


**Figure 4.23** Load versus Longitudinal Strain Charts

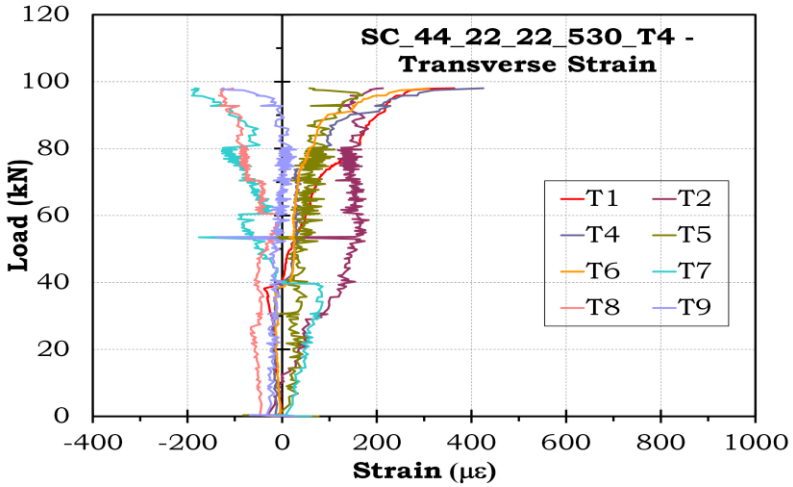


**Figure 4.24** Load versus Transverse Strain Charts

Support displacements were measured very low as expected. The overlap of the left and right tip deflections indicates that the load was applied symmetrically. The mid-deflection was much lower than the tip deflections. The total deflection can be calculated by adding both the tip and mid deflections.

First, flexural cracks formed on the side and bottom cover of the specimen. As it was expected, side splitting occurred by longitudinal cracks on the side cover due to inadequate side cover and spacing between bars.

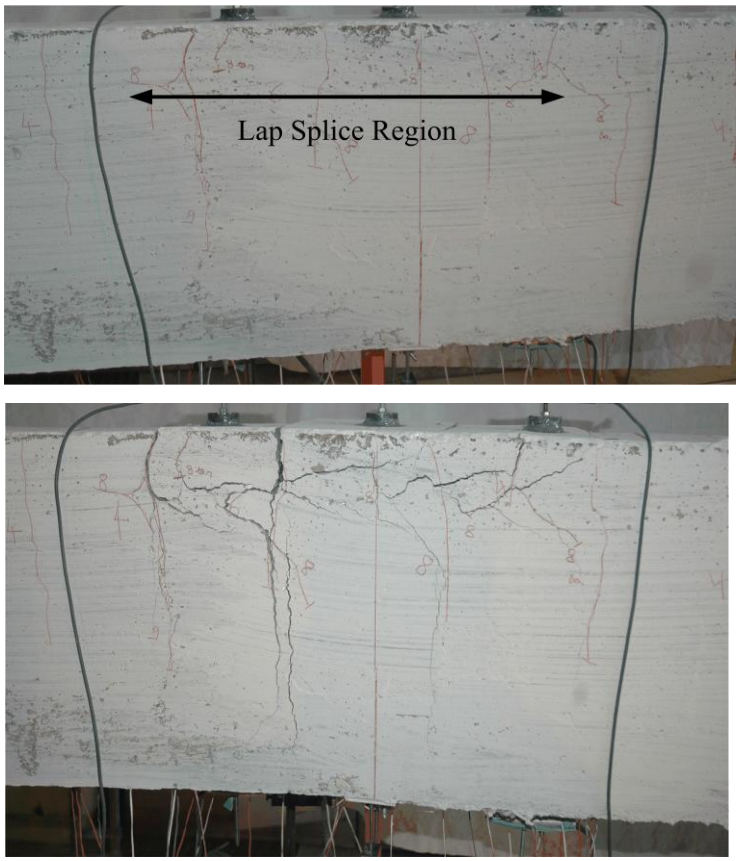


**Figure 4.25** Cracks formation and side splitting occurrence on the side cover of the specimen

### 4.3.6. Specimen SC_44_22_22_530_T6

Specimen SC_44_22_22_530_T6 was the very same specimen with SC_44_22_22_530_T4 except number of transverse reinforcement along the splice. In this specimen, six transverse reinforcements were put within the splice region to observe effect of increased stirrups on the bond behavior. The idea of the increased transverse reinforcement was to prevent bond failure and get flexural yielding at the ultimate stage even with small cover dimensions. The bar stress according to ACI 408 equation for $24d_b$ splice length was calculated as 341.7 MPa. The contribution of transverse reinforcement was calculated as 96.8 MPa. Total expected steel stress was 438.5 MPa. Note that, the yield strength was 459 MPa. In this specimen, the first crack initiated at 22.6 kN according to the deflection graphs. Prior to yielding, the beam specimen failed at 95.3 kN due to the side splitting. Failure was brittle and occurred suddenly. Tip and mid deflections, support displacements, longitudinal, and transverse reinforcement strain are represented graphically in Figures 4.26-4.29.

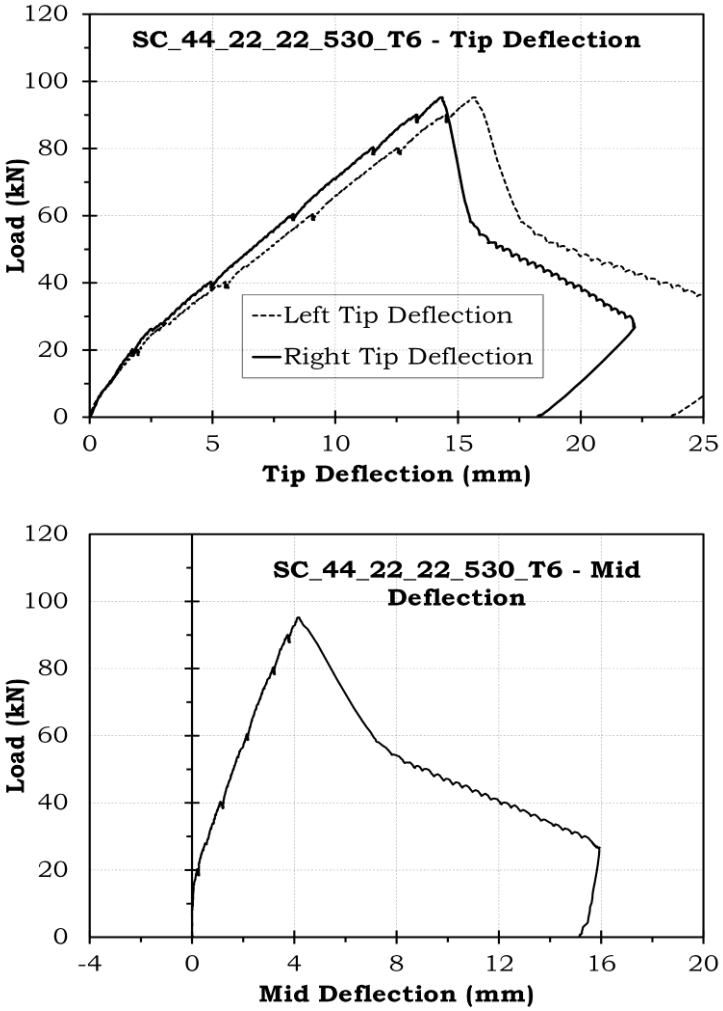


**Figure 4.26** Load versus Deflection Charts

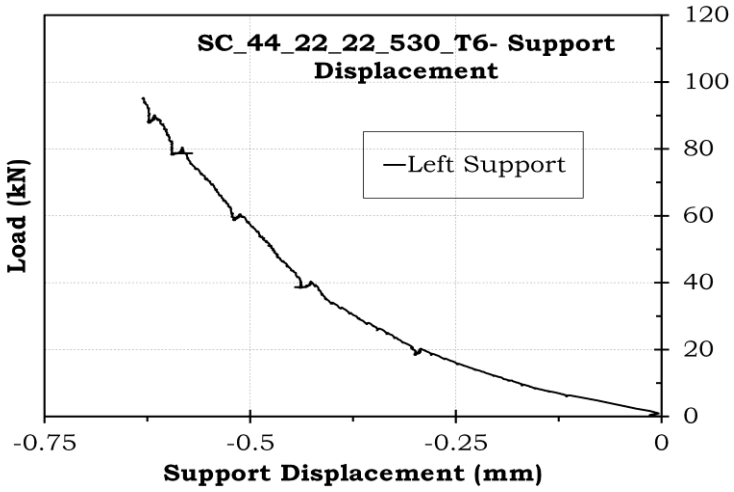


**Figure 4.27** Load versus Support Displacement

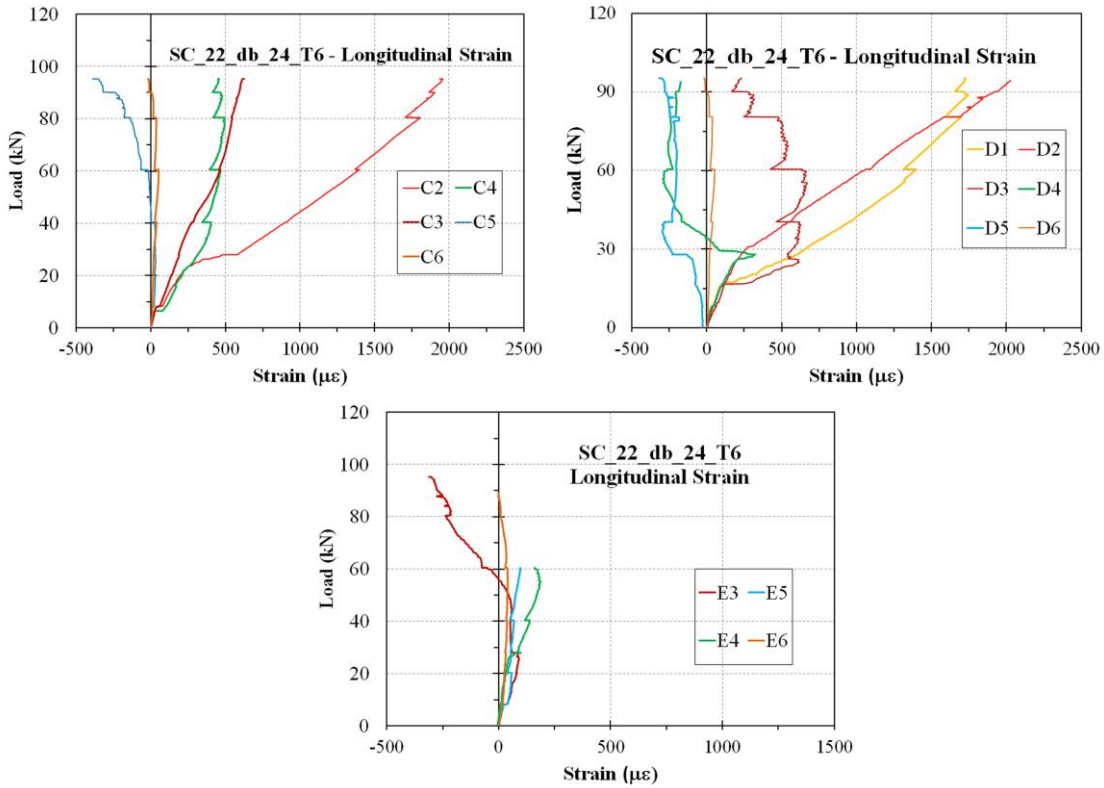


**Figure 4.28** Load versus Longitudinal Strain Charts

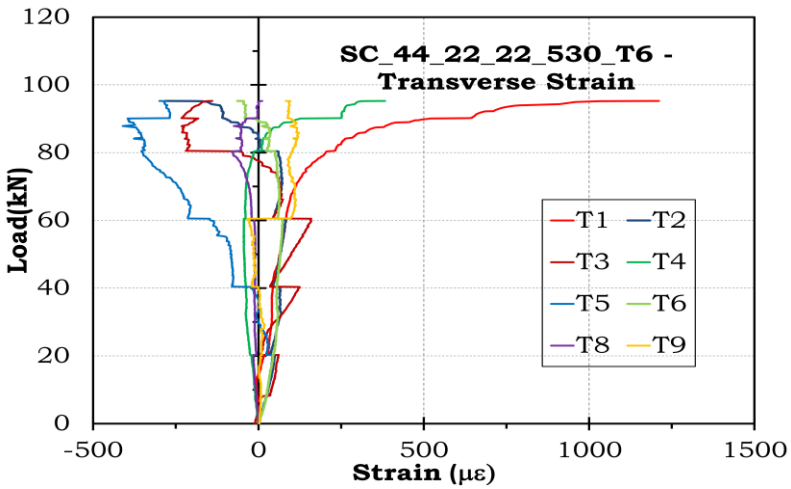


**Figure 4.29** Load versus Transverse Strain

Similar to the other specimens, vertical flexural cracks formed first. Although, the number of stirrups were increased from four to six, inadequate cover could not carry the tensile stresses and with the formation of longitudinal side cracks, failure occurred by side splitting, Figure 4.30.

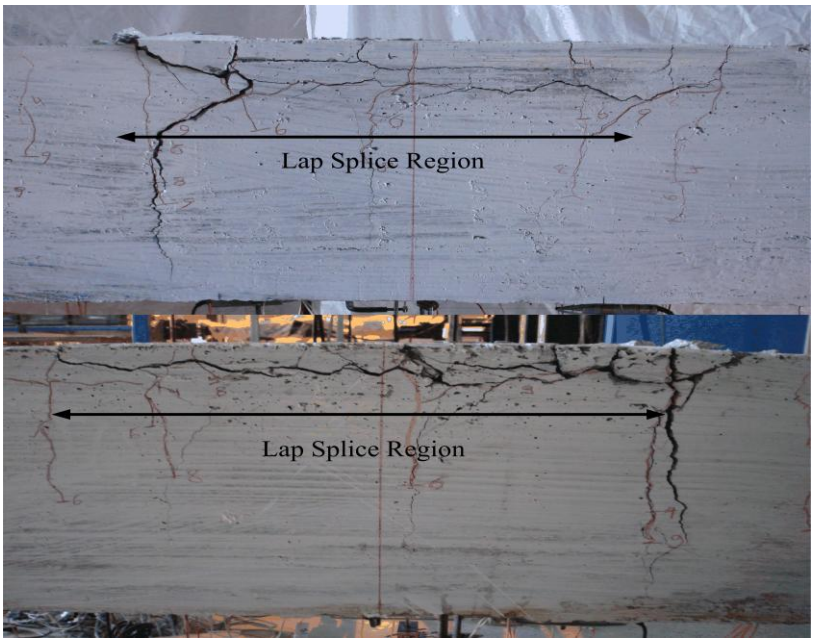


**Figure 4.30** Cracks formation and side splitting occurrence on the side cover of the specimen

# CHAPTER 5

# ANALYSIS AND DISCUSSION OF RESULTS

## 5.1. General

In this chapter, test results were compared with analytical results. First, experimental and analytical cracking loads are compared. Subsequently, experimental load-deflection and moment-curvature curves are compared with the analytical ones. The theoretical approaches are described in detail in this chapter.

## 5.2. Crack analysis

As it was stated in chapter 4, cracks were marked during testing. Generally, first cracks initiated at the free end of the lap splice region. Crack initiation can also be recognized from the load-displacement curves. For the analytical cracking load calculation uncracked transformed section was used, Figure 5.1. Flexural tensile strength and elastic modulus of concrete was calculated according to TS 500.

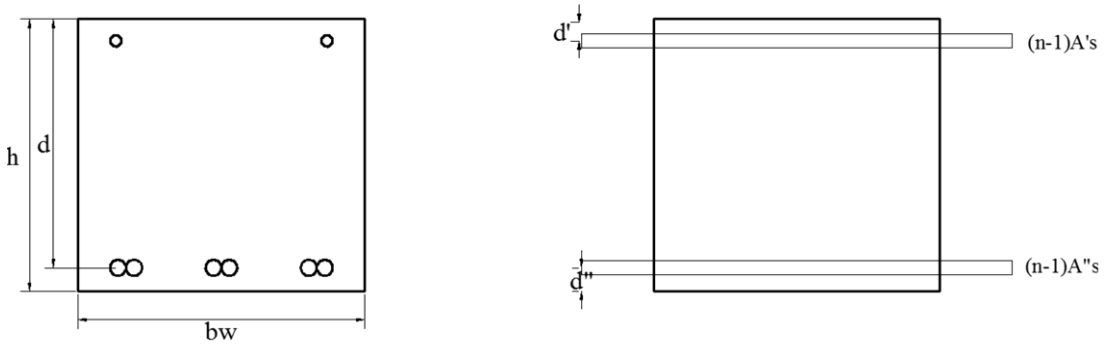


**Figure 5.1** Real and Transformed Cross Section

$$\bar{y} = \frac{b_w \times h \times \frac{h}{2} + (n-1) \times A_s'' \times d'' + (n-1) \times A_s' \times d'}{b_w \times h + (n-1) \times A_s'' + (n-1) \times A_s'} \tag{5.1}$$

$$I = \frac{b_w \times h^3}{12} + b_w \times h \times \left(\frac{h}{2} - \bar{y}\right)^2 + (n-1) \times A_s'' \times \left(\bar{y} - d'\right)^2 + (n-1) \times A_s' \times \left(h - \bar{y} - d''\right)^2 \tag{5.2}$$

$$M_{cr} = \frac{f_{ctf} \times I}{\bar{y}} \tag{5.3}$$

$$P_{cr} = \frac{M_{cr}}{1.4} \tag{5.4}$$

$$n = \frac{E_s}{E_c} \tag{5.5}$$

$$E_c = 3250\sqrt{f_c} + 14000 \tag{5.6}$$

$$f_{ctf} = 0.7\sqrt{f_c} \tag{5.7}$$

In Figure 5.2 shows determination of the experimental cracking load for specimen SC_22_44_88_530. The total deflection was calculated by summing up tip and mid deflections. Two tangents were drawn on the Load-Total Deflection curve of specimen and the intersection point of the lines was considered as cracking load. In Table 5.1, experimental and analytical cracking loads are demonstrated.

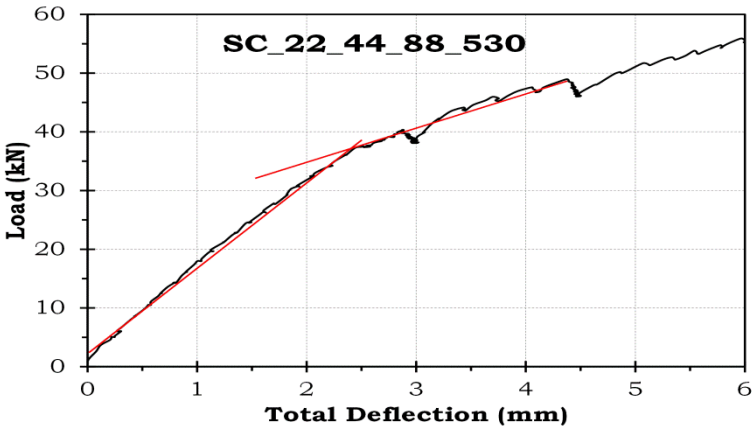


**Figure 5. 2 Experimental cracking load determination**

**Table 5.2** Measured and calculated Cracking load

| Test Specimen | Calculated $P_{cr}$ (kN) | Measured $P_{cr}$ (kN) | Error (%) |
|---|---|---|---|
| SC_22_44_88_530 | 34.90 | 37.40 | -7.20 |
| SC_22_44_88_800 | 34.9 | 34.80 | 0.30 |
| SC_44_44_44_710 | 30.60 | 30.80 | -0.65 |
| SC_44_44_44_530_T4 | 30.60 | 30.40 | 0.65 |
| SC_44_22_22_530_T4 | 23.10 | 21.30 | 7.8 |
| SC_44_22_22_530_T6 | 23.10 | 22.60 | 2.2 |

## 5.3. Comparison of the Load-Deflection Curves

In this part, analytically calculated load-deflection curves are compared with those obtained experimentally. First, moment-curvature diagrams were calculated. The non-commercial software called RESPONSE 2000 was utilized in the moment-curvature calculations of the sections. The moment area procedure for the theoretical load-deflection calculation can be summarized as follows:

- Figure 5.3 shows moment diagram of the specimens. Moment is linearly increasing along the shear span. Within support region, the moment is

maximum and constant. The maximum moment can be calculated simply by multiplying the moment arm with the applied load (1.4×$P$). In order to get finer result especially for tip deflection values, moment diagram along shear span was divided to 10 equal strips and moment value for each strip was determined.

- Curvature values of the corresponding moments were taken from moment curvature diagram. Load increment value which was used in load-deflection calculations was equal to 1kN. During the determination of curvature values for the corresponding moments, interpolation was done between two curvature values.
- After the formation of curvature diagram, second-moment area theorem was applied to determine the mid- and tip deflection of specimens. Equations 5.8 - 5.11 were used to calculate tip deflection (deflection at point A). At point C rotation is zero as shown in figure 5.4. The tangential deviations between points A and C and between points B and C are $t_{A/C}$, and $t_{B/C}$, respectively. Difference between $t_{A/C}$ and $t_{B/C}$ gives the deflection at point A ($\Delta_A$). Deflection at point C ($\Delta_C$), the mid-point, is directly equal to $t_{B/C}$. Tip and mid deflections were calculated for 1 kN increments until reaching a nonlinear behavior of the beam.

$$t_{A/C} = \sum_{1}^{10} A_i \times \delta_{A_i} + A_{11} \times \delta_{A_{11}/A} \tag{5.8}$$

$$t_{B/C} = A_{11} \times \delta_{A_{11}/B} \tag{5.9}$$

$$\Delta_A = t_{A/C} - t_{B/C} \tag{5.10}$$

$$\Delta_B = t_{B/C} \tag{5.11}$$

The analytical moment-curvature curves are provided in Appendix A.

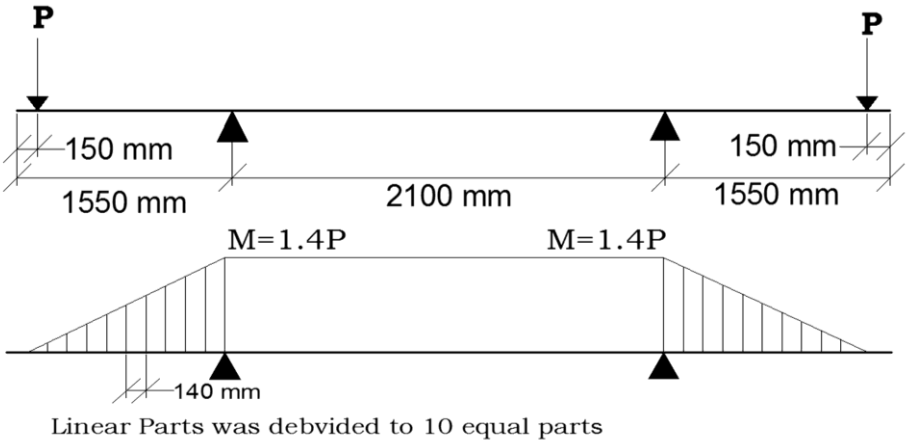


**Figure 5.3** Moment Diagram of test specimens

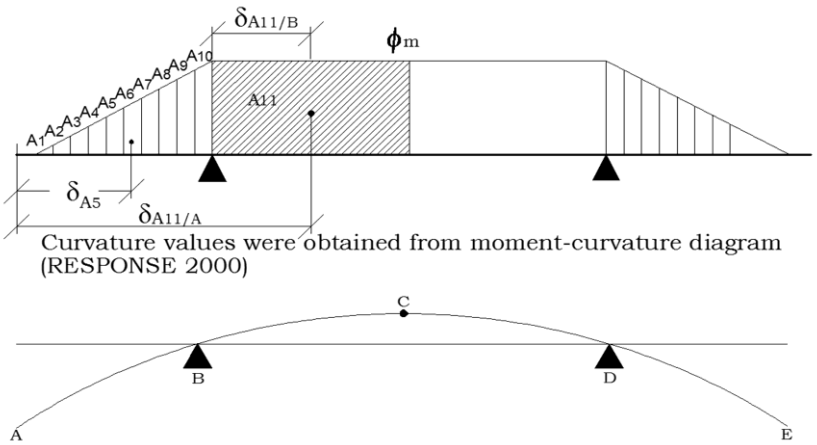


**Figure 5.4** Curvature and Deflection Diagrams of test specimens

Measured and calculated load – total deflection curves are presented in Figures 5.5, 5.7, 5.9, 5.11, 5.13, and 5.15. On total deflection charts, the x and y axis indicate load and total deflection respectively.

In the analytical calculation of load – deflection curves, material and geometric properties of the specimens given in Chapter 3 were used. Material properties include yield and ultimate strength for longitudinal, transverse and assembly reinforcement and compressive strength of self-compacting concrete. Geometric properties include the section dimensions and clear cover dimensions which had been determined after the tests.

In all elastic, post cracking and post yielding regions, the match between the experimental and analytical curves are extremely good. All beam specimens except specimens SC_22_44_88_800, and SC_44_44_44_710 have undergone bond failure. They failed before reaching their flexural capacities in a brittle manner. Therefore, they deviated from the analytical curve prematurely. Specimens SC_22_44_88_800, and SC_44_44_44_710 showed flexural failure. Therefore, the experimental and analytical curves over the whole range of testing coincide particularly satisfactory.

For the comparison of the load-deflection curves, the overlap of the slopes is particularly of importance because the slope dictates the stiffness of the specimens. In all specimens, the slopes are calculated very close to the real behavior.

In Figures 5.6, 5.8, 5.10, 5.12, 5.14, and 5.16, the moment curvature diagrams are provided both measured during testing and analytically calculated. As can be seen from the figures, the deviation between the experimental and analytical curves is very high. The experimental curvature values are almost half of the analytical ones. The main reason of this deviation is mainly the method for the curvature measurements. Curvature at the mid span was measured over a gage length of 400 mm whereas analytical curvatures were calculated for a section which has infinitely small length.

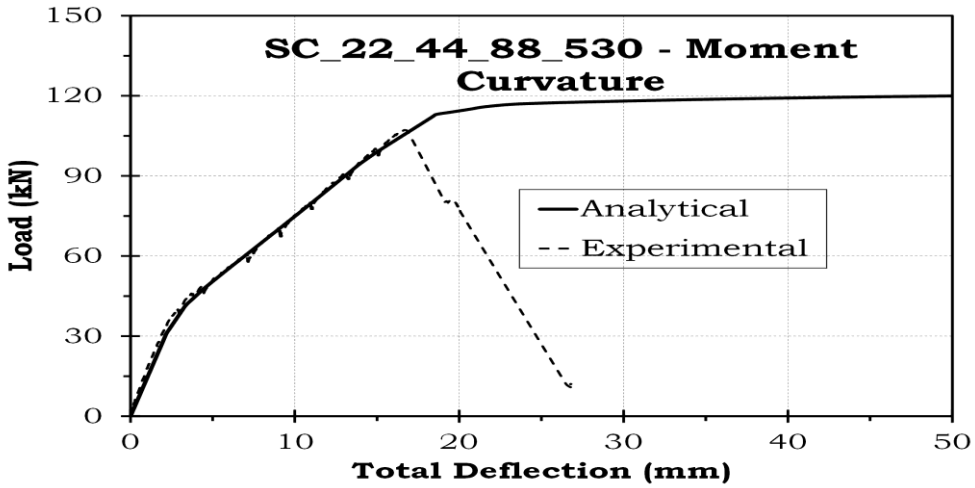


**Figure 5.5** Load versus Total Deflection curves for SC_22_44_88_530

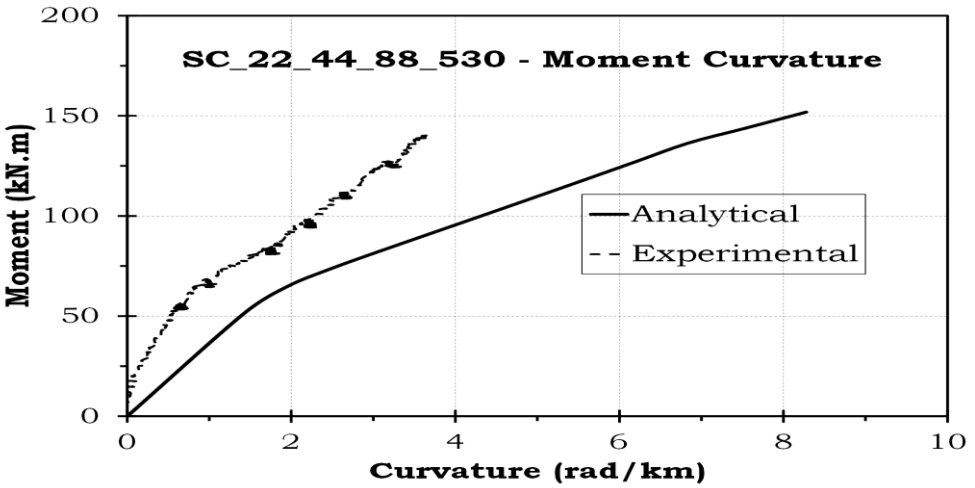


**Figure 5.6** Moment-Curvature Diagram for SC_22_44_88_530

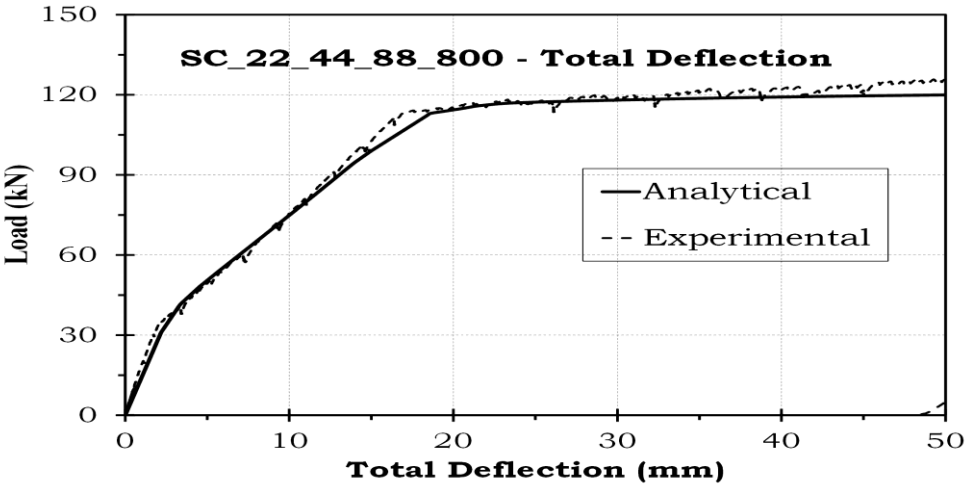


**Figure 5.7** Load versus Total Deflection curves for SC_22_44_88-800

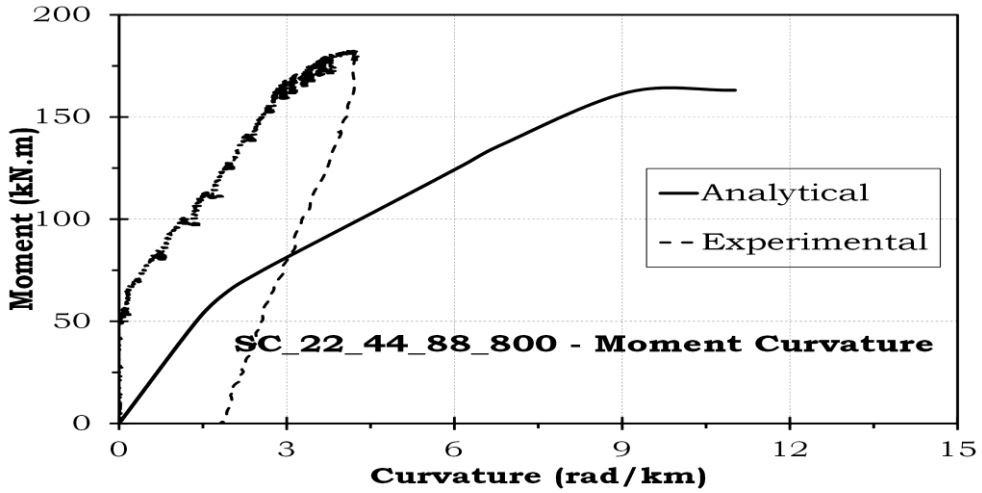


**Figure 5.8** Moment-Curvature Diagram for SC_22_44_88_800

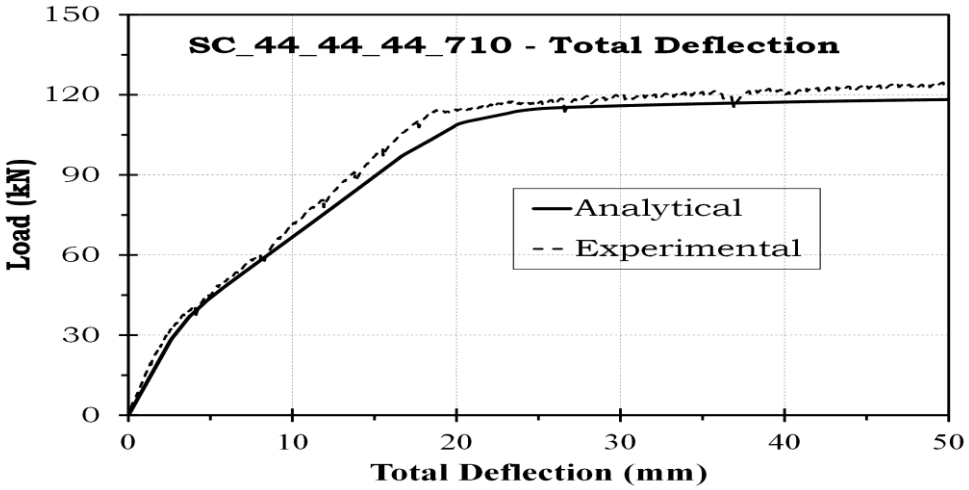


**Figure 5.9** Load versus Total Deflection curves for SC_44_44_44_710

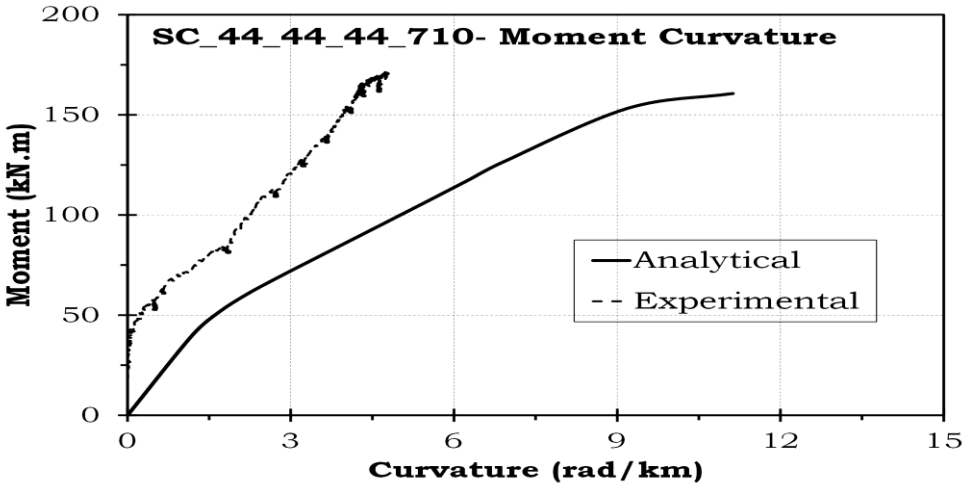


**Figure 5.10** Moment-Curvature Diagram for SC_44_44_44_710

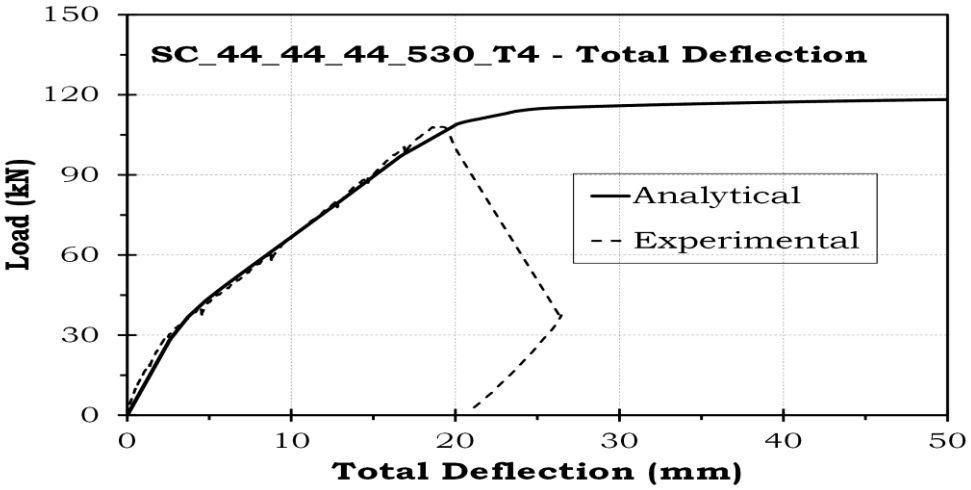


**Figure 5.11** Load versus Total Deflection curves for SC_44_44_44_530_T4

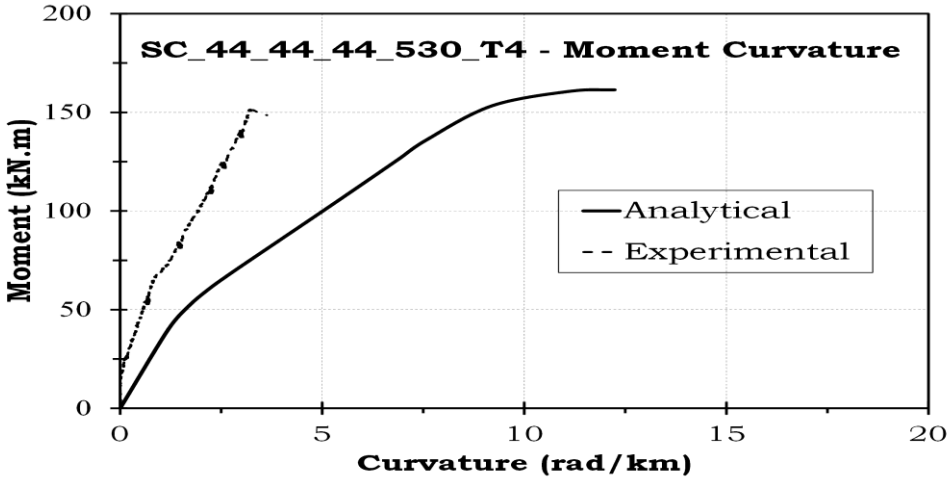


**Figure 5.12** Moment-Curvature Diagram for SC_44_44_44_530_T4

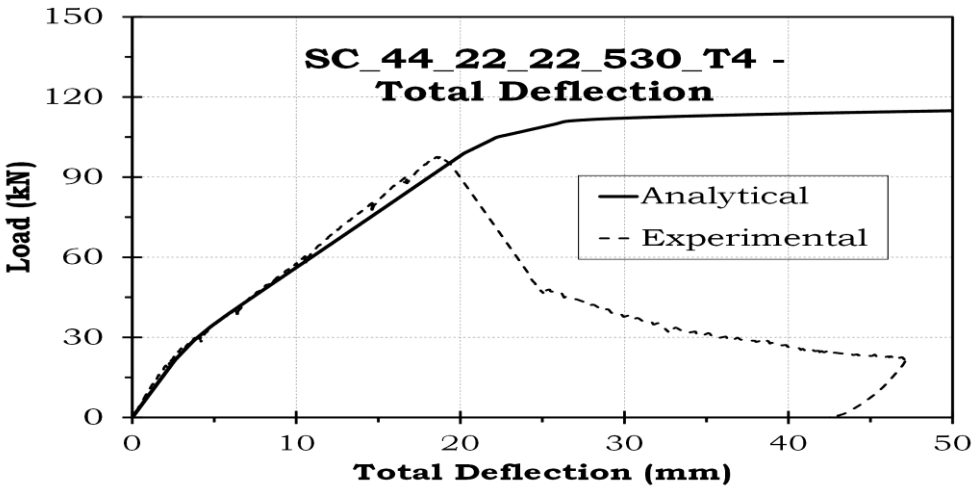


**Figure 5.13** Load versus Total Deflection curves for SC_44_22_22_530_T4

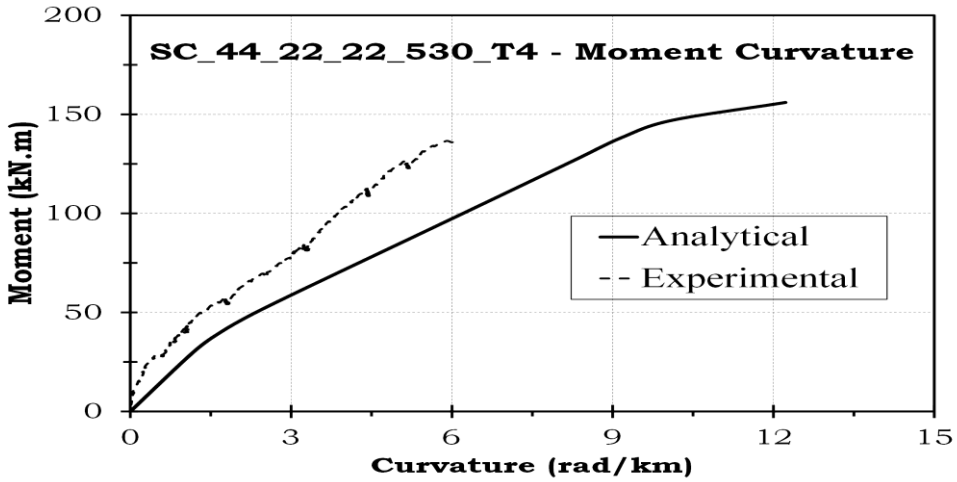


**Figure 5.14** Moment-Curvature Diagram for SC_44_22_22_530_T4

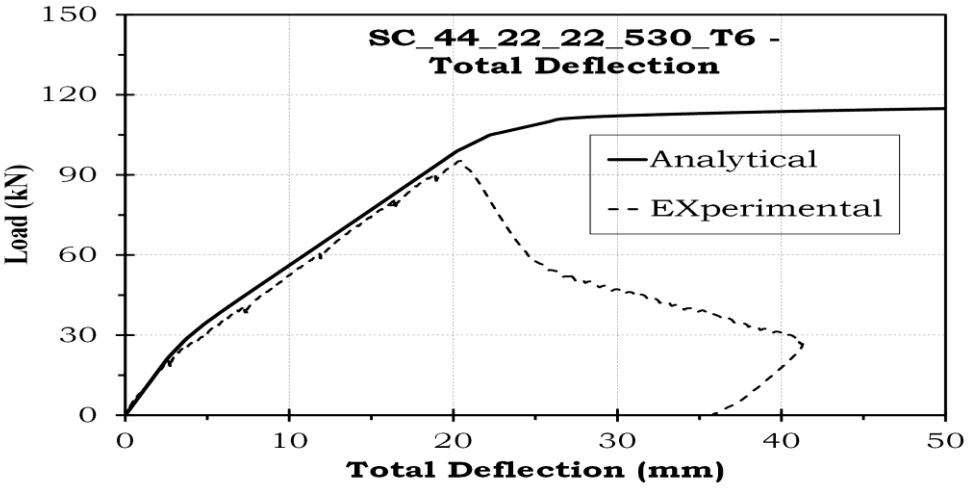


**Figure 5.15** Load versus Total Deflection curves for SC_44_22_22_530_T6

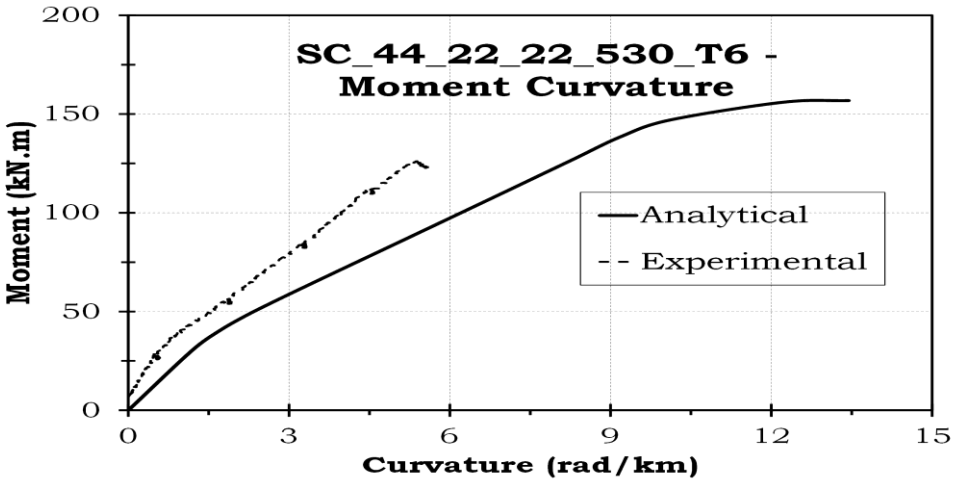


**Figure 5.16** Moment-Curvature Diagram for SC_22_db_24_T6

## 5.4. Strain Profiles on Longitudinal Reinforcement

The strains of the longitudinal and transverse reinforcement were measured during the test. As expected strain reached its maximum value at the continuous end of the lap splice and approached to zero at the free end. Longitudinal strain values are presented between Figures 5.18 and 5.31. As shown in Figure 5.17, on each longitudinal bar, 6 strain gages were attached. A and B strain gages were placed on the side lap spliced longitudinal bars. C and D strain gages were attached on the middle lap spliced longitudinal bars. E and F strain gages were mounted on the other side lap spliced longitudinal bars. The first strain gages, #1, were attached on the continuous side and therefore it was expected to measure the maximum strain on these gages. The last strain gages, #6, were mounted on the free end and consequently zero strain was expected on these gages.

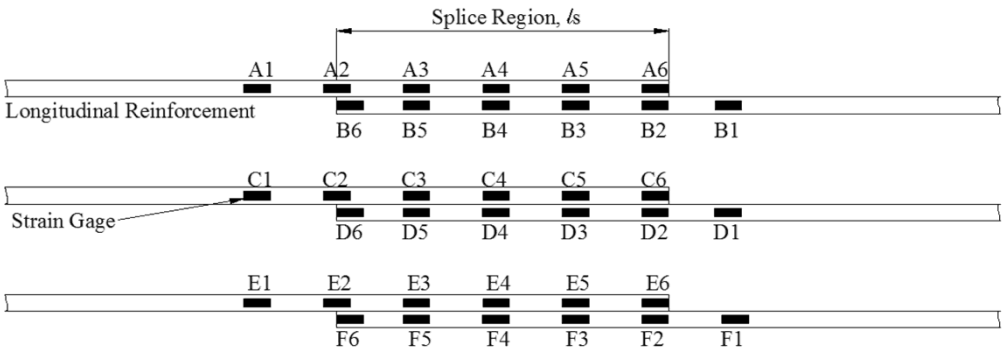


**Figure 5.17** Longitudinal strain gage locations

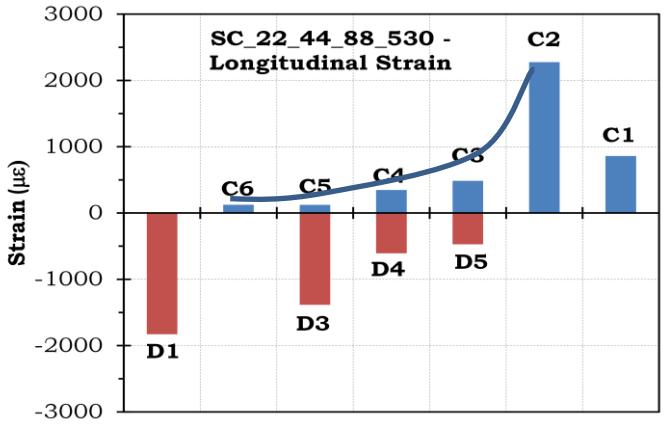


**Figure 5.18** Longitudinal strains at the ultimate stage for SC_22_44_88_530

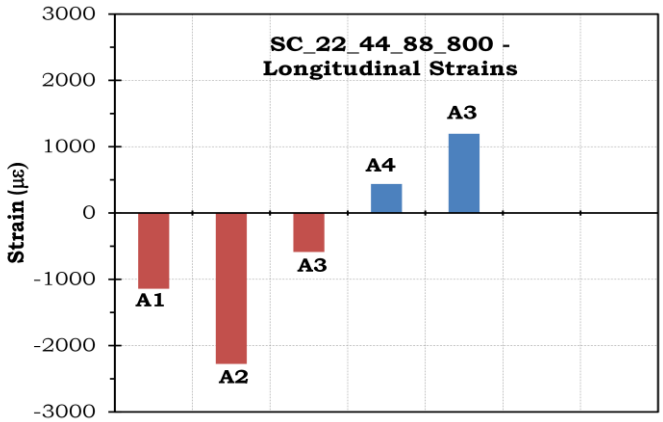


**Figure 5.19** Longitudinal strains at the ultimate stage for SC_22_44_88_800

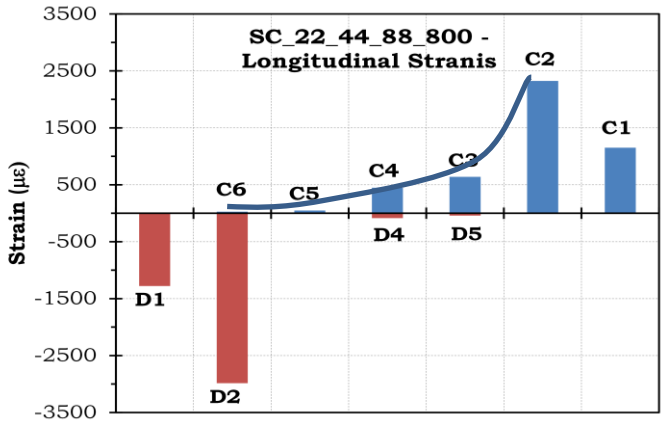


**Figure 5.20** Longitudinal strains at the ultimate stage for SC_22_44_88_800

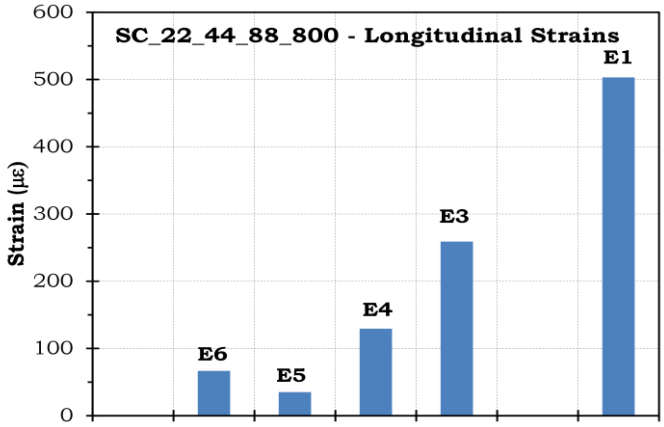


**Figure 5.21** Longitudinal strains at the ultimate stage for SC_22_44_88_800

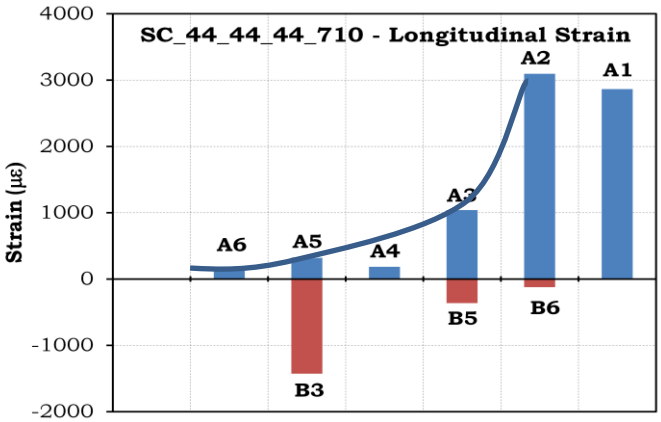


**Figure 5.22** Longitudinal strains at the ultimate stage for SC_44_44_44_710

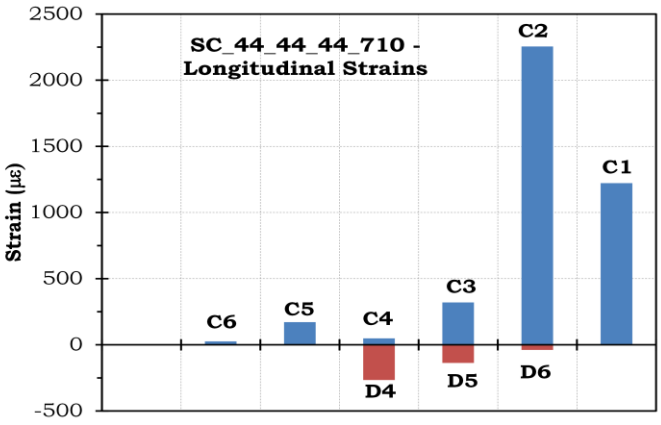


**Figure 5.23** Longitudinal strains at the ultimate stage for SC_44_44_44_710

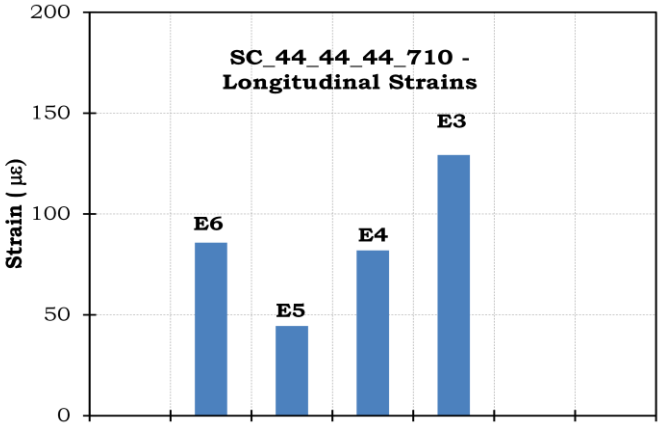


**Figure 5.24** Longitudinal strains at the ultimate stage for SC_44_44_44_710

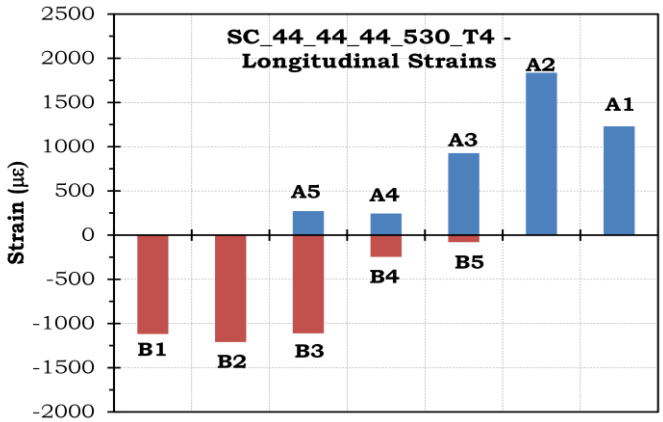


**Figure 5.25** Longitudinal strains at the ultimate stage for SC_44_44_44_530_T4

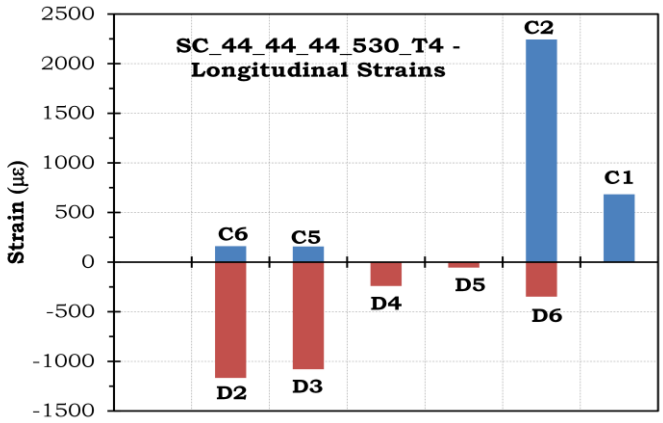


**Figure 5.26** Longitudinal strains at the ultimate stage for SC_44_44_44_530_T4

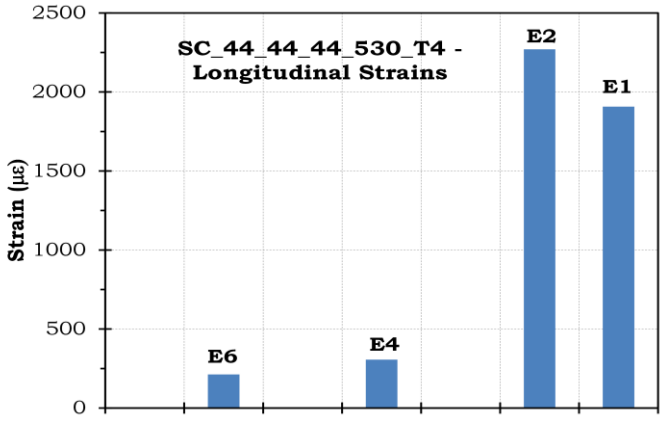


**Figure 5.27** Longitudinal strains at the ultimate stage for SC_44_44_44_530_T4

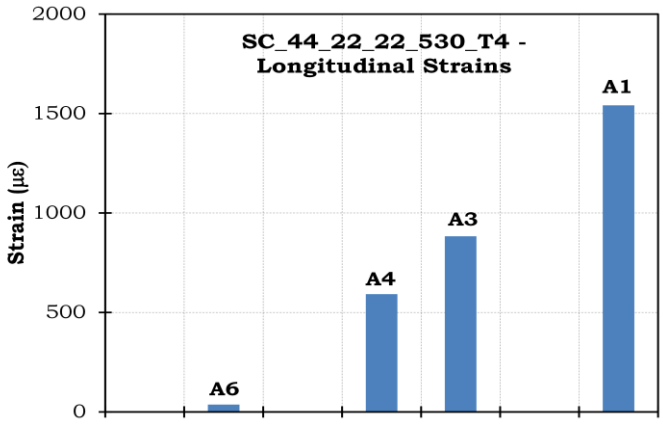


**Figure 5.28** Longitudinal strains at the ultimate stage for SC_44_22_22_530_T4

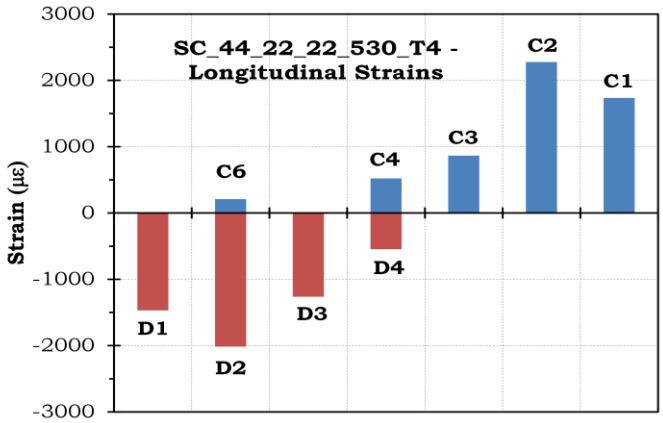


**Figure 5.29** Longitudinal strains at the ultimate stage for SC_44_22_22_530_T4

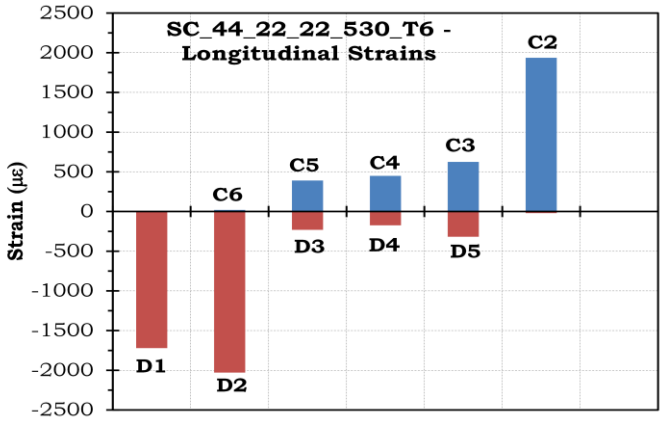


**Figure 5.30** Longitudinal strains at the ultimate stage for SC_44_22_22_530_T6

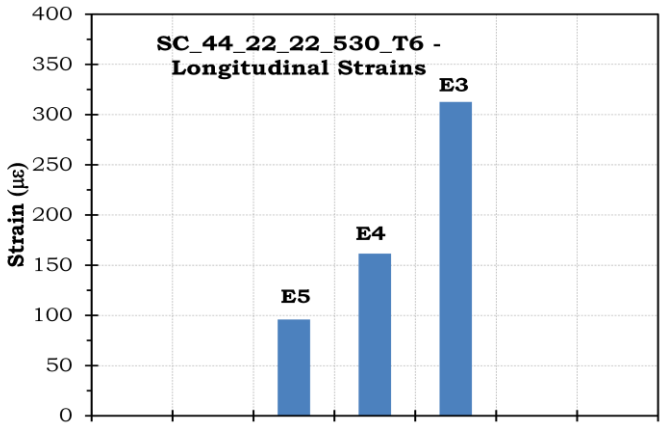


**Figure 5.31** Longitudinal strains at the ultimate stage for SC_44_22_22_530_T6

As expected, maximum strains occurred at the continuous side of the bars and minimum strains at the free end. Generally, #1 gages showed lower strains as compared to #2 gages. However, similar strains were expected on both gages. #2 strain gages were located on the end of lap splice whereas #1 gages were attached away from the lap splice. Generally, the main flexural cracks were observed at the both end of the lap splices. Therefore, #2 gages met generally these main flexural cracks. Strains accumulate at the cracked regions and therefore, cracked sections cause increase in the strain as compared to uncracked sections.

Like specimens SC_22_44_88_800 and SC_44_44_44_710, the strains are not close to each other on the three splices. The reason may be the uneven crack distribution.

As can be observed from the above figures, the longitudinal strain variation on the splice is not linear. The strain increases in accelerated manner.

## 5.5. Strain Profiles on Transverse Reinforcement

The locations of the strain gages on the transverse reinforcement are given in Figure 5.32. For 4 stirrup case, the last two strain gaged stirrups are symmetrical and should give similar results. For 6 stirrup case, the first stirrup (T1, T2, T3) is at the end of lap splice whereas the last stirrup (T7, T8, T9) is located at the middle of lap splice. Figures 5.33 - 5.35 shows strain variation of transverse reinforcement at the ultimate stage.

As shown in the above figures and in the previous chapter, strain variations on the transverse reinforcement are not smooth and show high variations. While some gages show compressive strains other can give tensile strains. Therefore it is hard to conclude from the strain readings on the transverse reinforcement. However, it can be generalized that, strain gages at the corner of the transverse reinforcement (T4, and T6) gave higher strains as compared to the middle strain gages (T5). Additionally, it can be concluded that strain values measured on transverse reinforcement adjacent to the free ends were higher than that of strain values measured closer to mid of the lap splice. The average strain on the transverse reinforcement for specimen SC_44_22_22_530_T4 can be taken as 200 με.

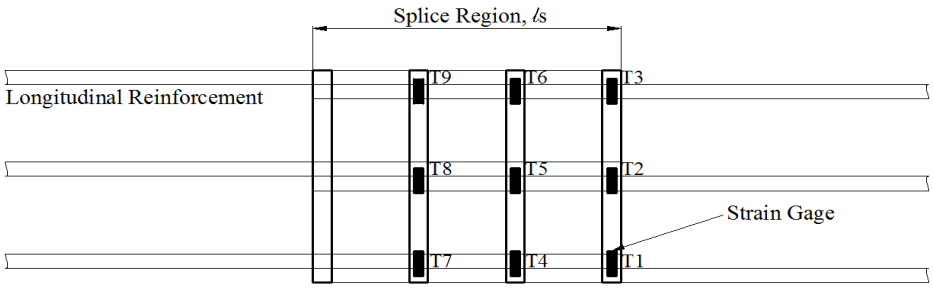


**Figure 5.32** Longitudinal strains at the ultimate stage for SC_44_22_22_530_T6

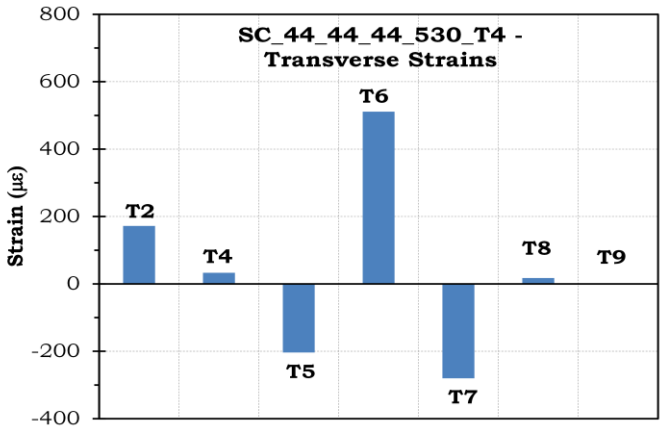


**Figure 5.33** Strain value at ultimate for transverse reinforcements of SC_44_44_44_530_T4

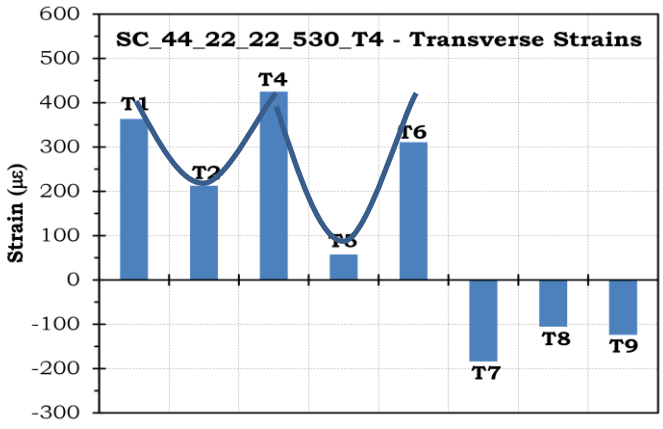


**Figure 5. 34** Strain value at ultimate for transverse reinforcements of SC_44_22_22_530_T4

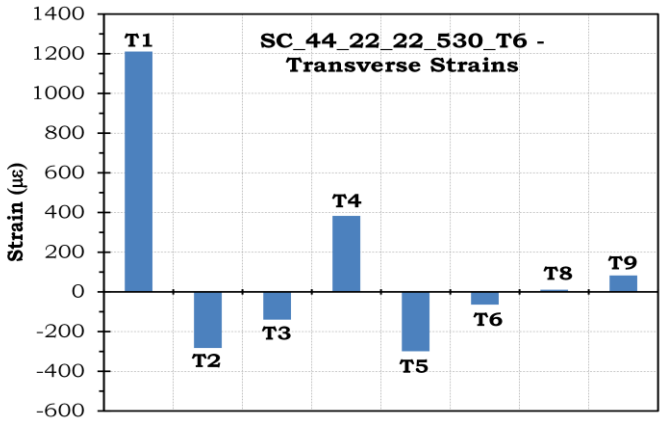


**Figure 5.35** Strain value at ultimate for transverse reinforcements of SC_44_22_22_530_T6

## 5.6. Comparison of the Measured and Calculated Ultimate Stresses

The reinforcement stress values were calculated theoretically by using ACI 408 descriptive equation, Equation 5.12. The SI version of the equations is provided below for steel stress $f_s$:

$$f_s = \left[1.43\ell_s\left(c_{\min} + 0.5d_b\right) + 57.4A_b\right]\left(0.1\frac{c_{\max}}{c_{\min}} + 0.9\right)\frac{\left(f_c'\right)^{1/4}}{A_b} + \left(8.90t_r t_d\frac{NA_{tr}}{n} + 558\right)\frac{f_c'^{3/4}}{A_b} \leq f_y \quad (5.12)$$

$f_s$: stress in reinforcing bar,
$\ell_s$: splice length,
$c_{min}$: min($c_b$; $c_s$)
$c_b$: bottom concrete cover,
$c_s$: min($c_{so}$; $c_{si}$+6.35mm)
$c_{so}$: side concrete cover,
$c_{si}$: ½ of the bar clear spacing,
$d_b$: diameter of bar,
$A_b$: area of bar being spliced,
$c_{max}$: max($c_b$; $c_s$)
$f_c$': concrete compressive strength,
$t_r$: term representing the effect of relative rib area on $T_s$. Taken as 0.978 for regular bars.
$T_s$ : the additional bond strength provided by the transverse steel,
$t_d$: term representing the effect of bar size on $T_s$.
$N$: the number of transverse reinforcement within the splice length,
$A_{tr}$: area of each stirrup crossing the potential plane of splitting adjacent to the reinforcement being spliced,
$n$: number of bars being spliced,
s: spacing of transverse reinforcement,
$f_y$: yield strength of steel.

The measured bar stresses were determined from the ultimate load. The ultimate stress reached during the test was calculated by using the ultimate load. The bar stresses were computed by back solving iteratively the force and moment equilibrium equations.

Table 5.2 shows the bar stresses determined from the tests and calculated analytically. For unconfined specimens, the error between the measured and calculated bars stress varies between 3.4% and 6.5 %. It can be concluded that the ACI 408 bond stress descriptive equation for normal vibrated concrete predicts very successfully the bar stresses of unconfined beams made of SCC.

According to Table 5.2, the error between the measured and calculated bar stresses varies between 10.6% and 34.5 %. In general, bar stress prediction for confined beams is poor even for normal vibrated concrete. However, the error was enormous in this series of tests. The main reason of this high difference is mainly inadequate cover dimensions. According to ACI 318-11, Clause 7.6.1, the minimum clear spacing between parallel bars in a layer shall be 1 bar diameter, $1d_b$, but not less than 1 in. (25.4 mm). For the last two specimens, this limitation is not satisfied and set to 22 mm which is less than 25.4 mm. According to ACI 318-11 Clause 7.7.1, specified cover for reinforcement shall not be less than 1.5 in. (38.1 mm) for beams not exposed to weather or in contact with ground. The given distance for clear cover should be measured from the outside of the transverse reinforcement. The face cover of all confined specimens was 44 mm which was measured from outside of the longitudinal bars. The clear face cover was 36 mm which is slightly less than the given limit. The side clear cover for specimen SC_44_44_44_530_T4 was 36 mm. However, for specimens SC_44_22_22_530_T4, and SC_44_22_22_530_T4, the side clear cover was 14 mm which was far below the given limit. These inadequate covers and spacing caused unpredictable and low bars stresses. Briefly, the descriptive equation cannot predict bar stresses adequately if covers are very small.

The last specimen SC_44_22_22_530_T6 should have behaved better than specimen SC_44_22_22_530_T4 because it had more transverse reinforcement. The calculated bar stress of this specimens was 5.7% higher than specimen with less stirrups. However, the measured bar stress of SC_44_22_22_530_T6 was 4.4% less than that of SC_44_22_22_530_T4. The main reason is again inadequate cover dimensions. The side cover dimensions for these two specimens were extremely low. Increased number of transverse reinforcement inside this small cover caused weak plane instead of increase in bar stress. Briefly, small cover along with a large number of transverse reinforcement weakened tensile capacity of cover concrete and resulted in a decrease in the capacity.

**Table 5.2** Test results

| | $f_c$ (MPa) | $f_{cts}$ (MPa) | Measured $f_s$ (MPa) | ACI 408 $f_s$ (MPa) | Error (%) |
|---|---|---|---|---|---|
| SC_22_44_88_530 | 44.0 | 3.4 | 373.5 | 349.1 | -6.5 |
| SC_22_44_88_800 | 44.0 | 3.4 | 459 | 441.1 | -3.9 |
| SC_44_44_44_710 | 44.5 | 3.7 | 459 | 443.4 | -3.4 |
| SC_44_44_44_530_T4 | 44.5 | 3.7 | 400.0 | 442.4 | 10.6 |
| SC_44_22_22_530_T4 | 45.6 | 3.9 | 341 | 414.8 | 21.6 |
| SC_44_22_22_530_T6 | 45.6 | 3.9 | 326 | 438.5 | 34.5 |

# CHAPTER 6

# CONCLUSIONS

Due to insufficient experimental study on the bond behavior of full scale beams with Self Compacting Concrete (SCC), this study was conducted to fill the gap of lacking experimental data. In this study 6 beams were prepared, with different variables affecting bond behavior. These variables are side cover, bottom cover, free spacing between lap-spliced bars and transverse reinforcement. These specimens were tested under flexure. All beams had lap splice at mid span where constant moment exists. The reinforcement stresses were calculated analytically by using ACI 408-R03 descriptive equations and compared with those obtained experimentally. Based on the experimental and analytical studies and therefore limited to number of tests conducted, the following conclusions are inferred:

- In Turkey, ready-mix concrete companies may not design concrete mix for SCC properly and may cause bleeding in SCC. The main reason of the bleeding can be attributed to exclusion of the viscosity modifying agent in the mix design.

- Specimen SC_22_44_88_530 with $24d_b$ lap splice length showed bond failure with face splitting as expected.

- The expected failure for Specimen SC_22_44_88_800 with $36d_b$ lap splice was bond failure. This specimen, however, showed flexural failure. Increased lap splice length and adequate covers succeeded flexural failure. Test continued approximately until reaching 4 times the yield displacement.

- The expected failure for Specimen SC_44_44_44_710 with $32d_b$ lap splice was bond failure. This specimen showed yielding primarily. With the increasing loading and increasing displacements, however, bond failure occurred with side splitting. Bond failure occurred at about 3 times the yield displacement.

- Specimen SC_44_44_44_530_T4 with $24d_b$ lap splice length and 4 stirrups within the lap splice showed bond failure with side splitting as expected.

- Specimen SC_44_22_22_530_T4 with $24d_b$ lap splice length and 4 stirrups within the lap splice showed bond failure with side splitting as expected.

- Specimen SC_44_22_22_530_T6 with $24d_b$ lap splice length and 6 stirrups within the lap splice showed bond failure with side splitting as expected.

- ACI 408 descriptive equation for normal vibrated concrete predicted bar stresses of the unconfined specimens produced with SCC acceptably well. The predicted values were lower than the measured values to be on the safe side. The error varied between 3.4% and 6.5%.

- All predictions of the ACI408 descriptive equation gave higher bar stresses than measured values of the confined specimens produced with SCC. All

the calculated values were unsafe. The error varied between 10.6% and 34.5%.

- Although specimen SC_44_44_44_530_T4 with $24d_b$ lap splice length followed almost all the limitation for cover dimension the error of the bar stress prediction was 10.6%. In this specimen, side and face cover was only 5.5% less than the ACI 318 limits and spacing between bars was 13.4% less than the ACI 318 limits.

- Although, specimen SC_44_22_22_530_T4 with $24d_b$ lap splice length should have shown high bar stresses according to ACI 408 prediction, this calculated value was 21.6% higher than the measured value. The main reason of the deviation was inadequate cover dimensions. In this specimen, face cover was only 5.5% less than the ACI 318 limits, whereas side cover and spacing between bars were 63.3% and 56.7% less than the ACI 318 limits.

- In specimen SC_44_22_22_530_T6 with $24d_b$ lap splice length to overcome the small cover and spacing problem, number transverse reinforcement was increased to 6 stirrups. However, this increase had a negative effect on the bar stress and measured values were lower than specimen SC_44_22_22_530_T4. The main reason of the decreasing bar stress was the weak plane created due to the increased number of stirrups inside a small side and face cover.

- Cover dimensions or spacing between bars lower than code minimums cause unpredictable bar stresses and cause premature bond failure. Lap splice length provision alone cannot ensure flexural failure. Cover dimensions and bar spacing limitations should be strictly followed in design.

## REFERENCES


*The European Guidlines for Self-Compacting Concrete; Specification, Production and Use.* (2005).

Abrams, D. (1913). *Tests of Bomnd Between Concrete and Steel.* University of Illinois.

ACI 237R-07. (2007). *"Self-Consolidating Concrete Reported by ACI Committe 237".* Farmington Hills, MI: American concrete Institute.

ACI 408R-03. (2003). *"Bond and Develoement of Straight Reinforcing Bars in Tension Reported by ACI Committe 408".* Farmington Hills, MI: American Concrete Institute.

Bentz, E. (2000). Response-2000, Reinforced Concrete Sectional Analysis using the Modified Compression Field Theroy, Version 1.0.5. Toronto, CA.

Canbay, E. (2009). Bond of Lap-Spliced Bars in Self-Compacting Concrete. Canada.

Daoud, A., & Lorrian, M. (2003, May). Influence of bar position on bond between reinforcement and self-compacting concrete: interpretation using image analysis. *Materials and Structures/, 38*, 231-237.

de Almeida Filho, F., El Debs, M. K., & El Debs, A. H. (2008). Bond-slip behavior of self-compacting concrete and vibrated concrete using pull-out and beam tests. *Materials and Structures, 41*, 1073–1089.

de C. El Debs, A. H., & de Almeida Filho, F. M. (2007). THEORETICAL AND NUMERICAL APPROACH OF THE BOND BEHAVIOR IN BEAM TESTS USING SELF-COMPACTING AND ORDINARY CONCRETE WITH THE SAME COMPRESSIVE STRENGTH. *Ciência & Engenharia,, 16*(1/2), 99-106.

De Schutter, G., Bartos, P. J., Domone, P., & Gibbs, J. (2008). *Self-Compacting Concrete.* New York: Whittles Publishing.

Desnerk, P., De Schutter, G., & Taerwe, L. (2010). Bond Behavior of reinforcing bars in self-compacting concrete: experimental determination by using beam test. *Material and Structures, 43*, 53-62.

Domone, P. (2007). A review of the hardened mechanical properties of self-compacting concrete. *Cement & Concrete Composites, 29*, 1-12.

Esfahani, M. R., Kianoush, M. R., & Lachemi, M. (2005, June 4). *Bond strength of glass fibre reinforced polymer reinforcing bars in normal and self-consolidating concrete*. Retrieved from http://cjce.nrc.ca

Hayakawa, M., Matsouka, Y., & Shindoh, T. (1993). Developement and Applicatioon of Super Workable Cocncrete. *Universiyi of Pasiley* (p. 8). RILEM.

Hossain, K., & Lachemi, M. (2008, September 1). Bond Behavior of Self-Consolidating Concrete with Mineral and Chemical Admixtures. *Journal of Materials in Civil Engineering, 9*(9), 608-616.

Mazaheripour, H., Barros, J., Sena-Cruz, J., Pepe, M., & Martinelli, E. (2013). Experimental study on bond performance of GFRP bars in self-compacting steel fiber reinforced concrete. *Composite Structure*, 202-212.

Miura, N., Takeda, N., Chikamatsu, R., & and Sogo, S. (1993). Developement and Utilization of High Performance Concrete fo the Construction of the Akashi Kaikyo Bridge. 25-51.

Okamura, H., Maekawa, K., & Ozawa, K. (1993). *Highe Performance Concrete.* Gihodo Publishing.

Ozawa, K., Maekawa, K., Kunishima, M., & Okamura, H. (1989). Developement of high performance concrete based on the durability design of concrete structures. *East-Asia and Pacific Conference on Structural Engineering and Construction (EASEC-2), 1*, pp. 445-450.

Pandurangan, K., Kothandaraman, S., & Sreedaran, D. (2010). A study on the bond strength of tension lap splices in self compacting concrete. *Materials and Structures, 43*, 1113-1121.

Sonebi, M., & Bartos, P. ( September 1999). Hardened SCC and its Bond with Reinforcement. *The Firts Internatioan RELIM Symposym on SCC.* Stockhom, Sweden.

Sonebi, M., & Bartos, P. (September 1999). Hardened SCC and its Bond with Reinforcement. *The Firts Internatioan RILEM Symposym on SCC.* Stockhom, Sweden.

Tanaka, K., Sato, K., Watanabe, S., Arima, I., & and Suenaga, K. (1993). Development and Utilization of High Performance Concrete for the Construction of the Akashi Kaikyo Bridge. In *High-Performance Concrete in Severe Environments* (Vol. 140, pp. 25-51).

Tanaka, K., Sato, K., Watanabe, S., Arima, I., & and Suenaga, K. (n.d.). Development and Utilization of High Performance Concrete for the Construction of the Akashi Kaikyo Bridge. (P. Zia, Ed.)

Türk, K., Benli, A., & Calayır, Y. (2008, January 12). Bond Strength of Tension Lap-Splice in Full Scale Self-Compacting Concrete Beams. *Turkish J. Eng. Env. Sci, 32*, 377-386.

Türk, K., Karataş, M., & Ulucan, Z. C. (2010). Effect of the use of different types and dosages of mineral additions on the bond strength of lap-spliced bars in self-compacting concrete. *Materials and Structures, 43*, 557-570.

Valcuende, M., & Parra, C. (2009). Bond behaviour of reinforcement in self-compacting concretes. *Construction and Building Materials, 23*, 162-170.

Yin-Wen, C., Chen, Y.-S., & Liu, Y.-S. (2003, July - August). Developement of Bond Strength of Reinforcement Steel in Self-Consolidating Concrete. *ACI STRUCTURAL JOURNAL, 100*(4).

Zhu, W., Sonebi, M., & Bartos, P. (2004, August - September). Bond and Interficial properties of reinforcement in self-compacting concrete. *Material and Sructures, 37*, 442-448.

## APPENDIX A

### THEORETICAL MOMENT CURVATURE DIAGRAMS OF SPECIMENS

In this appendix theoretical moment curvature diagrams, acquired from RESPONSE-200, are shown.

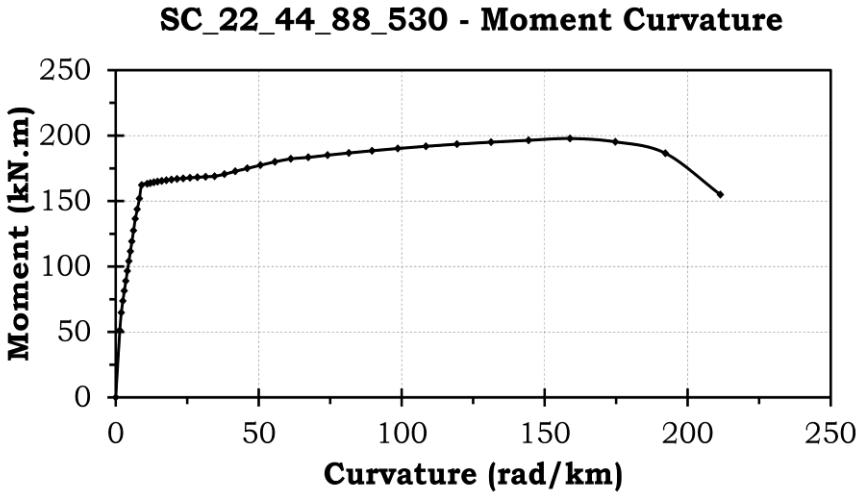


**Figure A.1** Moment Curvature Diagram – SC_22_44_88_530

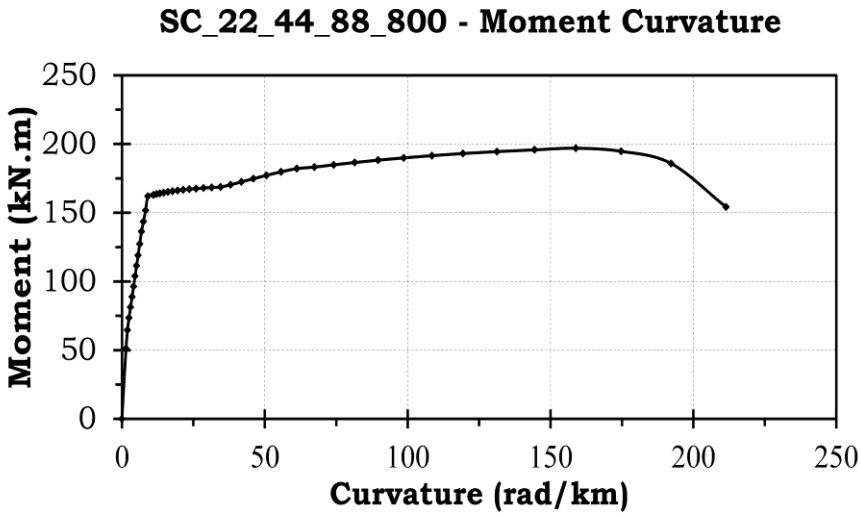


**Figure A.2** Moment Curvature Diagram – SC_22_44_88_800

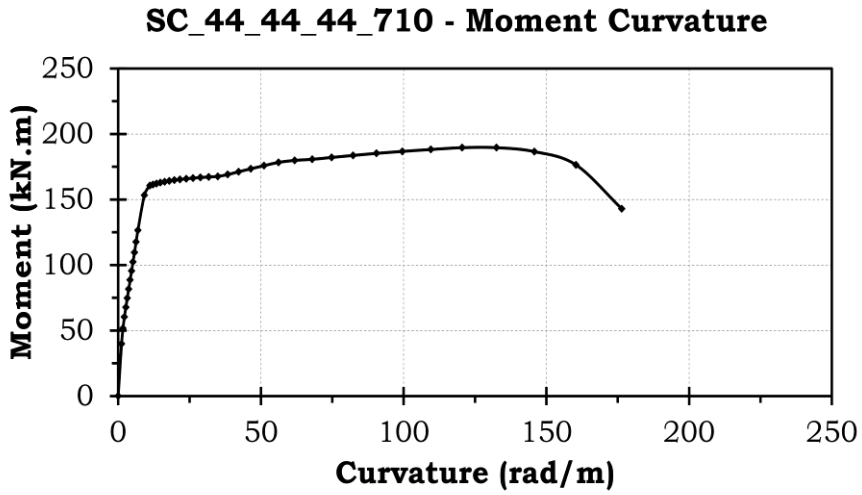


**Figure A.3** Moment Curvature Diagram – SC_44_44_44_710

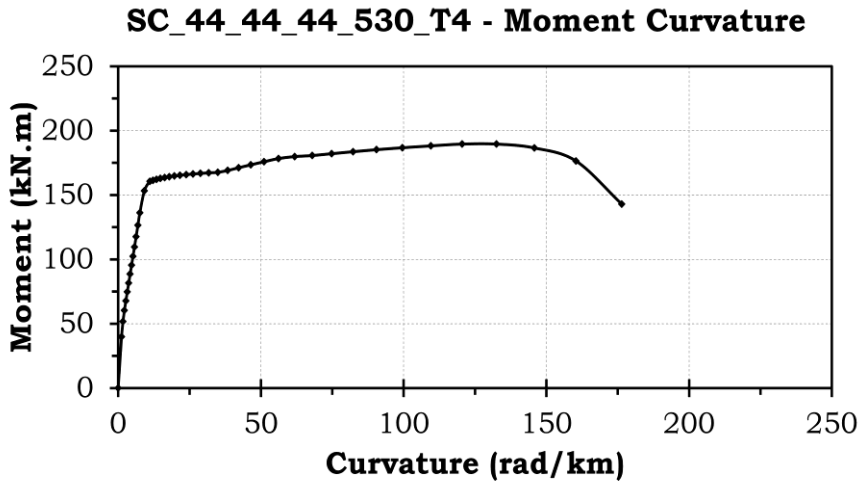


**Figure A.4** Moment Curvature Diagram – SC_44_44_44_530_T4

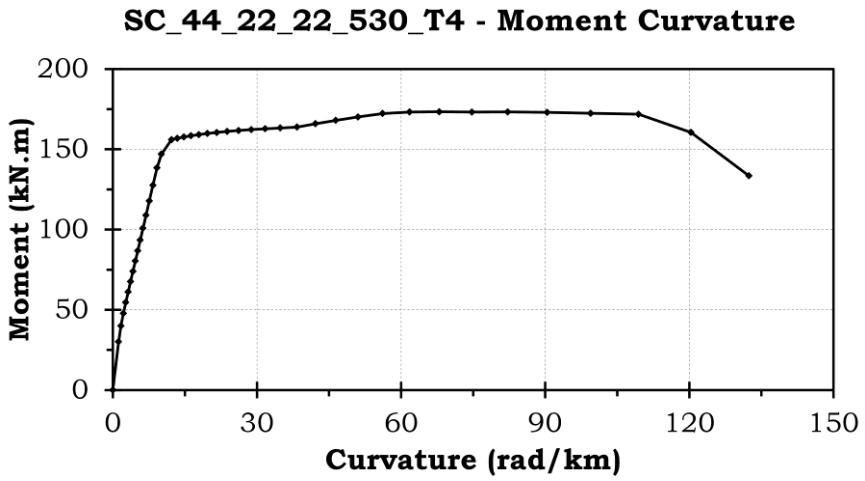


**Figure A.5** Moment Curvature Diagram – SC_44_22_22_530_T4

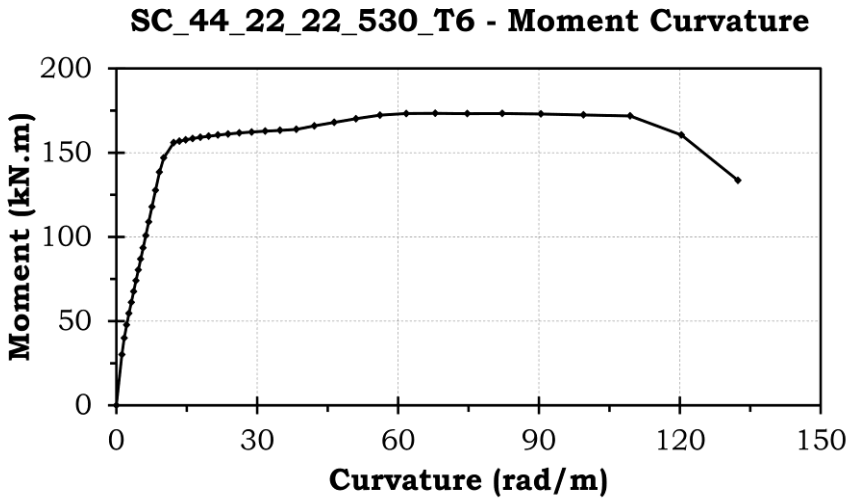


**Figure A.6** Moment Curvature Diagram – SC_44_22_22_530_T6